ÉCOLE DE TECHNOLOGIE SUPÉRIEURE
UNIVERSITÉ DU QUÉBEC

THESIS PRESENTED TO
ÉCOLE DE TECHNOLOGIE SUPÉRIEURE

IN PARTIAL FULFILLMENT OF THE REQUIREMENTS FOR
THE DEGREE OF DOCTOR OF PHILOSOPHY
Ph.D.

BY
Souleman NJOYA MOTAPON

DESIGN AND SIMULATION OF A FUEL CELL HYBRID EMERGENCY POWER SYSTEM FOR A MORE ELECTRIC AIRCRAFT: EVALUATION OF ENERGY MANAGEMENT SCHEMES

MONTREAL, MARCH 27 2013

BOARD OF EXAMINERS

THIS THESIS HAS BEEN EVALUATED

BY THE FOLLOWING BOARD OF EXAMINERS:

Mr. Louis-A. Dessaint, Thesis Director
Département de génie électrique de l'École de technologie supérieure

Mr. Roger Champagne, Committee President
Département de génie logiciel et des TI de l'École de technologie supérieure

Mr. Kamal Al-Haddad, Examiner
Département de génie électrique de l'École de technologie supérieure

Mrs. Susan Liscouet-Hanke, Invited Examiner
Bombardier Aerospace

Mr. Christophe Turpin, External Independent Examiner
Chercheur CNRS. Laboratoire Laplace, Institut national polytechnique de Toulouse

THIS THESIS WAS PRESENTED AND DEFENDED

IN THE PRESENCE OF A BOARD OF EXAMINERS AND PUBLIC

ON MARCH 13 2013

AT ÉCOLE DE TECHNOLOGIE SUPÉRIEURE

ACKNOWLEDGEMENTS

This work is part of the CRIAQ ENV405 project and is supported by a NSERC (Natural Sciences and Engineering Research Council of Canada) grant, in collaboration with CRIAQ (Consortium for Research and Innovation in Aerospace in Quebec), Bombardier Aerospace and Transtronic Inc.

The project started back in mid 2008, right after the completion of my M. Eng. degree in electrical engineering at École de technologie supérieure (ETS). As my previous work involved fuel cell modelling and power electronic converters, this new project was right on track with my research area. Therefore, I was very motivated and excited when I was approached by professor Dessaint, to contribute to this highly challenging and interesting field of study.

I would like to sincerely thank professor Dessaint for his trust in me in undertaking this project and for his financial assistance, which enabled me to focus effectively on my research activities. Moreover, his constructive guidance and support throughout the project period was very much appreciated.

I would also like to thank the ETS electrical department technical team, particularly Daniel Bérubé and Yves Robitaille, Bruno Côté from the ETS "Service de l'équipement", Pierre Giguère from the ETS "Bureau de la santé et de la sécurité au travail" and Javier Beltran-Galindo from the ETS "Bureau du développement durable", for their excellent work in setting up the ETS fuel cell laboratory, the first fuel cell laboratory in Montreal! Large Mexican hats to all of you. Without you this laboratory wouldn't have been ready as scheduled and my experimental validation wouldn't have been possible.

My sincere thanks go to Jorge Rojas Abad and Christian Talbot, for their assistance and patience during all my experimental tests. These folks were always there when I needed them, even after their regular working hours and week-ends.

I would like to thank the technical staffs from the industries that supported this project, particularly Claude Lavoie, Susan Liscouet-Hanke, Sylvain Morel, Dominic Lavoie, Francois Pel-

letier and Makram de Freige from Bombardier Aeropace, Louis Monnin, Pierre Merette and Emmanuel Zanré from Transtronic inc, for providing technical data for validation purposes and for their guidance and critiques throughout the project.

I would like to thank Kevin Rocard, an intern from the “Université de Toulouse”, who helped in developing the LabVIEW software for control and monitoring.

I would like to thank the project manager Pierre Mercier for his enthusiasm and persistence throughout the project. Without you the project wouldn’t have been completed as planned.

I would also like to thank my family for their support and encouragements. It has not been easy to live miles away from you for years, but you always make me feel you were right there. Without you I wouldn’t have make it this far.

Finally, with all my heart, I would like to express my gratitude to my wife Fiona, for her time reviewing this report, her support and encouragements and most importantly her love. I know I have been a work-alcoholic for the past months and haven’t been able to spend as much time with you and our newborn Malik. Thank you for your patience and tolerance.

DESIGN AND SIMULATION OF A FUEL CELL HYBRID EMERGENCY POWER SYSTEM FOR A MORE ELECTRIC AIRCRAFT: EVALUATION OF ENERGY MANAGEMENT SCHEMES

Souleman NJOYA MOTAPON

ABSTRACT

As the aircraft industries are moving toward more electric aircraft (MEA), the electrical peak load seen by the main and emergency generators becomes higher than in conventional aircraft. Consequently, there is a major concern regarding the aircraft emergency system, which consists of a ram air turbine (RAT) or air driven generator (ADG), to fulfill the load demand during critical situations; particularly at low aircraft speed where the output power is very low. A potential solution under study by most aircraft manufacturers is to replace the air turbine by a fuel cell hybrid system, consisting of fuel cell combined with other high power density sources such as supercapacitors or lithium-ion batteries.

To ensure the fuel cell hybrid system will be able to meet the load demand, it must be properly designed and an effective energy management strategy must be tested with real situations load profile. This work aims at designing a fuel cell emergency power system of a more electric aircraft and comparing different energy management schemes (EMS); with the goal to ensure the load demand is fully satisfied within the constraints of each energy source. The fuel cell hybrid system considered in this study consists of fuel cell, lithium-ion batteries and supercapacitors, along with associated DC-DC and DC-AC converters. The energy management schemes addressed are state-of-the-art, most commonly used energy management techniques in fuel cell vehicle applications and include: the state machine control strategy, the rule based fuzzy logic strategy, the classical PI control strategy, the frequency decoupling/fuzzy logic control strategy and the equivalent consumption minimization strategy (ECMS). Moreover, a new optimal scheme based on maximizing the instantaneous energy of batteries/supercapacitors, to improve the fuel economy is proposed. An off-line optimization based scheme is also developed to ascertain the validity of the proposed strategy in terms of fuel consumption.

The energy management schemes are compared based on the following criteria: the hydrogen consumption, the state of charges of the batteries and supercapacitors and the overall system efficiency. Moreover the stress on each energy source, which impacts their life cycle, are measured using a new approach based on the wavelet transform of their instantaneous power. A simulation model and an experimental test bench are developed to validate all analysis and performances.

The main results obtained are as follows: the state machine control scheme provided a slightly better efficiency and stresses on the batteries and supercapacitors. The classical PI control and the proposed scheme had the lowest fuel consumption and more use of the battery energy. As expected, the lowest fuel cell stress and lowest use of the battery energy was achieved with the frequency decoupling and fuzzy logic scheme, but at the expense of more fuel consumption and

lower overall efficiency. The DC bus or supercapacitor voltage was maintained nearly constant for all the schemes. Also, the proposed strategy performed slightly better than the ECMS in terms of efficiency and fuel consumption, with an increase in fuel economy by 3 %.

The energy management scheme suitable for a MEA emergency system should be a multi-scheme EMS such that each scheme is chosen based on a specific criterion to prioritize. As an example, depending on the operating life of each energy source, the energy management strategy can be chosen to either minimise the stress on the fuel cell system, the battery system or supercapacitor system, hence maximizing the life cycle of the hybrid power system. Also if the target is to reduce the fuel consumption, the proposed or the classical PI strategies are better alternatives.

Keywords: Fuel cell, Batteries, Supercapacitors, DC-DC converters, Energy management, Hybridization, Optimization

CONCEPTION ET SIMULATION D'UN SYSTÈME D'ALIMENTATION DE SECOURS POUR UN AVION PLUS ÉLECTRIQUE: ÉVALUATION DES SYSTÈMES DE GESTION D'ÉNERGIE

Souleman NJOYA MOTAPON

RÉSUMÉ

Dans le but de réduire la consommation de combustibles fossiles et les coûts liés à la maintenance, l'industrie aéronautique vise à remplacer la plupart des systèmes hydrauliques et pneumatiques des avions conventionnels par des systèmes électriques. Ces nouveaux avions du futur sont appelés « avion plus électrique ». Dans ces avions plus électrique, l'augmentation de la demande électrique rend l'utilisation du système de secours actuel basé sur une éolienne traditionnelle impossible. Surtout lors des atterrissages et décollages où la puissance fournie par celle-ci est presque nulle. L'une des solutions considérée par les avionneurs est de remplacer l'éolienne par un système hybride basé sur une pile à hydrogène, assistée par les batteries et/ou les super condensateurs.

Afin de s'assurer que le système hybride pourra satisfaire à la demande, il doit être correctement conçu et une stratégie efficace de gestion d'énergie doit être testée avec un vrai profil de vol. Ce travail vise à concevoir un système d'alimentation de secours basé sur une pile à hydrogène pour un avion plus électrique, et à comparer différentes stratégies de gestion d'énergie; avec pour but de s'assurer que la demande en situation d'urgence est entièrement satisfaite, et ce, dans les limites de chaque source d'énergie. Le système hybride considéré est constitué d'une pile à hydrogène, d'un bac de batteries aux ions de lithium et de super condensateurs, ainsi que leur convertisseurs CC-CC et CC-CA associés. Les stratégies de gestion d'énergie considérées sont les plus courantes de l'état de l'art, utilisées dans les véhicules hybrides, à savoir: la stratégie de commande par état de la machine, la stratégie basée sur la logique floue, la stratégie de commande par régulateur PI, la stratégie de commande basée sur le découplage de la fréquence et la stratégie de minimisation de la consommation équivalente (ECMS). D'autre part, une nouvelle stratégie optimale basée sur la maximisation de l'énergie instantanée des batteries/super condensateurs, est proposée afin d'en améliorer l'économie en hydrogène. En plus, un algorithme basé sur l'optimisation hors-ligne a été également développé afin de valider la stratégie proposée.

Les critères principaux de comparaison des différentes stratégies sont les suivants: la consommation d'hydrogène, l'état de charge des batteries/super condensateurs et l'efficacité globale du système. En plus, le niveau de sollicitations de chaque source d'énergie, qui influence énormément leur cycle de vie, est mesuré avec une nouvelle approche basée sur la transformée en ondelettes de leur puissance instantanée.

Un modèle de simulation et un banc d'essai expérimental ont été développés pour valider toutes les analyses et les différentes performances.

Les principaux résultats obtenus sont les suivants : la stratégie de commande par état de la machine a fourni une performance légèrement meilleure en termes d'efficacité globale et du niveau de sollicitations des batteries et des super condensateurs. La stratégie de commande par régulateur PI et celle proposée ont eu la plus basse consommation d'hydrogène, mais avec un taux d'utilisation de l'énergie des batteries plus élevé. Comme prévu, le plus bas niveau de sollicitations de la pile à hydrogène ainsi que le plus bas taux d'utilisation de l'énergie des batteries ont été réalisés avec la stratégie de commande basée sur le découplage de la fréquence, mais aux dépens d'une consommation d'hydrogène plus élevée et d'une efficacité globale plus faible. Pour toutes les stratégies, la tension du bus DC ou des super condensateurs est presque maintenue constante. En outre, la stratégie proposée a été légèrement meilleure comparée à l'ECMS en termes de consommation d'hydrogène et d'efficacité globale avec une augmentation sur l'économie en hydrogène de 3 %.

La stratégie de gestion d'énergie appropriée au système de secours des avions plus électrique devrait être de type multi-stratégies telle que chaque stratégie est choisie basée sur un critère spécifique prioritaire. Par exemple, selon la durée de fonctionnement de chaque source d'énergie, la stratégie de gestion d'énergie peut être choisie avec pour but de réduire au minimum le niveau de sollicitations du système de pile à hydrogène, des batteries ou des super condensateurs, ainsi augmentant le cycle de vie du système d'alimentation hybride. Par ailleurs, si la cible est de réduire la consommation d'hydrogène, la stratégie proposée ou celle classique par régulateur PI sont de meilleurs candidats.

Mots-clés: Pile à hydrogène, batteries, super condensateurs, système hybride, convertisseurs CC-CC, optimisation

CONTENTS

LIST OF TABLES

LIST OF FIGURES

LIST OF ABBREVIATIONS

ETS	École de Technologie Supérieure
FCPM	Fuel Cell Power Module
ECU	Engine Control Unit
BMS	Battery Management System
EMS	Energy Management Scheme
ECMS	Equivalent Consumption Minimization Strategy
EEMS	External Energy Maximization Strategy
UMU	Ultracapacitor Management Unit
MEA	More Electric Aircraft
CRIAQ	Consortium for Research and Innovation in Aerospace in Quebec
NSERC	Natural Sciences and Engineering Research Council of Canada
EHA	Electro-Hydrostatic Actuator
EMA	Electro-Mechanical Actuator
EBHA	Electro-Backup Hydraulic Actuator
RAT	Ram Air Turbine
ADG	Air Driven Generator
TRU	Transformer Rectifier Unit
KEAS	Knots Equivalent Air Speed
SOC	State OF Charge
SOE	State OF Energy

APU	Auxiliary Power Unit
HBMU	Heater/Brake Monitoring Unit
SPS	SimPowerSystems
CAN	Controller Area Network
PXI	PCI eXtensions for Instrumentation
ELDC	Electric Double Layer Capacitor
PWM	Pulse-Width-Modulated

LIST OF SYMBOLS

E_n	Nernst voltage (V)
P_{H2}	Hydrogen partial pressure (atm)
P_{O2}	Oxygen partial pressure (atm)
Uf_{H2}	Hydrogen utilization
Uf_{O2}	Oxygen utilization
V_{fuel}	Fuel flow rate ($lmin^{-1}$)
V_{air}	Air flow rate ($lmin^{-1}$)
K_c	Voltage constant
k	Boltzmann's constant ($JK^{-}1$)
h	Planck's constant (Js)
α	Charge transfer coeffcient
ΔG	Activation barrier (J)
K_u	Voltage undershoot constant
Uf_{O2nom}	Nominal oxygen utilization
V	Fuel cell output voltage (V)
E_{oc}	Fuel cell open circuit voltage (V)
V_{act}	Activation voltage (V)
V_r	Charge transport voltage (V)
A	Tafel slope (V)
i_0	Exchange current (A)

i_{fc}	Fuel cell current (A)
r_{ohm}	Combined cell and diffusion resistance (Ω)
T_d	Fuel cell settling time (s)
N	Number of cells
V_{fc}	Stack voltage (V)
P_{fuel}	Fuel inlet pressure (bar)
P_{air}	Air inlet pressure (bar)
T	Stack temperature (^oC)
V_{batt}	Battery voltage (V)
E_0	Battery constant voltage (V)
K	Polarization constant (V $(Ah)^{-1}$)
Q	Battery capacity (Ah)
i	Battery current (A)
i^*	Filtered battery current (A)
it	Battery charge (Ah)
A_b	Exponential zone amplitude (V)
B	Exponential zone time constant inverse ($(Ah)^{-1}$)
R_b	Battery internal resistance (Ω)
Pol_{res}	Polarization resistance (Ω)
C	Cell capacitance (F)
C_H	Helmholtz capacitance (F)

C_{GC}	Gouy-Chapman capacitance (F)
N_e	Number of electrode layers
ϵ	Permittivity of the electrode material (F m^{-1})
ϵ_0	Permittivity of free space (F m^{-1})
A_i	Inter-facial area between electrode and electrolyte (m^2)
d	Helmholtz layer length (m)
Q_c	Cell electric charge (C)
c	Molar concentration (mol m^{-3})
R	Ideal gas constant (J mol^{-1} K)
F	Faraday constant (A s mol^{-1})
N_s	Number of cells in series
N_p	Number of cells in parallel
C_T	Total capacitance (F)
V_{SC}	Supercapacitor output voltage (V)
Q_T	Total electric charge (C)
R_{SC}	Supercapacitor module resistance (Ω)
i_{SC}	Supercapacitor current (A)
V_L	Voltage at low voltage side (V)
V_H	Voltage at high voltage side (V)
I_L	Current at low voltage side (A)
I_H	Current at high voltage side (A)

D	Duty cycle
η	Converter efficiency
K_{pi}	Current controller proportional gain
K_{pv}	Voltage controller proportional gain
K_{ii}	Current controller integral gain
K_{iv}	Voltage controller integral gain
ω_{ni}	Current controller bandwidth
ω_{nv}	Voltage controller bandwidth
ζ	Damping coefficient
T_{Ri}	Current controller response time (s)
T_{Rv}	Voltage controller response time (s)
V_{Pnom}	Nominal RMS phase voltage (V)
P_p	Phase active power (W)
Q_p	Phase reactive power (W)
S	3-phase apparent power (VA)
$cos\theta$	Power factor
P_{fc}	Fuel cell power at the DC bus (W)
α_p	Penalty coefficient
P_{batt}	Battery power at the DC bus (W)
ΔT	Sampling time (s)
P_{fcmin}	Minimum fuel cell power at the DC bus (W)

P_{fcmax}	Maximum fuel cell power at the DC bus (W)
$P_{battmin}$	Minimum battery power at the DC bus (W)
$P_{battmax}$	Maximum battery power at the DC bus (W)
SOC_{min}	Minimum battery state of charge (%)
SOC_{max}	Maximum battery state of charge (%)
μ	SOC balance coefficient
V_{dc}	DC bus voltage (V)
ΔV	Supercapacitor charge/discharge voltage (V)
C_r	Rated capacitance (F)
V_{dcmin}	Minimum DC bus voltage (V)
V_{dcmax}	Maximum DC bus voltage (V)
V_{battr}	Rated battery voltage (V)
P_{load}	Load power (W)
$ConsH2^{opt}$	Optimal H2 consumption (g)
n	Number of samples
T_p	Load profile duration (s)
F^{opt}	Optimal total fuel cell energy (W s)
P_{fcnom}	Nominal fuel cell power (W)
$ConsH2_{nom}$	Nominal fuel consumption (g)
$efficiency$	Overall efficiency
P_{fcin}	Fuel cell power at the DC/DC converter input (W)

P_{battin}	Battery power at the DC/DC converter input (W)
P_{capin}	Supercapacitor power (W)

INTRODUCTION

In the fast moving and competitive world of aeronautics, aircraft manufacturers are eager to develop new systems that will greatly improve the weight and efficiency of the whole aircraft architecture and therefore reduce fuel consumption and maintenance costs. For this reason, most aircraft manufacturers are moving toward a more electric aircraft (MEA) which involves the replacement of some parts of hydraulic, mechanical and pneumatic systems with electrical systems. The major modifications performed on a conventional aircraft to obtain a MEA are the following (Langlois *et al.* (2005)), (Faleiro (2006)), (Rosero *et al.* (2007)):

- the hydraulic actuators necessary for flight controls and landing gear are replaced by other types of actuators such as the electro-hydrostatic actuator (EHA), the electro-mechanical actuator (EMA) and the electro back-up hydraulic actuator (EBHA). The main hydraulic pumps with their heavy and inflexible piping are removed;
- the bleed air off-takes (which account for the largest non propulsive power off-take from the engine) required for air-conditioning and wing ice protection are replaced by new electrical systems (air compressors, re-circulating fans, refrigeration units, heating resistors, etc);
- the gear box which is used to connect the main engine (gas turbine) to other electrical or hydraulic systems may be removed. The power generated by the main engine is converted into electrical energy by generators mounted directly on the engine shaft (s).

Figure 0.1 and Figure 0.2 depict the differences between a conventional and a MEA aircraft. These modifications reduce the non-propulsive power required as the power off-take to supply the aircraft systems (flight control actuators and environmental control system) is adjusted to match the demand, rather than being wasted unusable heat. That means the efficiency of the aircraft will be improved and consequently less fuel will be used (Faleiro (2005)).
Airbus and Boeing have started to introduce this technology on their recent aircraft (A380 and Boeing 787 respectively). On the A380, a hydraulic circuit for the primary flight controls

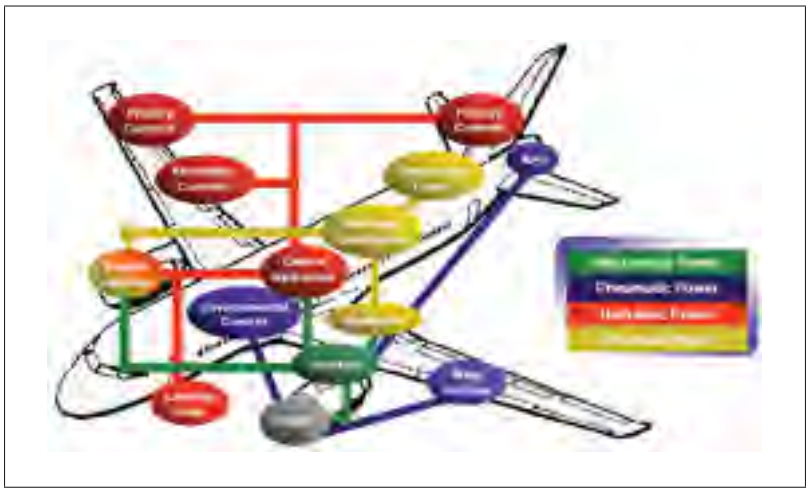

Figure 0.1 Conventional aircraft power distribution
Adapted from Faleiro (2006)

is replaced by EHAs. The Boeing 787 Dreamliner is even more electric with its brake, ice protection systems, engine start and environmental control systems all being electric-based. These aircrafts are claimed to be very beneficial in terms of fuel consumption, maintenance costs, efficiency and reliability.

Figure 0.2 MEA aircraft power distribution
Adapted from Faleiro (2006)

The power source commonly used in most aircraft during emergency situations is the ram air turbine (RAT) or the air driven generator (ADG). An example of RAT is shown in Figure 0.3 for

a Boeing 757 (Wikipedia (2012)). The RAT or ADG is automatically deployed into the airflow upon loss of all engine supplied power. The RAT consists of an air driven turbine coupled to a central hydraulic pump and an electrical generator. It provides electric power to essential loads and hydraulic power to the flight control surfaces and landing gear systems. The ADG on the other hand is an air driven turbine coupled only to an electrical generator to supply the essential loads and to power electrically a central hydraulic pump (Prats (2007)).

Figure 0.3 Ram air turbine of a Boeing 757
Adapted from Wikipedia (2012)

In a MEA, the RAT produces only electrical power (just as the ADG) and supplies the EHA, EMA and EBHA through the AC essential bus (to be more precise, the RAT is replaced by the ADG in MEA). The AC essential bus is connected to the DC essential bus (which supplies all the critical DC loads) through transformer-rectifier units (TRUs).

The addition of new electrical devices to the flight controls and landing gear systems results in extra peak power requirements during critical situations (flap/slat actuation, landing gear deployment and braking). This is mainly due to power electronics converters in EHA, EMA and EBHA which generate high currents and voltages at starting and during transients (Langlois (2006)). Therefore there is a potential risk of overloading the existing RAT/ADG, which will cause the latter to stall.

Another problem associated with the RAT/ADG is the decrease of output power with the air speed. At low airspeed, the loading of the RAT/ADG must be limited. For the Global express, at 145 KEAS (Knots Equivalent Air Speed), the RAT is off-loaded to ensure that the required hydraulic power is supplied to the flight control surfaces (Bombardier (2004)).

The risk of overloading the existing ADG in a MEA has been one of the major concerns of aircraft companies. In most aircraft, the ADGs are usually over-dimensioned as they are designed based on peak power requirement during emergency situations. To fulfil the load demand in a MEA, these power sources will have to be redesigned for higher peak power delivery. This means the ADGs of MEA will excessively be larger in size and volume. Consequently they will be heavier and their installation and maintenance will be challenging (especially for medium and small size aircraft). Fuel consumption will be increased as more weight is added to the system.

Besides the risk of overloading the ADG, there are some other challenges in MEA which need to be overcome, during total loss of main engines and during landing/braking. On conventional aircraft, when the main engines are lost, the main AC generators drop off-line almost immediately. The ADG is available only after a short time (needed for deployment and starting) during which the flight controls remain powered via the central hydraulic pumps which keep operating due to turbine inertia. During landing and braking, as the ADG output power reduces, a safe landing and braking is achieved through hydraulic accumulators. A MEA with no mechanically driven central hydraulic pump and electric brakes will require an alternative power source during ADG deployment and during landing/ braking (Langlois (2006)).

One interesting idea to solve these problems could be to connect the ADG in parallel with batteries via power electronic converters to fulfil the load requirement (Langlois (2006)), (Wells *et al.* (2008)). The ADG could be designed for nominal power while the batteries could be used for peak power requirement. This will effectively reduce the weight and size of the ADG and therefore facilitate its installation and maintenance. For longer emergency situations, there are still risks of overloading the ADG (especially at low speed) if the charging/discharging of the batteries is not well controlled. Therefore, this method requires a complex power management

strategy. Several energy management techniques have been proposed for successful power sharing between the ADG and the batteries, but these techniques can not be validated due to the difficulty to test the performance of the hybrid system. Currently testing ADG's requires a dedicated test flight.

A more efficient and robust power source is desired for emergency situations. A preliminary analysis made by Bombardier aerospace (Prats (2007)) and a theoretical study by Garcia (2007) shows that a potential power source to replace the ADG are fuel cell. Compared to conventional internal combustion engines, fuel cell produce power (from several W to multi- MW) with low toxic emissions, low noise and vibrations, high efficiency (especially at light loads), easy installation and low maintenance cost. fuel cell are compatible with several types of fuel and can provide the required power as long as the fuel is supplied.

With the recent technological advances on fuel cell components (electrodes, membrane and catalysts) and pressurized hydrogen tanks, the power density of fuel cell has greatly improved. Ballard Power Systems has developed fuel cell stacks for motive or stationary power applications (Mark9 SSL) with power density greater than 1kW/kg (Ballard (2012)). Honda also presented in 2009 a new vertical-flow fuel cell stack of 100 kW with a size which can be compared to a computer case and a power density close to 1.5kW/kg (Honda (2009)). Recently (in October 2011), Nissan revealed a new fuel cell stack with the world's best power density of 2.5 kW/kg (Nissan (2011)).

This has motivated MEA manufacturers for more in-depth studies to make the fuel cell onboard, a commercial reality. Figure 0.4 shows a prototype of a 25 kW fuel cell emergency power system (FCEPS) developed by Liebherr Aerospace, where the fuel cell stack is fed directly with hydrogen and oxygen, using pressurized tanks to improve the system efficiency. As shown, the system is fully integrated in the aircraft fuselage, with the power available as needed, regardless of the external airflow or weather conditions. Figure 0.5 shows another fuel cell emergency power system of 20 kW developed by DLR that have been successfully tested in a A320 Airbus at flight altitude up to 25000 feet (Renouard-Vallet *et al.* (2011)), (Renouard-

Vallet *et al.* (2010)).

Figure 0.4 FCEPS prototype from Liebherr Aerospace
Adapted from Liebherr (2007)

Figure 0.5 Fuel cell emergency power system developed and tested by DLR
Adapted from DLR (2010)

Problem statement

Due to the slow response of fuel cell to highly fluctuated demand, hybridization of fuel cell with new energy storage devices such as lithium-ion batteries or supercapacitors is required. This hybridization allows the fuel cell system to be optimized to achieve better fuel economy and performance as part of the load is provided by the batteries/supercapacitors. This optimization is accomplished through an energy management strategy (EMS) which distributes the load power among the energy sources. The design of such EMS should be made in such a way to

achieve an optimal fuel economy while ensuring each energy source operates within its limits. Also the EMS impact on the life cycle of the whole hybrid power system should be limited as possible.

Different EMSs for fuel cell hybrid power systems have been reported in the literature. However, most of these EMS have been mainly applied to hybrid vehicle load profile, which is regenerative with low fluctuations compared to aircraft emergency load profile. Moreover, existing comparative studies between these EMS cover only few of them without (or not enough) experimental validation. Also, the impact of the EMS on the overall efficiency and life cycle of the whole system is often omitted. This has motivated the author of this work for further analysis to verify experimentally which EMS strategy fits better with MEA load profile.

Another point concerns the modelling of the hybrid power system, in previous studies reported in the literature, the models of components are either valid for a specific test bench or require parameters that are difficult to determine (cell area, volume of electrolyte, etc.). An accurate and more generic simulation model of the hybrid system will allow energy management strategies to be tested and properly tuned via simulation, to ensure the fulfilment of the aircraft electrical network requirements.

Project objectives

The objectives of this project are:

- to design and model the fuel cell hybrid emergency power system for a MEA. The model parameters must be easily deduced from specifications or from simple experiments;
- to test and compare the performance of common energy management strategies;
- to develop an experimental test bench for validation purpose.

The main challenges are as follows:

a. The estimation of model parameters from specifications or experiments: most manufacturers provide few meaningful data, fully dependent on operating conditions;

b. The identification of existing EMS from the literature: require an extensive review;

c. Test bench development security: there exist severe guidelines for the H_2 supply system safety;

d. Software development for control and monitoring: most drivers for device communication and tasks synchronization are not provided by manufacturers.

Contributions

The main contributions of this work are as follows:

a. A validated performance comparison of common EMS strategies for an aircraft emergency system based on fuel cell, with criteria that include the overall efficiency and life cycle of the whole system. The latter is measured using a new approach based on wavelet transform of each energy source instantaneous power;

b. The design and validation of a new optimal EMS strategy based on maximizing the instantaneous energy of the batteries/supercapacitors. The strategy performs slightly better than the existing real time equivalent consumption minimization based strategies, in terms of efficiency and fuel economy.

3 Journal and 2 conference papers have been submitted for review, they include:

[1] **Souleman Motapon**, L-A Dessaint, Kamal Al-Haddad, "A comparative study of energy management schemes for a fuel cell hybrid emergency power system of More Electric Aircraft", IEEE Transactions on industrial electronics, 2012 (Accepted).

[2] **Souleman Motapon**, L-A Dessaint, Sylvain Morel, "H2 consumption minimization based energy management strategy for a fuel cell hybrid emergency power system of More Electric Aircraft", Journal of Power Sources, 2012 (Under review).

[3] **Souleman Njoya Motapon**, Olivier Tremblay, Louis-A. Dessaint, "Development of a Generic Fuel Cell Model: Application to a Fuel Cell Vehicle Simulation", International Journal of Power Electronics, 2012, (Accepted).

[4] **Souleman Njoya M.**, Olivier Tremblay and Louis-A Dessaint, “A generic fuel cell model for the simulation of fuel cell power systems”, IEEE Power & Energy Society 2009 General Meeting Proceedings (Published).

[5] **Souleman Njoya M.**, Olivier Tremblay and Louis-A Dessaint,“A generic fuel cell model for the simulation of fuel cell vehicles”, IEEE 2009 Vehicle Power and Propulsion Conference (Published).

Thesis outline

This thesis is organized as follows:

Chapter 1: Literature review

This chapter presents a literature survey of energy management schemes for fuel cell hybrid systems and mention existing comparative studies of their performances.

Chapter 2: Design of the hybrid power system

This chapter describes the design procedure of the hybrid power system and select all the components (fuel cell, batteries, supercapacitors and power converters) based on a typical emergency load profile. Also state-of-the-art topologies are evaluated (in terms of efficiency, weight and cost) and the hybrid power system architecture is selected.

Chapter 3: Modelling of the hybrid power system

Chapter 3 presents the modelling approach of the hybrid power system after a brief review of the literature. The model parameters are obtained from specification and simple experimental tests. The model performance are compared with experiments to confirm the validity of the developed models.

Chapter 4: Design of the energy management schemes

In this chapter, the most common energy management schemes are implemented for performance comparison. A new scheme based on cost function optimization is proposed and an off-line optimization based scheme is developed for comparison purpose. The chapter also evaluates the performance of each energy management scheme through simulations. The criteria for comparison are the fuel consumption, the batteries/supercapacitors state of charge and the overall efficiency.

Chapter 5: Experimental validation

Here, the test bench is briefly described and the schemes are implemented in the real system using LabVIEW real time software. The results are compared to simulations and the performance of each scheme is validated. Beside the criteria considered in the simulation, the impact of each EMS on the life cycle of the hybrid power system is studied.

Conclusion

The final section concludes with a synopsis of the thesis and identifies topics for further studies.

CHAPTER 1

LITERATURE REVIEW

Over the last decade, the interest of transportation industries to develop efficient and environmentally friendly tractions systems have made fuel cell vehicles a reality. In these vehicles the fuel cell system is usually assisted by batteries or supercapacitors, for fast starting and acceleration as well as for regenerative braking. A lot of work has been done on developing fuel efficient energy management strategies for these vehicles, which can also be applied to fuel cell hybrid system of more electric aircraft. This chapter presents different energy management schemes reported in the literature and mention comparative studies that have been done to evaluate their performances.

1.1 State–of–the–art energy management schemes

Different energy management strategies for fuel cell hybrid power systems have been reported in the literature. The use of state machine control is a simple and well-known rule based strategy (Fernandez *et al.* (2010)) , (Fernandez *et al.* (2011)), (Attaianese *et al.* (2012)), (Yang *et al.* (2012)), each EMS rule or state is defined based on heuristic or empiric past experience. Therefore, the performance of this strategy depends on how well the designer is familiar with the operation of each component in the system. Figure 1.1 shows a summary of this approach, implemented on a fuel cell vehicle. As shown the fuel reference power is obtained based on the conditions (battery SOC and load power), the states as well as the speed of the vehicle. The fuel cell operates in load following (LF) or load levelling (LL) mode and an hysteresis controller is used for switching between each state.

Another widely used strategy is the rule based fuzzy logic energy management technique, where the power distribution is accomplished through membership functions and the set of if-then rules (Li *et al.* (2012)), (Caux *et al.* (2010)), (Zandi *et al.* (2011)), (Chun-Yan and Guo-Ping (2009)). This strategy can be easily tuned to achieve optimal operation and its performance is less sensitive to measurement imprecision and component variations. Nevertheless,

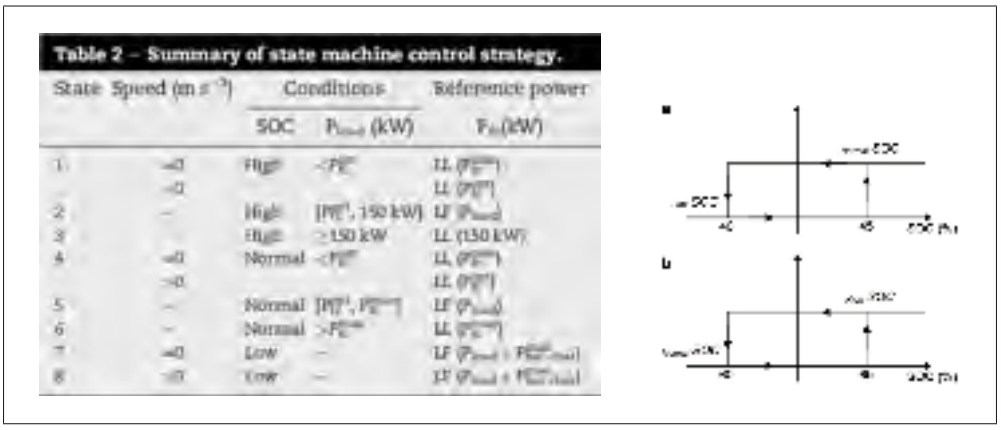

Figure 1.1 State machine control strategy
Adapted from Fernandez *et al.* (2010)

the heart of the fuzzy logics controller resides on the if-then rules which require the knowledge and past experience of an expert. Figure 1.2 shows an example where the fuel cell reference power is obtained using this approach. The membership functions of the battery state of energy (SOE), load power and fuel cell power are first defined. Then a set of rules (or the inference matrix table) is created. The outcome is the fuzzy logic control surface which gives the fuel cell reference power in terms of the battery SOE and load power.

Recently, energy management based on classical PI controllers have been proposed. This strategy is based on the control of the main performance parameters such as the battery state of charge (SOC), the supercapacitor voltage or DC bus voltage using PI controllers (Thounthong *et al.* (2011)), (Wong *et al.* (2011)), (Wilhelm *et al.* (2010)), (Thounthong and Raël (2009)). The knowledge of an expert is not necessary and the PI controllers can be easily tuned on-line for better tracking. The load power is distributed in such a way to allow the fuel cell system to provide the steady state load demand. Figure 1.3 depicts this strategy, where the fuel cell current is obtained using 2 PI loops (an outer loop for the battery SOC and an inner loop for the battery current).

The frequency decoupling strategy ensures the fuel cell provide low frequency demand while the other energy sources deal with high frequency demand (Zhang *et al.* (2008)), (Ates *et al.*

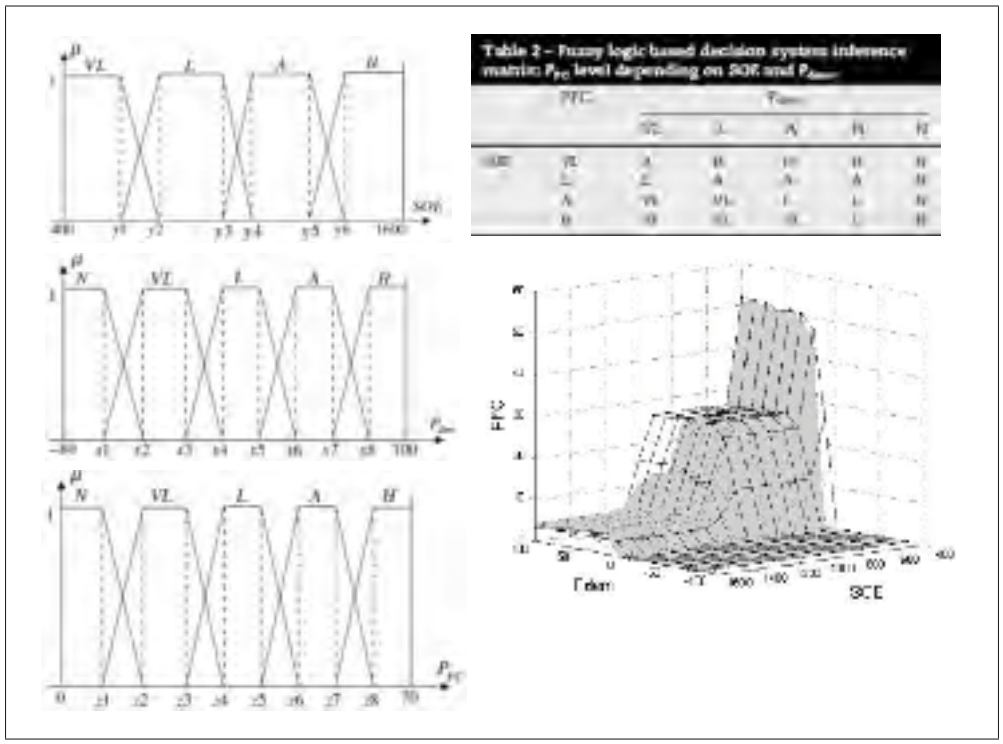

Figure 1.2 Rule based fuzzy logic strategy
Adapted from Caux *et al.* (2010)

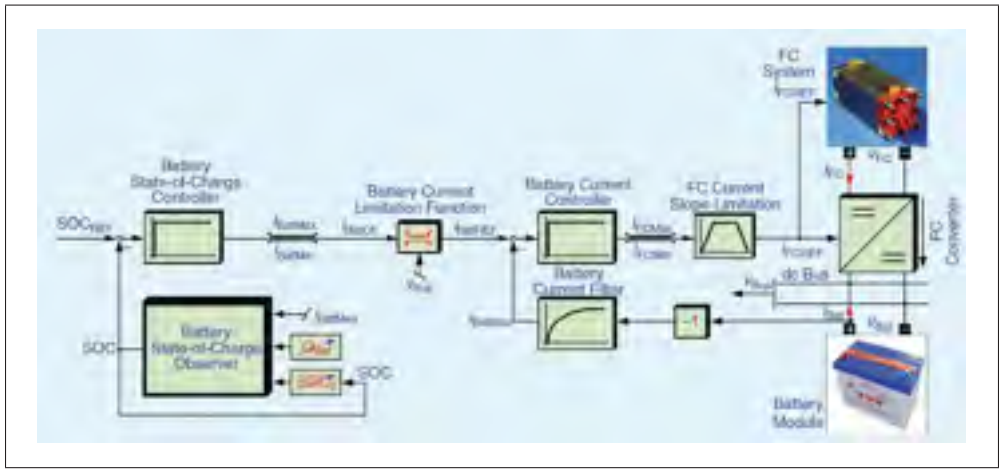

Figure 1.3 Classical PI control strategy
Adapted from Thounthong and Raël (2009)

(2010)), (Vural *et al.* (2010)), (Erdinc *et al.* (2009)), (Garcia (2007)). This is achieved through the use of low pass-filters, wavelet or fast Fourier transforms (FFT) techniques. This strategy

improves the life time of the fuel cell system as the dynamic stress on the fuel supply system is prevented. Here, the fuel cell system supplies a nearly constant mean load power while the other energy sources discharge or recharge when the load power is above or below its mean value respectively. This strategy is shown in Figure 1.4 where a three level wavelet transform is used to decompose the load power into low and high frequency components. Also a fuzzy logic controller is necessary for SOC control of the battery and supercapacitor.

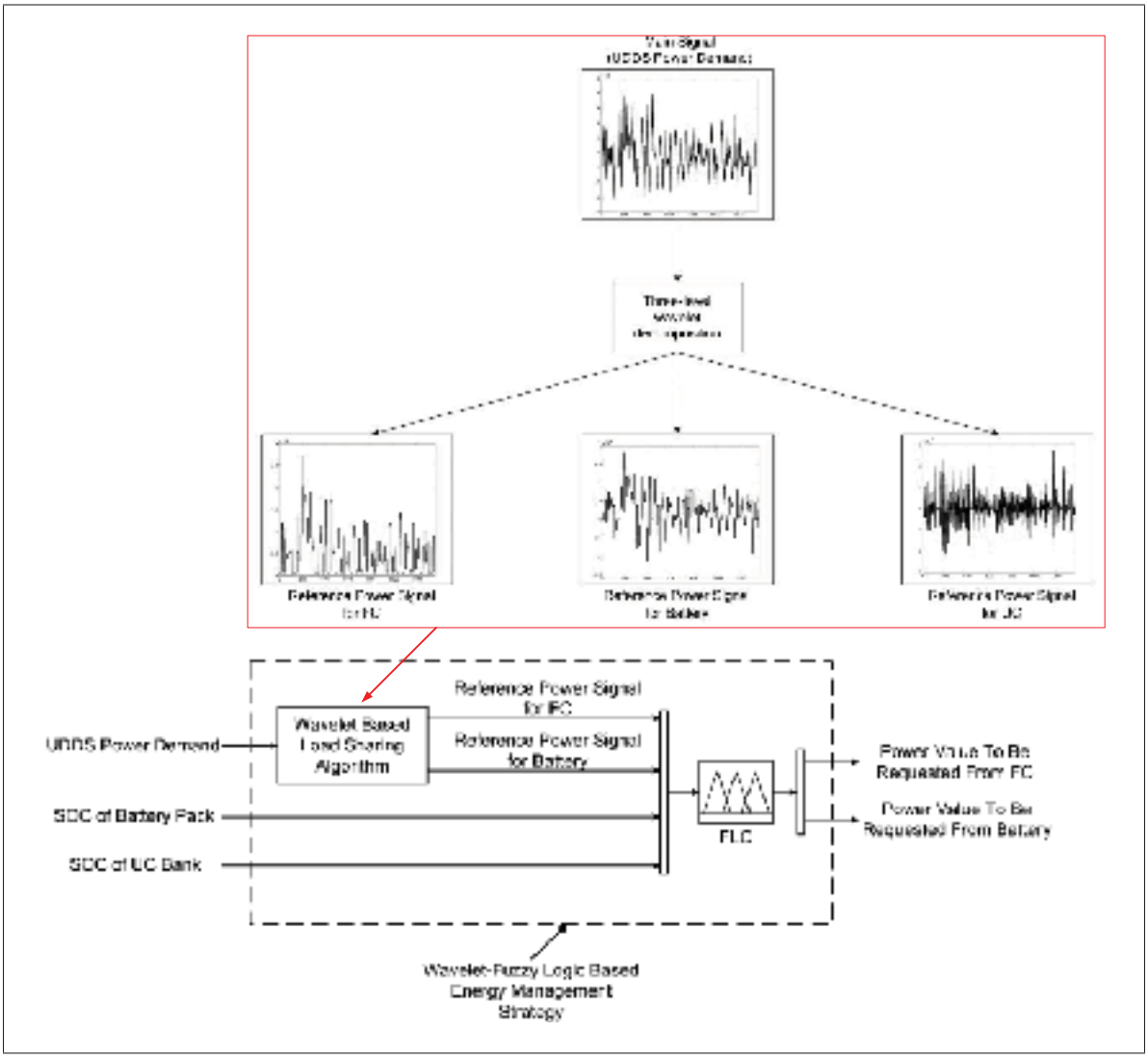

Figure 1.4 Frequency decoupling and fuzzy logic strategy
Adapted from Erdinc *et al.* (2009)

To ensure optimal operation of the fuel cell system for maximum fuel economy or maximum global efficiency, a cost function optimization strategy is used (Zheng *et al.* (2012)), (García *et al.* (2012)), (Torreglosa *et al.* (2011)), (Rodatz *et al.* (2005)), (Sciarretta *et al.* (2004)), (Liangfei *et al.* (2009)). The most common strategy for real time implementation is the equivalent fuel consumption minimization strategy (ECMS). The power distribution is determined from the minimization of an instantaneous cost function, which consists of the fuel consumption of the fuel cell system and the equivalent fuel consumption of the other energy sources. The principle of the ECMS is shown in Figure 1.5 for a fuel cell/supercapacitor hybrid vehicle.

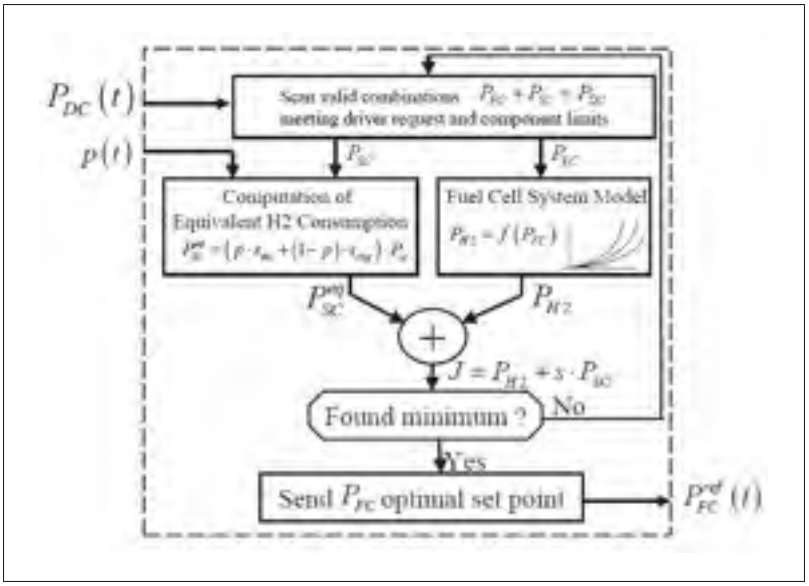

Figure 1.5 The ECMS strategy
Adapted from Rodatz *et al.* (2005)

The equivalent fuel consumption is obtained in terms of the charge and discharge equivalence factors (s_{chg} and s_{dis}), the probability ($p(t)$) of the supercapacitor energy being positive and the supercapacitor power. The fuel cell power reference is the optimal fuel cell power which minimize the summation of the equivalent fuel consumption and the fuel consumed by the fuel cell.

Other real time energy management strategies for fuel cell hybrid power systems have also been reported. They include strategies based on model predictive control (MPC) (Bordons *et al.* (2010)), (Kermani *et al.* (2012)), stochastic dynamic programming (Min-Joong and Huei (2007)), neural networks (Moreno *et al.* (2006)), (Ates *et al.* (2010)) adaptive optimal control (Lin and Zheng (2011)) and H_∞ control (Pisu and Rizzoni (2007)). These strategies are very complex and require large computations which could potentially affect the response time of the energy management system. Hence, they are not appropriate when the control is designed based on standard microprocessors based solutions. Table 1.1 shows a summary of the pros and cons of the existing energy management schemes (Erdinc and Uzunoglu (2010)).

Table 1.1 Brief comparison of EMS approaches
Adapted from Erdinc and Uzunoglu (2010)

Energy management approach	Advantages	Disadvantages
Fuzzy logic	Independent from a overall mathematical model, adaptation to more complex structures, computational efficiency, robustness to modelling uncertainties	Dependent on designer's knowledge about the problem
Neural networks	Provides adequate and quick responses to new information	Requires a training procedure
Global optimization approaches	Guarantees the optimum solution	Not applicable to real-time applications, not computationally efficient
Local optimization approaches	Applicable to real-time applications	Does not guarantee the optimum solution, not computationally efficient
Frequency decoupling techniques	Applicable to real-time applications, provides a load sharing suitable for the individual characteristics of hybrid sources	Does not include the control of multi-objectives if used alone
Linear controllers (PI, etc.)	Easy to implement in embedded systems and realize with analog circuits	Not suitable for multi-objective control of complex systems
Adaptive, robust, etc. based approaches	Applicable to systems with uncertainties	Robust approach is static and does not adapt to measurement and implementation variations, both techniques require a detailed mathematical knowledge on system

1.2 Comparative study of energy management schemes

There exist few comparative studies of energy management scheme in the literature. But these studies are mainly theoretical with less emphasis on the experimental validation. In (Valero *et al.* (2006)), the classical PI control, the state machine control (based on the fuel cell global efficiency) and an optimization based approach similar to the ECMS are compared through simulations. The study were performed for a tramway, an urban bus and a office building. For

all cases, the optimization approach performed better in terms of fuel consumption, follow by the state machine control strategy. No experiments were done to validate these results. Also other criteria such as the overall system efficiency and life cycle of the component were not considered.

In (Pisu and Rizzoni (2007)), the state machine control is considered together with a modified ECMS, where the equivalence factor is updated on-line based on the predicted load profile (adaptive ECMS or A-ECMS) as shown in Figure 1.6. Also an H_∞ control was implemented. In this case too, the simulation of each EMS performance was done using urban drive cycles and the A-ECMS was found to be the best strategy in term of fuel consumption. No impact of the EMS on component life cycle and efficiency was considered. Moreover, there was no experimental validation.

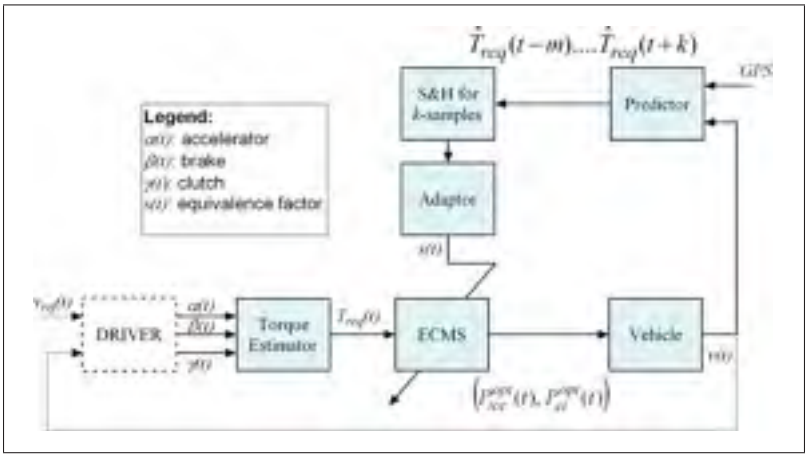

Figure 1.6 Adaptive ECMS
Adapted from Pisu and Rizzoni (2007)

In (Fadel and Zhou (2011)), the study included the classical PI control, the rule based fuzzy logic and the ECMS strategies. Here, the main criteria for performance comparison were the fuel efficiency and battery cycling. The latter was evaluated by counting the number of battery charge and discharge cycle. Here too, the ECMS was found to perform better, follow by the fuzzy logic approach in terms of fuel consumption. But at the expense of larger battery cycles compared to the classical PI control strategy. The work was validated experimentally, but using

a programmable DC source to represent the fuel cell system. Moreover, a urban vehicle drive cycle was also used to derive the load profile.

In all these studies, the performances of the EMS were evaluated using typical tramway or urban vehicle drive cycles. The load demand seen by the fuel cell hybrid system is regenerative and has low fluctuations compared to MEA emergency load profile. As an example, Figure 1.7 illustrates the differences between a typical urban tramway drive cycle and a MEA emergency system load demands. As shown, for the MEA, the demand is highly fluctuating, which will generates more stress on the energy sources. The EMS must be designed accordingly to ensure a long life cycle of the hybrid power system as well as high overall efficiency. To determine, which existing EMS is more suitable for MEA emergency load profile, their performances have to be tested and compared using a real test bench setup, which is the goal of this study.

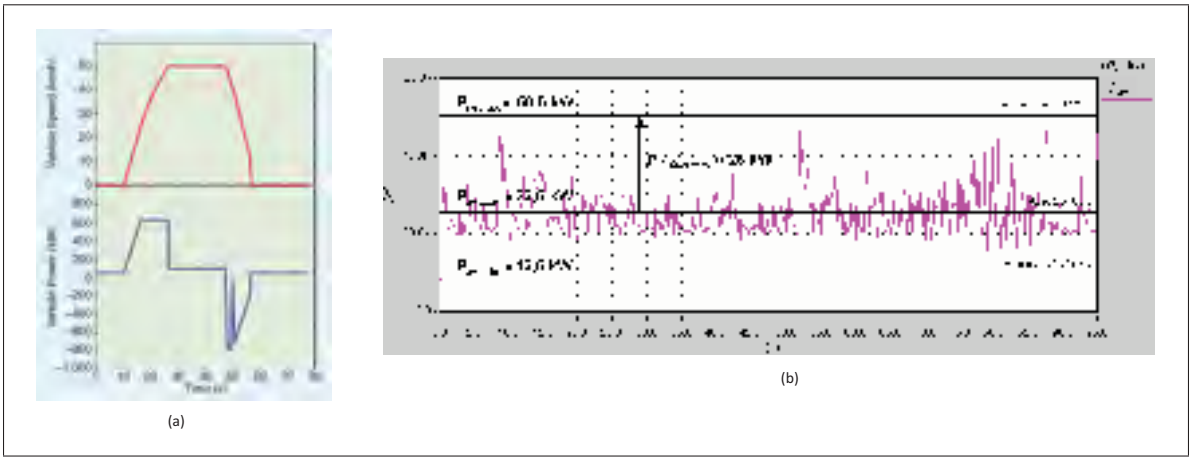

Figure 1.7 Load profiles:
(a) European urban tramway (b) MEA emergency power system
Adapted from Thounthong and Raël (2009) and Langlois (2006)

The next chapter starts with the design of the fuel cell hybrid emergency system of a MEA. Afterwards, the performances of common energy management schemes are simulated and validated experimentally.

CHAPTER 2

DESIGN OF THE FUEL CELL HYBRID POWER SYSTEM

2.1 Introduction

This chapter describes the design approach of the hybrid power system. At first, the power and energy requirement for the hybrid system are derived using a typical emergency load profile of a MEA. Then, the topology of the hybrid power system is selected based on criteria such as weight, cost and efficiency. The fuel cell system is designed to meet the average load power, while batteries and supercapacitors provide extra power during transients and overload. This does not only reduce the size of the fuel cell system, but also improve the dynamic response of hybrid power system. As for the battery and supercapacitor systems, they are designed based on the extra power required, the total mission duration and the topology of hybrid power system.

2.2 Hybrid power system power/energy requirement

The hybrid power system is designed based on the power and energy requirement for a typical emergency landing scenario. In this study, a representative emergency landing cycle (Figure 2.1) provided by Bombardier Aerospace, is considered for all analysis. More details including the description of events are provided in Appendix 4. As described in Figure-A IV-2 , when the main generators are lost, the critical loads are supplied by the avionic and APU batteries for about 20 s, before the RAT kicks in. When the RAT is ON, the batteries are turned OFF and the heater/brake monitoring units (HBMUs) are turned ON for preparation for landing. Afterwards, the flap/slat and landing gear are put into motion. As the aircraft gets close to landing, its speed reduces below 147 Knots and the RAT goes off-line. Then, within 20 s, the RAT tries to get back on-line when the critical load is reduced. Later, at aircraft touch down, the RAT power reduces to zero.

This 5 min. landing cycle shows the behavior of the RAT during an emergency situation. However in real life, the aircraft may need the RAT to operate not just during approach and

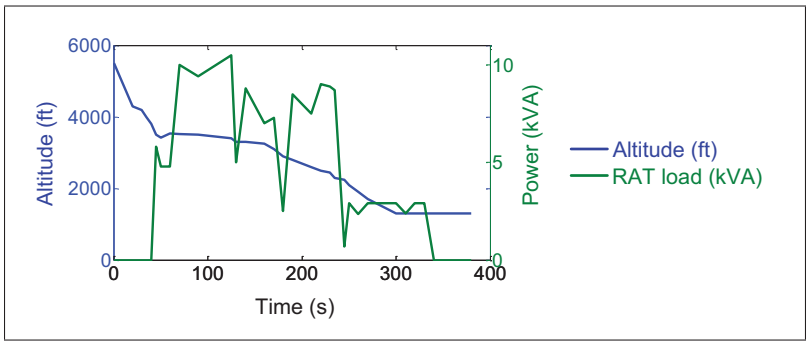

Figure 2.1 Rat power during a 5 min. emergency landing

landing, but also during cruising as well. That is, the RAT may need to provide power for 0.5 - 4 h. For this study, the component of the hybrid power system are selected assuming the emergency system will operate for half an hour. The emergency load profile considered is derived from Figure 2.1 for a 30 min. flight scenario as shown in Figure 2.2.

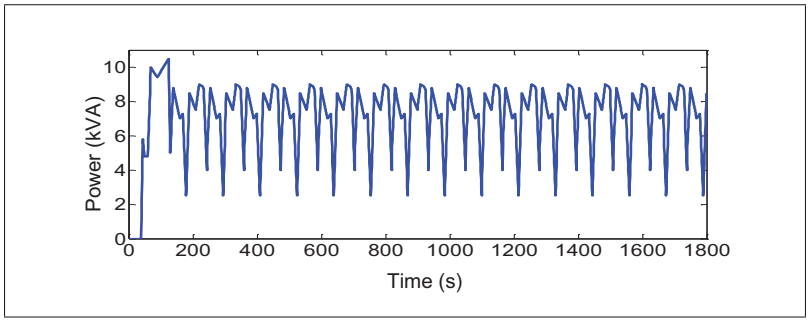

Figure 2.2 Rat power during a 30 min. emergency landing

From Figure 2.2, the emergency load characteristics can be derived as shown in Table 2.1.

Table 2.1 Emergency load characteristics

LOAD CHARACTERISTICS	Value
Average power	7.5 kW
Peak power	10.5 kW (1 min.)
Maximum continuous power	8.5 kW (30 min.)
Transient peak power	10 kW (5 sec.)
Load voltage	115/200 V AC, 400 Hz

The fuel cell system is designed to meet the average demand while the batteries and supercapacitors are designed to assist the latter during continuous and transient peak demand respectively. Assuming the transfer (DC/DC converter) efficiency between the energy source and the load is around 80% and a typical DOD (depth-of-discharge) of 30% for the batteries and supercapacitors, the power and energy requirements of the hybrid system are derived and summarized in Table 2.2.

Table 2.2 Hybrid system power/energy requirement

COMPONENTS	POWER/ENERGY REQUIREMENT
FUEL CELL SYSTEM	
Continuous power	7.5/0.8 = 9.375 kW
BATTERY MODULES	
Maximum power	(10.5 - 7.5)/0.8 = 3.75 kW
Usable energy	((8.5 - 7.5)/0.8 x 30 x 60)/3.6 = 625 Wh
DOD	30%
Total energy content	625/0.3 = 2.08 kWh
SUPERCAPACITOR MODULES	
Peak power	10 kW
Usable energy	(10000 x 5)/3600 = 19 Wh
DOD	30%
Total energy content	21 Wh

From Table 2.2, the fuel cell system has to have a nominal power of 10 kW, whereas the battery system should be able to provide 4 kW of power with a total energy content of 2 kWh. As for the supercapacitor system, it should be able to provide 10 kW of power with a total energy content of 21 Wh. With the power and energy requirement for each energy device known, the next step is to select the topology of the power system.

2.3 Hybrid power system topology and component selection

To ensure the hybrid power system is designed for low cost, weight and high efficiency, its topology must be properly selected. Several topologies have been reported in the literature. From (Erdinc and Uzunoglu (2010)), (Ramos-Paja *et al.* (2010)), (Sripakagorn and Limwuthigraijirat (2009)), (Bauman and Kazerani (2008)) and (Piyush *et al.* (2012)), different topologies are obtained and summarized in Figure 2.3. As shown, the energy devices can be connected

to the DC/AC converter directly (direct integration), or through one, two or three DC/DC converters. The peak power requirement and the direction of power flow of each converter are also depicted. The DC/AC converter input voltage is determined from the line voltage (200 V) and is equal to 270 V DC, which is typical for aircraft applications.

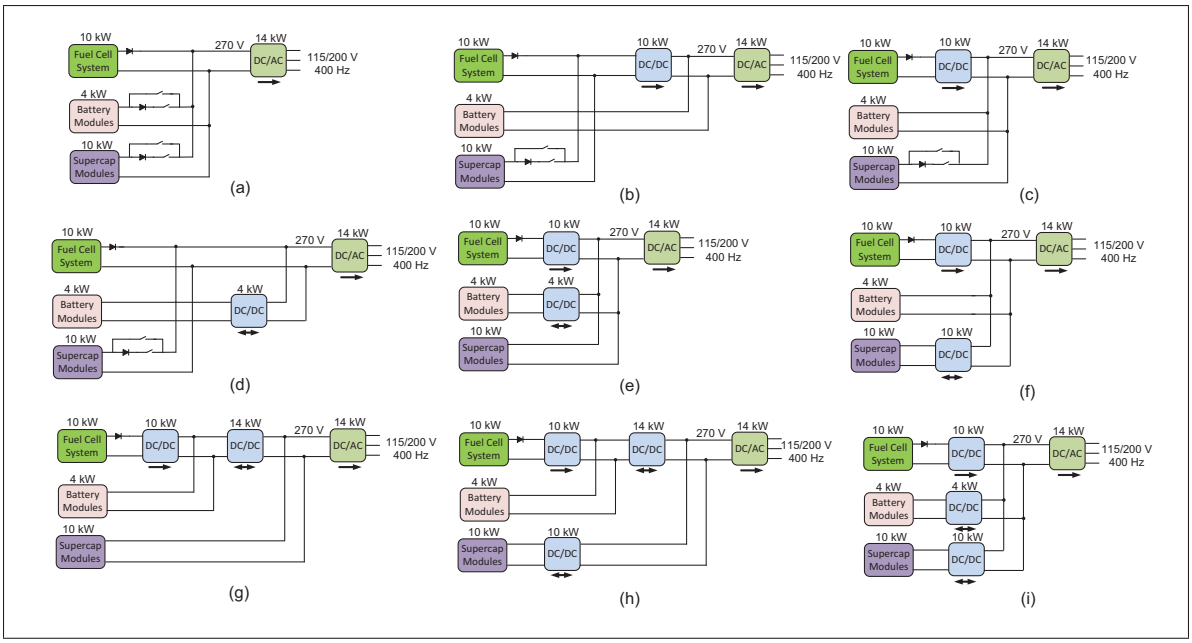

Figure 2.3 Hybrid power system topologies

Even thought the power density factor of the whole system is not considered in this study (as the primary goal is to investigate the performance of different energy management strategies). The topology is selected using off-the-shelf components and the main criteria are: the system efficiency, weight, cost and power controllability. The power controllability or ability to control the output power of each device allows the application of an effective energy management strategy.

The direct integration topology (Figure 2.3 (a)) together with topologies with one DC/DC converter (Figure 2.3 (b), (c) and (d)) are more attractive as better efficiency can be achieved. However, each energy device output power cannot be effectively controlled. Which is the reason this study will focus only on topologies from Figure 2.3 (e) - (i).

As a baseline for comparison, a 12.8 V, 40 Ah, Li-ion battery module from Valence and a 48.6 V, 88 F, supercapacitor module from NESSCAP are selected. These modules are considered for the analysis as data such as cost and weight were readily available. A 2 kW DC/DC converter module from TRACO POWER is also considered to evaluate the weight and cost of the DC/DC converters used in the topologies. The specifications of the baseline devices are summarised in Table 2.3. For analysis, the input voltage of the DC/DC converter is chosen to be 48 V for all topologies.

Table 2.3 Baseline devices specifications

BASELINE DEVICES	**Value**
Valence Li-ion U1-12XP battery module	
Nominal voltage	12.8 V
Nominal capacity	40 Ah
Max. Continuous current	80 A
Weight	6.5 kg
Cost	US$885
NESSCAP EMHSR-0088C0-048R0S supercapacitor module	
Rated voltage, Vr	48.6 V
Rated capacitance	88 F
Stored energy at Vr	28.9 Wh
Weight	11.5 kg
Cost	US$1,200
TRACO TSC 4738 isolated DC/DC converter	
Input voltage	40-58.4 V DC
Output	270 V DC, 7 A
Efficiency	85%
Weight	8 kg
Cost	US$3,483

For each energy source, the required number of module in series is determined from its operating voltage (which can be either 48 V or 270 V). Then, the module capacity or capacitance can be found using the energy requirement of Table 2.2. According to the specifications provided by Valence and NESSCAP for different battery and supercapacitor modules (Figures-A III-1 and III-2), the module weight tends to vary linearly with the capacity or capacitance as shown in Figure 2.4. As for the module cost, it is usually proportional to the capacity or capacitance

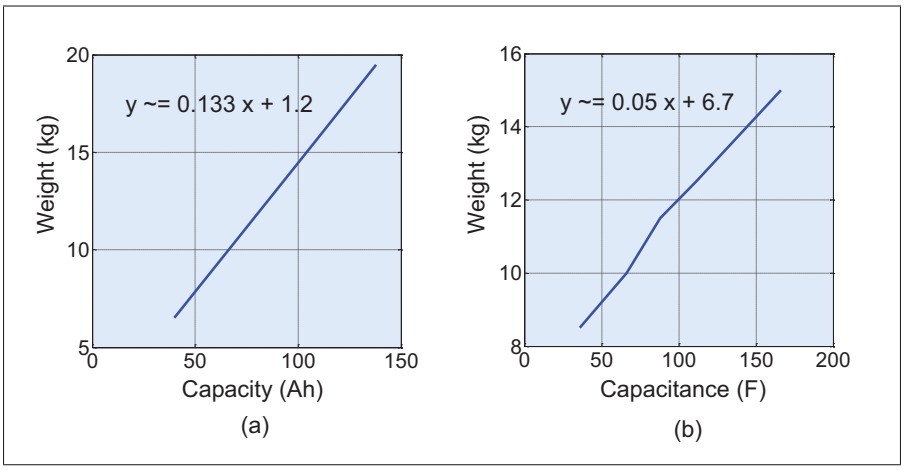

Figure 2.4 Module weight vs. capacity/capacitance: (a) Valence battery module (b) NESSCAP supercapacitor module

Battery system \ Topology	(e)	(f)	(g)	(h)	(i)
Voltage (V)	48	270	48	48	48
Module in series	4	21	4	4	4
Capacity (Ah)*	43	7.7	43	43	43
Weight (kg)**	27.67	46.7	27.67	27.67	27.67
Cost (US$)	3806	3578	3098	3098	3098

*Capacity=2080/Voltage
**Weight estimated using Figure 2.4 (a)

(a)

Supercap. system \ Topology	(e)	(f)	(g)	(h)	(i)
Voltage (V)	270	48	270	48	48
Module in series	6	1	6	1	1
Capacitance (F)*	13	65.6	13	65.6	65.6
Weight (kg)**	44.1	9.98	44.1	9.98	9.98
Cost (US$)	1063	895	1063	895	895

*Capacitance=2 x 21 x 3600 x (# of module in series)/Voltage^2
**Weight estimated using Figure 2.4 (b)

(b)

DC/DC converters \ Topology	(e)	(f)	(g)	(h)	(i)
Weight (kg)	56	80	96	136	96
Cost (US$)	24381	34830	41796	59211	41796

(c)

Figure 2.5 Component characteristics for each topology: (a) Battery system (b) Supercapacitor system and (c) DC/DC converters

and can be easily estimated. For the DC/DC converters, the cost and weight are assumed to be proportional to the output power.

Figure 2.5 summarises the results obtained with each topology, with regards to the weight and cost of each component.

Finally, the overall results considering all selection criteria are summarized in Table 2.4. As shown, the topology in Figure 2.3 (e) is more attractive in terms of efficiency, weight and cost. This topology is therefore selected for the study.

Table 2.4 Overall characteristics of each configuration

Criteria \ Topology	(e)	(f)	(g)	(h)	(i)
Efficiency (%)	**91.2**	87.5	86	79.7	85
Weight (kg)	**127.7**	136.7	167.7	173.65	133.65
Cost (US$)	**29250**	39803	45957	63204	45789
Power controllability	yes	yes	yes	yes	yes

Efficiency calculation example

Topology (g)

$\text{Efficiency} = P_{load}/(P_{fc}+P_{batt}+P_{cap})$

$= (10 \times 0.85 + 4) \times 0.85 + 10/(10+4+10)$

$= 0.86$

Based on the selected topology, the following devices are selected for the hybrid power system:

- fuel cell system: 1 x 12.5 kW PEM (proton exchange membrane) fuel cell power module (FCPM) from Hydrogenics, with a nominal power of 10 kW. The main specifications are shown in Table 2.5. More details are provided in Appendix 3;
- battery system: 4 x 12.8 V, 40 Ah, Li-ion battery module from Valence. These modules are connected in series;
- supercapacitor system: 6 x 48.6 V, 88 F, supercapacitor module from NESSCAP. These modules are also connected in series.

With this selection, the usable energy of the battery system and supercapacitor system is 615 Wh and 21.6 Wh respectively (assuming a minimum DC bus voltage of 250 V), which is close to the hybrid system energy requirement.

As for the converters, they are selected to match with the power requirement and consist of:

- fuel cell system DC/DC converter: 5 x 2.5 kW, 48 Vin, 270 Vout, DC/DC converter module from TRACO POWER. The modules are classical push-pull boost converters

Table 2.5 Fuel cell system specifications

PARAMETERS	Value
Model	HyPM® HD 12
Peak power	12.5 kW
Operating voltage	30-60 V
Peak efficiency	53%
Hydrogen consumption	≤ 190 l/min
Max. air flow rate	≤ 1300 l/min
Heat rejection	≤ 20 kW
H_2O collected	≤ 24 l/min
Time from Idle to Rated power	5 sec

with transformer isolation. These modules are output voltage controlled with input current limitation. That is, two control signals (output voltage and maximum input current) must be provided;

- battery system DC/DC boost converter: 2 x 2 kW, 48 Vin, 270 Vout, DC/DC converter module from TRACO POWER used for battery discharge. Similar to the fuel cell boost converter, these modules require two control signals (output voltage and maximum input current);
- battery system DC/DC buck converter: 1 x 1.2 kW, 270 Vin, 48 Vout, DC/DC converter module from TRACO POWER used for battery charge. This module also require two control signals (output voltage and maximum output current). For this study, two converters are used with the battery system due to time constraint as a bidirectional DC/DC converter was not readily available;
- inverter system: 3 x 5 kVA, 270 Vin, 200 VAC, 400 Hz, DC/AC converter module from TRACO POWER. These modules are all transformer isolated and does not require any control signals.

The complete system schematic is shown in Figure 2.6. As shown, the fuel cell and battery energies are controlled through their associated DC/DC converters using a National Instrument embedded controller (NI PXI-8108). The control signals for the DC/DC converters are determined from the energy management system (implemented in the controller). A battery management system is used to protect the battery system from overcharge, overtemperature

and overdischarge. A protecting resistor is also used to prevent the overvoltage of the supercapacitor system or the inverter input voltage. The emergency load profile is generated using a DC/AC programmable load. Chapter 5 describes in more details all the components.

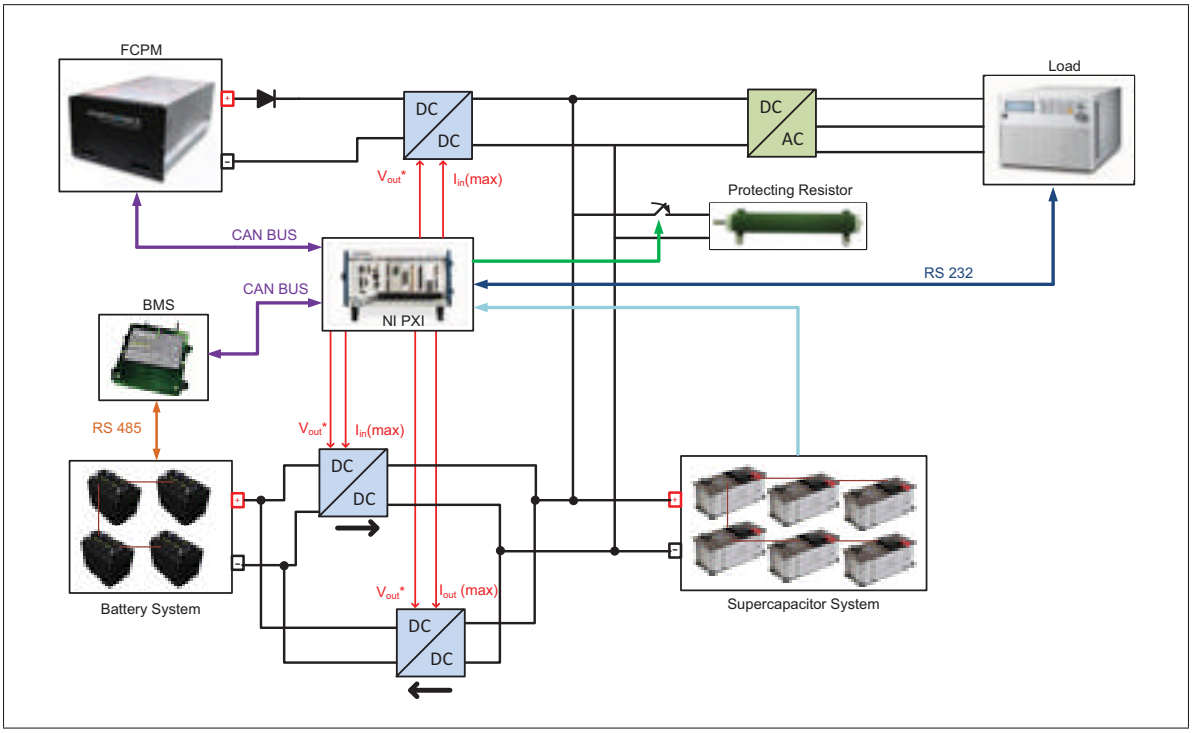

Figure 2.6 Overall system schematic of the hybrid power system

2.4 Conclusion

This chapter presented the approach used to design and select the components of the hybrid power system. The energy and power requirements were derived from a typical emergency landing load profile of a MEA. Based on the efficiency, cost, weight and power controllability, the topology of the hybrid system was selected. This topology consisted of using a separate DC/DC converter for the fuel cell and battery systems and connecting the supercapacitor system directly on the DC bus.

The components of the hybrid system were selected based on the characteristics of the selected topology and the emergency load profile. The specifications of these components were also provided. The hybrid power system consists of a 12.5 kW Fuel cell power module, with a nominal power of 10 kW along with 4x 12.8 V, 40 Ah battery module and 6x 48.6 V, 88 F supercapacitor module. Also, the DC/DC and DC/AC converters were selected appropriately to match with the power requirement.

The next chapter deals with the modelling of all the components and describes them in more details.

CHAPTER 3

MODELLING OF THE HYBRID POWER SYSTEM

3.1 Introduction

In the study of energy management strategies, it is necessary to develop a full and quite accurate model of each subsystem components. This helps in understanding the system behavior and allows an effective design of the energy management system. This chapter describes the modelling approach of each component of the hybrid power system. The fuel cell, batteries and supercapacitors are modelled using generic models available in Simulink/SimPowerSystems, where the model parameters are obtained from specifications or simple experiments. The power converters are modelled using average-value equivalent models, which greatly reduce the simulation time. As for the emergency load model, a 3-phase controlled current source is used to represent the emergency load profile provided by Bombardier.

3.2 Modelling of the fuel cell, batteries and supercapacitors

There exist different types of models for fuel cell, battery and supercapacitor in the literature. They can be classified into three categories: empiric or experimental model, electric-circuit based model and electro-chemical model.

Empiric models represent the behavior of fuel cell or batteries using curve fitting or lookup tables; obtained from the experimental polarization curves or charge/discharge characteristics. Examples of such models can be found in (Yongping *et al.* (2010)), (Kim *et al.* (2005)), (O'Hayre *et al.* (2005)), (Larminie and Dicks (2003)) and (Cadar *et al.* (2009)). The main drawback with this modelling approach are the fact that the system dynamics are not modelled.

The electric-circuit based models use electrical elements to represent the characteristics of the fuel cell, batteries or supercapacitors. Typically, the open circuit voltage, resistive losses and the capacity are modelled using an ideal voltage source, resistor and capacitor respectively. The model parameters are determined experimentally through current interrupt, impedance spec-

troscopy or frequency response tests. Examples of such model can be found in (Ferrero *et al.* (2012)), (Runtz and Lyster (2005)), (Buller *et al.* (2002)), (Zubieta and Bonert (2002)), (Sungwoo *et al.* (2012)) and (Xiaosong *et al.* (2012)). These models represent electrical dynamics effectively, however their validity is strongly dependent on the operating or test conditions.

Electro-chemical models involve modelling of each subcomponent (electrode, electrolyte, reactant diffusion and catalyst layers, heat transfer) using complex chemical and thermodynamics equations. These models are mainly used for design purpose and are able to represent the dynamics and the impact of the operating conditions. Examples of such models can be found in (Boaventura *et al.* (2011)), (Mingruo *et al.* (2004)), (Thanh-Son *et al.* (2012)), (Graham *et al.* (2012)) and (Parashuram *et al.* (2000)). The main drawback of these models is the fact that they require in-depth parameters such as cell area, thickness of electrode, porosity or volume of electrolyte, which are not easily available.

Recently, an interesting approach of modelling of fuel cell, batteries and supercapacitors has been proposed by the authors in (Njoya *et al.* (2009)), (Tremblay and Dessaint (2009)) and (Blaud, Pierre Clément (2012)). This approach combines the characteristics of curve fitting and electric-circuit based models, but with the advantage that the model parameters can be obtained from fairly simple experiments or directly from manufacturer's specifications. The proposed models have been included in Simulink/SimPowerSystems (SPS) and are publicly available (SimPowerSystems (2012)). For the analysis of power sharing or energy management strategies, these models are judged to be sufficient and adequate as dynamics are well represented. These models are selected for this study and are described briefly in the following sections.

3.2.1 The fuel cell model

PEMFCs (proton exchange membrane fuel cell) are the most common fuel cell used for automotive application. This is mainly due to the fact that they operate at low temperature (-20 - 100^{o}C), therefore a fast starting from idle to full load operation can be achieved.

Figure 3.1 shows the fuel cell operating principle along with electro-chemical reactions at electrodes (Xin *et al.* (2005)). The cell is fed with the fuel (hydrogen) and air at the anode and cathode respectively. Hydrogen gas, with the help of a catalyst, separates into electrons and hydrogen ions. These ions flow to the cathode through the electrolyte while the electrons flow through an external circuit (electricity is generated). At the cathode, the hydrogen ions combine with oxygen (from air) to form water.

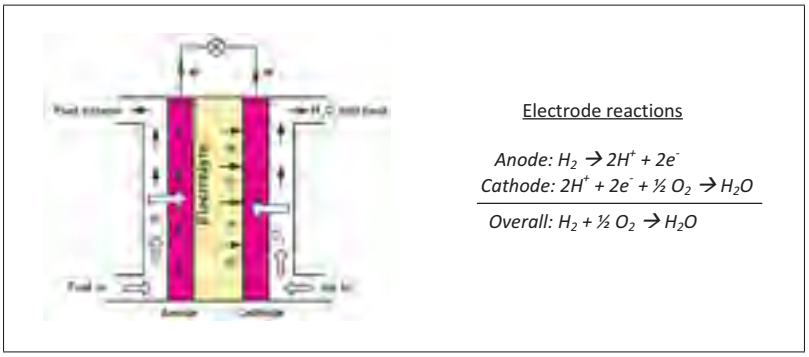

Figure 3.1 Fuel cell operation and electrode reactions
Adapted from Xin *et al.* (2005)

The fuel cell model available in SPS is a modified version of the approach proposed in (Padulles *et al.* (2000)) and (Pukrushpan *et al.* (2002)), where the dynamics of the reactant flow inside the electrode are neglected. Hence, the determination of partial pressure of reactants are decoupled from the electrode characteristics (such as anode/cathode volume and orifice area).

The thermodynamic voltage generated from the electro-chemical reactions is given by the Nernst equation as follows:

$$E_n = 1.229 + (T - 298) \cdot \frac{-44.43}{2F} + \frac{RT}{2F} ln \left(P_{H_2} P_{O_2}^{\frac{1}{2}} \right) \tag{3.1}$$

Where P_{H_2} and P_{O_2} are the hydrogen and oxygen partial pressures (atm), T is the operating temperature (K), F and R are Faraday constant (A s/mol) and ideal gas constant (J/mol K).

The partial pressures are determined in terms of the utilizations (rate of conversions) of reactants as follows (Njoya *et al.* (2009)):

$$P_{H_2} = (1 - Uf_{H_2})x\%P_{fuel} \tag{3.2}$$

$$P_{O_2} = (1 - Uf_{O_2})y\%P_{air} \tag{3.3}$$

Where Uf_{H_2} and Uf_{O_2} are the hydrogen and oxygen utilizations, P_{fuel} and P_{air} are the supply pressures of fuel and air (atm), x and y are the percentages of hydrogen and oxygen in the fuel and air ($\%$).

The reactant utilizations are expressed in terms of inlet flow rates and cell current as follows:

$$Uf_{H_2} = \frac{60000RTi_{fc}}{2FP_{fuel}V_{fuel}x\%} \tag{3.4}$$

$$Uf_{O_2} = \frac{60000RTi_{fc}}{4FP_{air}V_{air}y\%} \tag{3.5}$$

Where V_{fuel} and V_{air} are the fuel and air flow rates (l/min), i_{fc} is the cell current (A).

The cell open circuit voltage is proportional to the thermodynamic voltage and is given by:

$$E_{oc} = K_c \cdot E_n \tag{3.6}$$

Where K_c is the voltage constant.

Considering the losses due to reaction kinetics (activation losses) and species transport (resistive and diffusion losses), the cell output voltage is given by:

$$V = E_{oc} - V_{act} - V_r \tag{3.7}$$

With,

$$V_{act} = Aln\left(\frac{i_{fc}}{i_0}\right) \cdot \frac{1}{sT_d/3+1} \tag{3.8}$$

$$V_r = r_{ohm} \cdot i_{fc} \tag{3.9}$$

Where *A* is the Tafel slope (V), i_0 is the exchange current (A), r_{ohm} is the cell resistance (ohm), T_d is the cell settling time to a current step. It is assumed the cell voltage will exhibit a delay approximately equal to 3 times the time constant during a sudden change in cell current.

The exchange current and the Tafel slope are given by:

$$i_0 = \frac{2Fk(P_{H_2} + P_{O_2})}{Rh} \cdot exp(\frac{-\Delta G}{RT}) \tag{3.10}$$

$$A = \frac{RT}{2\alpha F} \tag{3.11}$$

Where ΔG is the activation energy barrier (J), α is the charge transfer coefficient, k and h are the Boltzmann's constant (J/K) and the Planck's constant (J s) respectively.

The fuel cell stack (multiple cells in series) output voltage is derived knowing the number of cells as:

$$V_{fc} = N \cdot V \tag{3.12}$$

Where N is the number of cells.

The effect of oxygen starvation (due to the air compressor/blower delay) on the stack voltage is modelled using the parameters for flow dynamics such as the peak utilization ($Uf_{O_2(peak)}$) and the corresponding voltage undershoot (V_u). The lack of oxygen inside the cell causes its utilization to increase above the nominal value and the Nernst voltage is modified as follows:

$$E_n = 1.229 + (T - 298) \cdot \frac{-44.43}{2F} + \frac{RT}{2F} ln\left(P_{H_2} P_{O_2}^{\frac{1}{2}}\right) - K_u(Uf_{O_2} - Uf_{O_2 nom}) \tag{3.13}$$

Where Uf_{O2nom} is the nominal oxygen utilization (%) and K_u is the voltage undershoot constant.

Figure 3.2 shows the model of the fuel cell stack implemented in SPS. Block A represents Equations 3.4 and 3.5. Block B represents Equations 3.1-3.3, 3.6 and 3.13. Block C represents Equation 3.11.

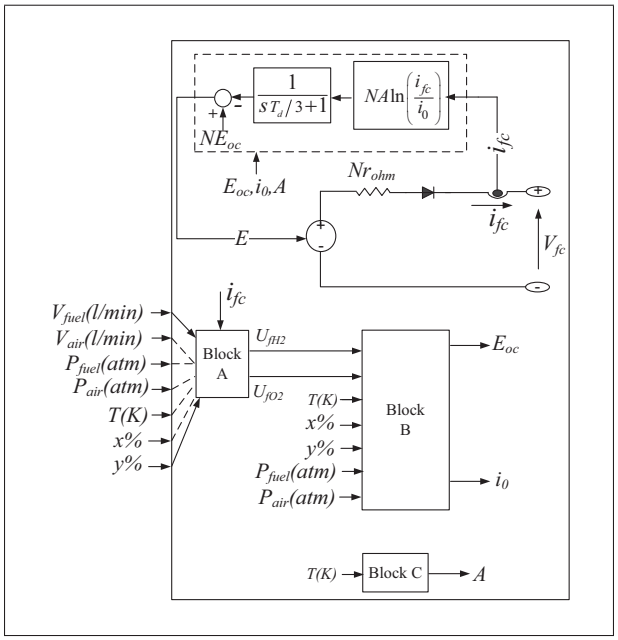

Figure 3.2 Fuel cell stack model

The parameters required by the model are obtained from a polarization curve test on the fuel Cell Power Module (FCPM). As shown in Figure 3.3, the FCPM electrical output is directly connected to a programmable load, which operates in DC mode, constant current demands. As soon as the FCPM is in RUN mode and no load, current steps are applied following the fuel cell maximum allowable current (this maximum current is provided by the FCPM controller, to avoid oxygen starvation). The FCPM and the programmable load are controlled from the NI PXI-8108 through CAN bus and RS 232 respectively. The parameters obtained are shown in Figure 3.4.

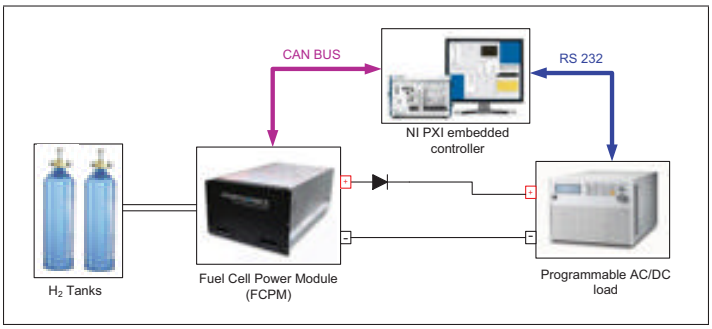

Figure 3.3 Fuel cell experimental setup

FUEL CELL MODEL INPUT PARAMETERS	
Voltage @ 0 A and 1 A [V_0 (V), V_1 (V)]	[52.5, 52.46]
Nominal operating point [Inom (A), Vnom (V)]	[250, 41.15]
Maximum operating point [Iend (A), Vend (V)]	[320, 39.2]
Number of cells	65
Nominal stack efficiency (%)	50
Operating temperature (Celcius)	45
Nominal Air flow rate (lpm)	732
Nominal supply pressure [Fuel (bar), Air (bar)]	[1.16, 1]
Nominal composition (%) [H2, O2, H2O (Air)]	[99.95, 21, 1]
Fuel cell voltage response time (sec)	1
Peak O2 utilization (%)	60
Voltage undershoot (V) @ Peak O2 utilization	2

(a)

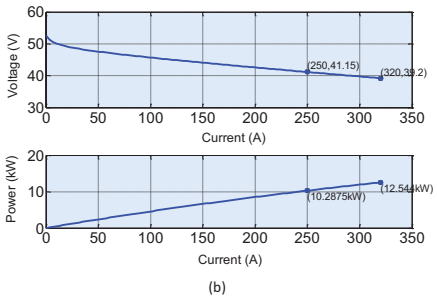

(b)

Figure 3.4 Fuel cell stack model: (a) input parameters (b) polarization curves

Figure 3.5 shows the simulation and test results (at nominal condition, $P_{fuel} = 1.16$ bar, $P_{air} = 1$ bar, $T = 45^{o}$C) along with the percentage error between the simulated and the real fuel cell output voltage.

It can be observed from Figure 3.5 that in the activation region (region with predominant activation losses), the steady state error is within $\pm$ 1% whereas the transient errors are within $\pm$ 4%. In the ohmic region (region with predominant resistive losses), the error is also within $\pm$ 1% for both transient and steady state conditions. This low error indicates the fuel cell system behavior is well represented by the model.

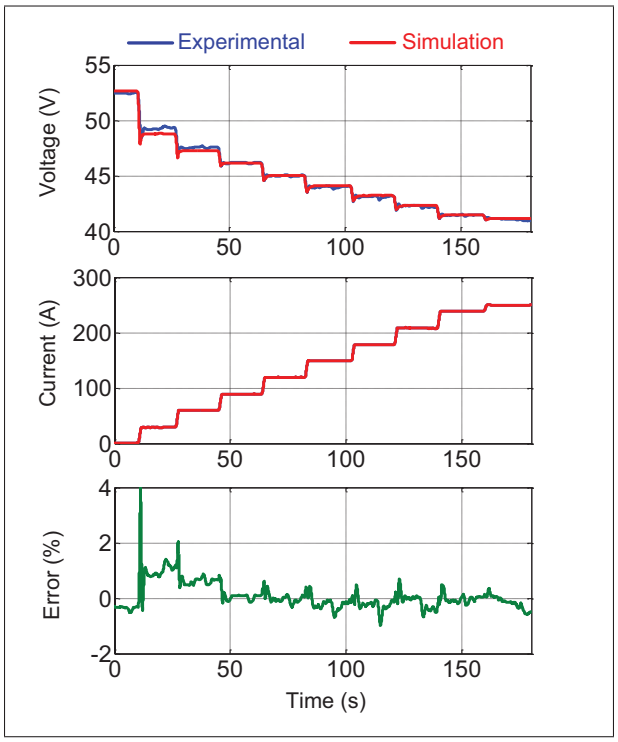

Figure 3.5 Fuel cell model validation: simulation vs. experimental results of the 12.5 kW fuel Cell Power Module (FCPM), $P_{fuel} = 1.16$ bar, $P_{air} = 1$ bar and $T = 45^{o}$C

3.2.2 The battery model

The batteries considered for this study are of type Li-ion as they have proven to exhibit a high energy density and efficiency compared to other battery types (such as lead-acid, NiCd or NiMH) (García *et al.* (2012)). This makes them more attractive for automotive or aircraft applications.

The battery model available in SPS is based on a modified Shepherd curve fitting model (Shepherd C. M (1963)), where an additional term (voltage polarization) is added to the battery discharge voltage expression to better represent the effect of the battery SOC on the battery performance. Also, to ensure the simulation stability, a filtered battery current instead of the actual battery current, is used to account for the polarization resistance. For a Li-ion battery

type, the battery voltage is expressed as (Tremblay and Dessaint (2009)):

$$V_{batt} = E_0 - K\frac{Q}{Q - it} \cdot it - R_b \cdot i + A_b exp(-B \cdot it) - K\frac{Q}{Q - it} \cdot i^* \tag{3.14}$$

Where E_0 is the battery constant voltage (V), K is the polarization constant $V/(Ah)$, Q is the battery capacity (Ah), i^* is the filtered battery current (A), it is the actual battery charge (Ah), A_b is the exponential zone amplitude (V), B is the exponential zone time constant inverse $(Ah)^{-1}$ and R_b is the battery internal resistance (Ω).

The term $K\frac{Q}{Q-it}it$ from Equation 3.14 is referred as polarization voltage while the term $K\frac{Q}{Q-it}$ is the polarization resistance (Pol_{res}).

During charging, the battery voltage increases abruptly after being fully charged, this behavior is represented by modifying the polarization resistance (only during charging) as follows:

$$Pol_{res} = K\frac{Q}{it - 0.1 \cdot Q} \tag{3.15}$$

Figure 3.6 shows the model of the battery implemented in SPS.
The parameters required by the model are obtained from the battery specifications and from the battery dynamic test for better accuracy. Figure 3.7 shows the experimental setup. The superpacitors are used to discharge and recharge the batteries. The charge and discharge currents are controlled through DC/DC converters. Figure 3.8 shows the model input parameters along with simulated discharge curves for the battery system (4x 12.8 V, 40 Ah, Valence Li-ion battery module).

Figure 3.9 shows the simulation and test results along with the percentage error between the simulated and the real battery system output voltage. As shown, the obtained error is less than $\pm$ 2% for both transient and steady state conditions, which confirms the validity of the battery model.

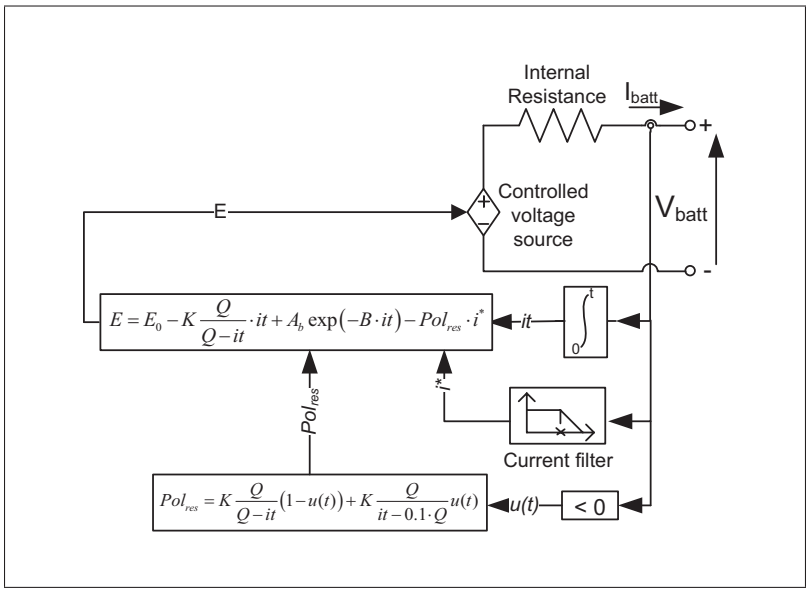

Figure 3.6 Li-ion battery model

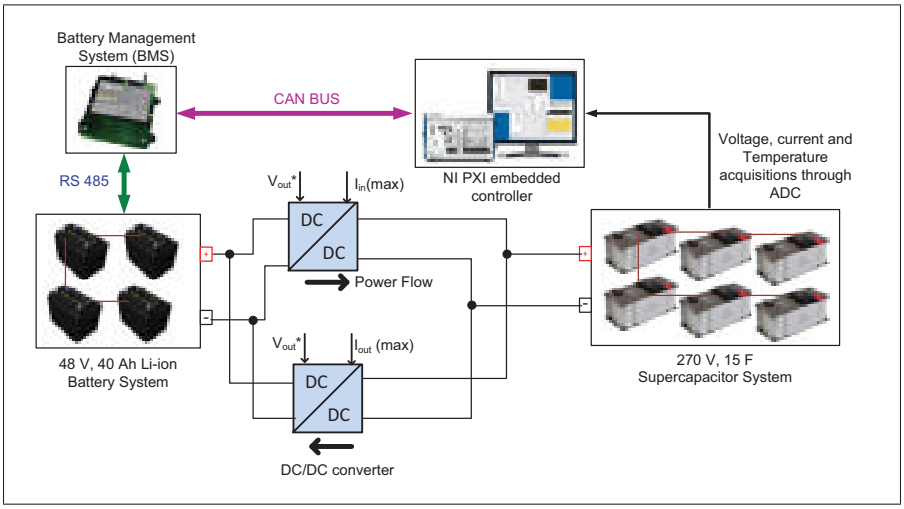

Figure 3.7 Battery and supercapacitor systems experimental setup

3.2.3 The supercapacitor model

Supercapacitors also known as Electric Double Layer Capacitors (EDLCs) are similar to conventional electrostatic or electrolytic capacitors, with the advantage that they can store or release more energy due to their high capacitance.

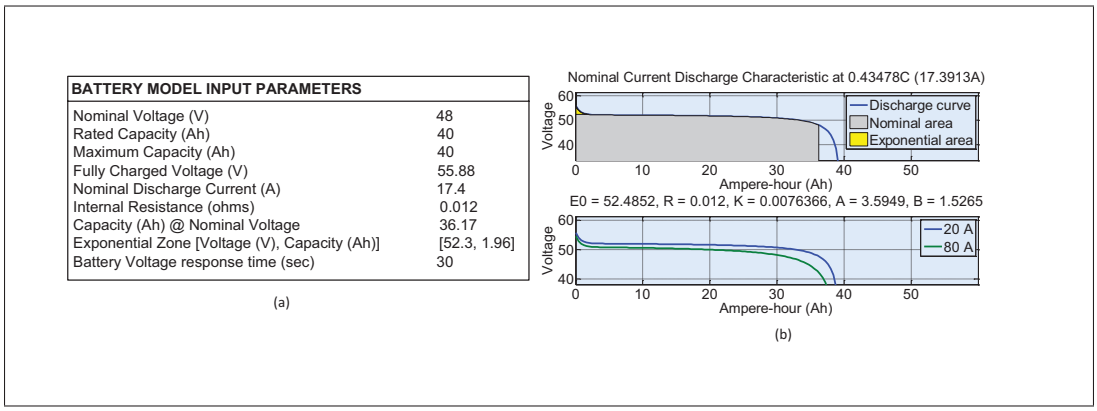

Figure 3.8 Battery model: (a) input parameters (b) discharge curves

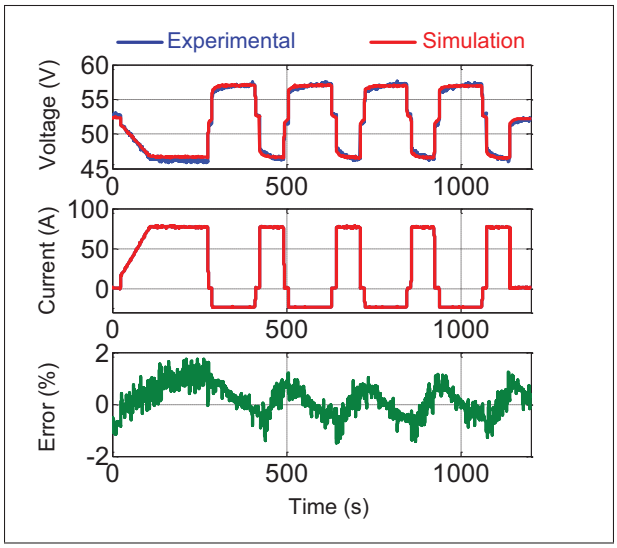

Figure 3.9 Battery model validation: simulation vs. experimental results, charge-discharge of the 48 V, 40 Ah, Li-ion battery system

The EDLC cell consists of two porous carbon electrodes immersed in an electrolyte. When a voltage is applied across the electrodes, the negative ions from the electrolyte migrate to the positive electrode while the positive ions migrate to the negative electrode. Two layers of charges are then formed (one layer at each electrode), hence the name double layer capacitor. Due to the porosity of the electrode and the extremely small distance separating the charges, a high capacitance is achieved.

The supercapacitor model implemented in SPS is based on the Stern model, which combines the Helmholtz and Gouy-Chapman models (Oldham (2008)), (Amokrane (1996)). The capacitance of a EDLC cell is expressed as (Blaud, Pierre Clément (2012)):

$$C = \left[\frac{1}{C_H} + \frac{1}{C_{GC}}\right]^{-1} \tag{3.16}$$

With,

$$C_H = \frac{N_e \epsilon \epsilon_0 A_i}{d} \tag{3.17}$$

$$C_{GC} = \frac{F Q_c}{2 N_e R T} \sinh\left(\frac{Q_c}{N_e^2 A_i \sqrt{8 R T \epsilon \epsilon_0 c}}\right) \tag{3.18}$$

Where C_H and C_{GC} are the Helmholtz and Gouy-Chapman capacitance (F) respectively, N_e is the number of electrode layers, ϵ and ϵ_0 are the permittivities (F/m) of the electrolyte material and free space respectively. A_i is the inter-facial area between electrodes and electrolyte (m^2), d is the Helmholtz layer length (or molecular radius) (m), Q_c is the cell electric charge (C) and c is the molar concentration (mol m^{-3}).

For a supercapacitor module of N_s cells in series and N_p cells in parallel, the total capacitance is given by:

$$C_T = \frac{N_p}{N_s} \cdot C \tag{3.19}$$

The supercapacitor output voltage is expressed considering resistive losses as:

$$V_{SC} = \frac{Q_T}{C_T} - R_{SC} \cdot i_{SC} \tag{3.20}$$

With,

$$Q_T = N_p Q_c = \int i_{SC} dt \tag{3.21}$$

Where Q_T is the total electric charge (C), R_{SC} is the supercapacitor module resistance (Ω) and i_{SC} is the supercapacitor module current (A).

Figure 3.10 shows the model of the supercapacitor implemented in SPS.

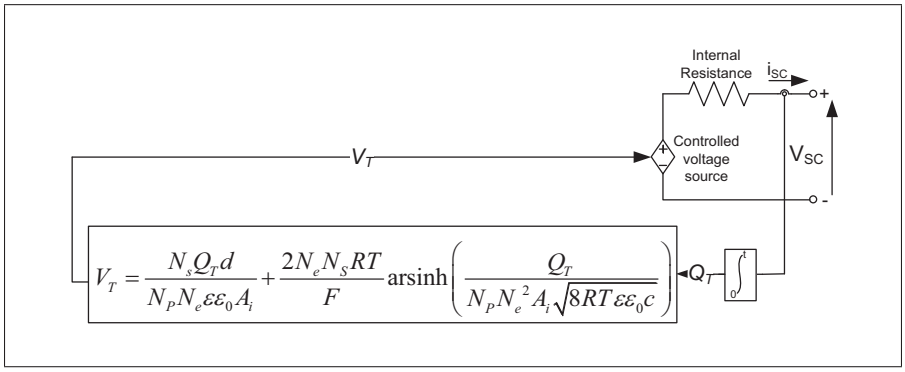

Figure 3.10 Supercapacitor model

The critical parameters required by the model are obtained from the specifications (rated capacitance and voltage, DC resistance), while the number of electrodes layers and the molecular radius are adjusted for better accuracy based on experiments. Figure 3.11 shows the model input parameters along with simulated discharge curves for the supercapacitor system (6x 48.6 V, 88 F, NESSCAP supercapacitor module).

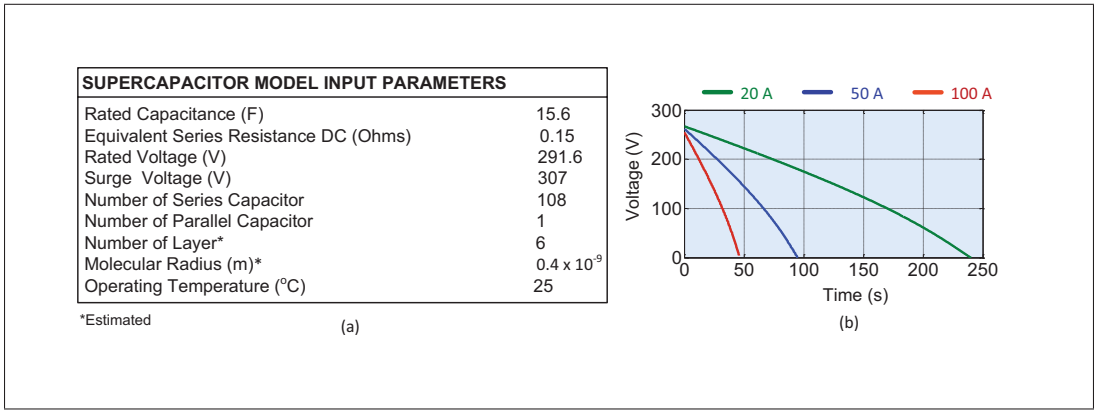

Figure 3.11 Supercapacitor model: (a) input parameters (b) discharge curves

Figure 3.12 shows the simulation and test results along with the percentage error between the simulated and the real supercapacitor system output voltage. It can be observed that the accuracy of the model is within $\pm$ 2%, which is sufficient for the study.

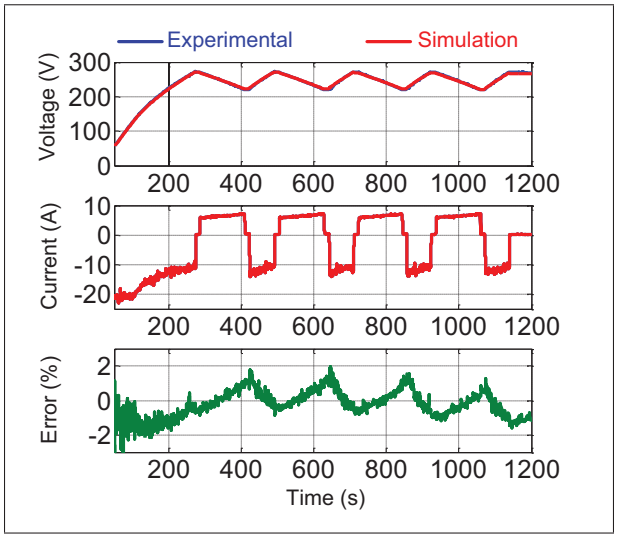

Figure 3.12 Supercapacitor model validation: simulation vs. experimental results, charge-discharge of the 270 V, 15 F supercapacitor system

3.3 Modelling of power converters

The fuel cell and battery system are connected to the DC/AC converter through DC/DC converters. This allows voltage conversion (from low voltage to high voltage and vice-versa) as well as full control of the fuel cell/battery current and DC bus voltage. The fuel cell system DC/DC converter is of boost type while the battery system converters consist of one DC/DC converter of boost type (discharge converter) and one DC/DC converter of buck type (charge converter). Preferably, to improve the system power density, a bidirectional DC/DC converter should be used for charging and discharging of the battery system.

DC/DC converters can be represented by two types of models which are: the switching models and the average-value models. The switching models are mainly used for design purpose and to investigate types of pulse-width-modulated (PWM) schemes with regards to switching harmonics and losses. These models require small sampling time to observe all the switch-

ing actions, which makes the simulation very time consuming. The average-value models on the contrary are less time consuming as the switches are replaced by controlled voltage/current sources. The switching harmonics are not represented, but all the converter dynamics are maintained, which makes these models attractive as larger sampling time can be used.

3.3.1 The DC-DC boost converter model and control

The DC/DC boost converter is modelled assuming a standard transformer-less DC/DC boost converter topology. Its circuit is shown in Figure 3.13 along with its averaged-value switch model equivalent. The switch is essentially replaced by a voltage controlled source at the low voltage side and a current controlled source at the high voltage side.

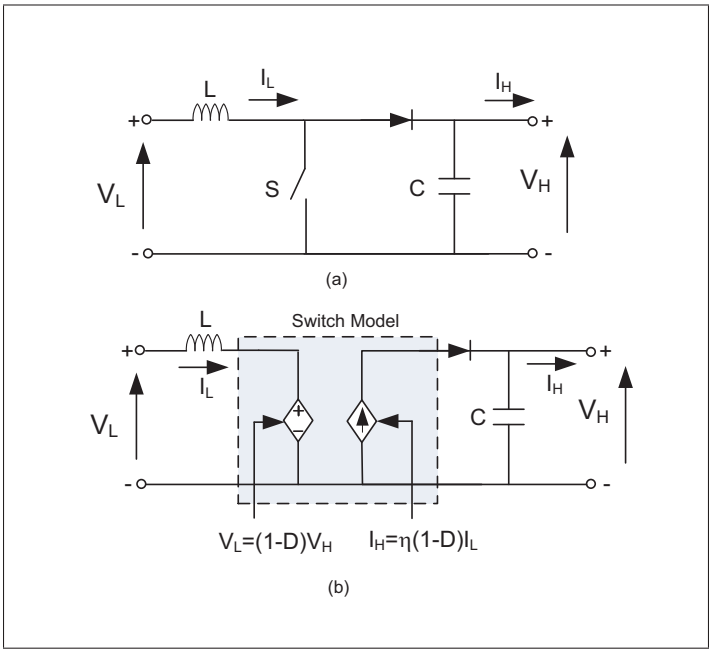

Figure 3.13 DC/DC boost converter: (a) standard transformer-less boost circuit (b) equivalent averaged-value switch model

The voltage and current of these controlled sources are obtained from steady state equations as (Erickson and Maksimovic (2001)):

$$V_L = (1 - D)\, V_H \tag{3.22}$$

$$I_H = \eta\,(1 - D)\,I_L \tag{3.23}$$

Where V_L and I_L are the voltage and current at the low voltage side respectively. V_H and I_H are the voltage and current at the high voltage side respectively. D is the duty cycle and η is the converter efficiency.

The converter efficiency is assumed to be constant below 10 % full load and then varies linearly with load afterwards. That is, the efficiency is expressed above 10 % full load as:

$$\eta = aI_H + b \tag{3.24}$$

Where the constants a and b are derived knowing the efficiency at rated and 10 % full load.

The converter is a regulated output voltage with input current limitation. These features are included to the model by adding an outer voltage control and inner current control loops as shown in Figure 3.14. The design of these control loops is made considering the average-value model dynamic behavior.

3.3.1.1 Design of boost converter control loops

From the average-value equivalent circuit (Figure 3.13 (b)), the inductor (L) voltage and capacitor (C) current can be expressed as:

$$L\frac{dI_L}{dt} = V_L - (1 - D)\,V_H \tag{3.25}$$

$$C\frac{dV_C}{dt} = \eta\,(1 - D)\,I_L - I_H \tag{3.26}$$

Which gives the inductor current and capacitor voltage in Laplace domain as:

$$I_L(s) = \frac{V_L - (1 - D)\,V_H}{Ls} \tag{3.27}$$

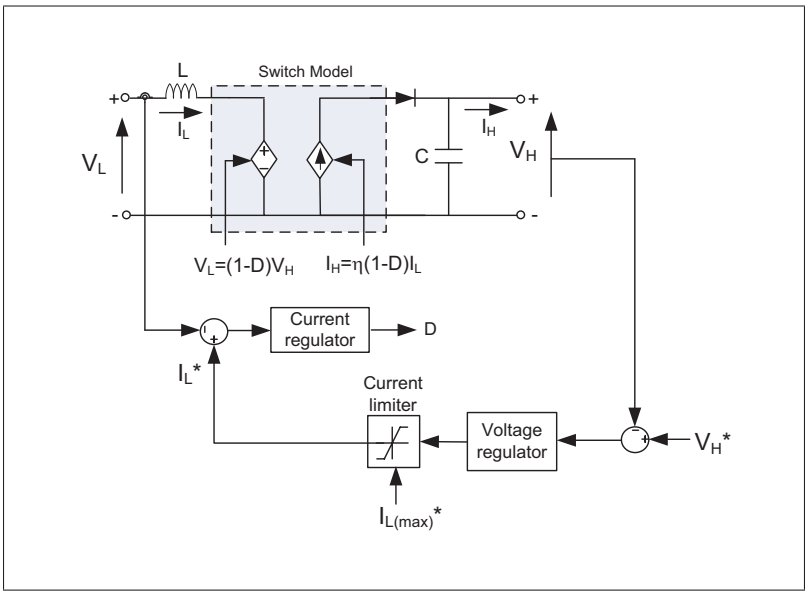

Figure 3.14 Control of the DC/DC boost converter

$$V_C(s) = V_H(s) = \frac{\eta\,(1-D)\,I_L - I_H}{Cs} \tag{3.28}$$

Using Equation 3.22, Equation 3.28 becomes:

$$V_C(s) = V_H(s) = \frac{\eta\left(\frac{V_L}{V_H}\right) I_L - I_H}{Cs} \tag{3.29}$$

The converter plants are reduced to first order transfer functions which can be controlled using simple PI regulators. This is shown in Figure 3.15.

The open loop transfer functions are given by:

$$H_i(s) = \frac{K_{pi}s + K_{ii}}{s} \cdot \frac{1}{Ls} \tag{3.30}$$

$$H_v(s) = \frac{K_{pvs} + K_{iv}}{s} \cdot \frac{1}{Cs} \tag{3.31}$$

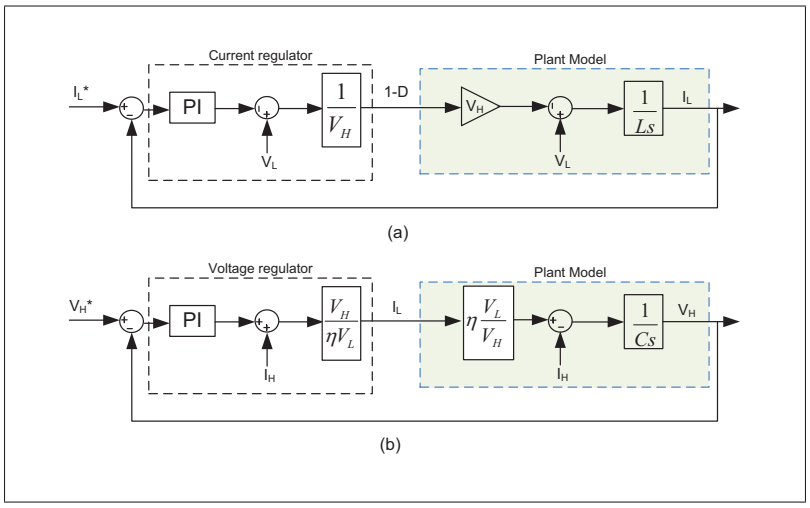

Figure 3.15 The DC/DC boost converter regulators:
(a) current regulator (b) voltage regulator

Where the proportional gains K_{pi}, K_{pv} and integral gains K_{ii}, K_{iv} are determined knowing the regulator response times as:

$$K_{pi} = 2\zeta\omega_{ni}L \tag{3.32}$$

$$K_{ii} = \omega_{ni}^2 L \tag{3.33}$$

$$K_{pv} = 2\zeta\omega_{nv}C \tag{3.34}$$

$$K_{iv} = \omega_{nv}^2 C \tag{3.35}$$

With,

$$\zeta\omega_{ni} = \frac{-ln\left[0.05\sqrt{1-\zeta^2}\right]}{T_{Ri}} \tag{3.36}$$

$$\zeta\omega_{nv} = \frac{-ln\left[0.05\sqrt{1-\zeta^2}\right]}{T_{Rv}} \tag{3.37}$$

Where ω_{ni} and ω_{nv} are the current and voltage controller bandwidth respectively, ζ is the damping coefficient and T_{Ri} and T_{Rv} are the current and voltage controller response times respectively. T_{Ri} is chosen to be one tenth of T_{Rv}.

The model parameters for the fuel cell converter and battery discharge converter are summarized in Figure 3.16. The efficiencies at 10% and 100 % full load are obtained from experiments along with the voltage regulator response time.

FUEL CELL BOOST CONVERTER MODEL INPUT PARAMETERS	
Full load current (A)	45
Efficiency @ 100% and 10% Full load (%) [n1, n2]	[85, 90]
Voltage regulator response time (s)	0.1
Load capacitance (F)	15.6

(a)

BATTERY BOOST CONVERTER MODEL INPUT PARAMETERS	
Full load current (A)	18
Efficiency @ 100% and 10% Full load (%) [n1, n2]	[80, 88]
Voltage regulator response time (s)	0.1
Load capacitance (F)	15.6

(b)

Figure 3.16 DC/DC converter model input parameters:
(a) fuel cell boost converter (b) battery boost converter

The performances of the DC/DC converter models are shown in Figure 3.17 for both the fuel cell and the battery system. As shown the boost converter models and the real converters have very close responses to load changes as well as during overload. The voltage is well regulated and the input current is well limited to its maximum reference current. For the fuel cell system, the slow response obtained both experimentally and in simulation is due to the current slope limitation (40 A/s) to deal with the problem of oxygen starvation.

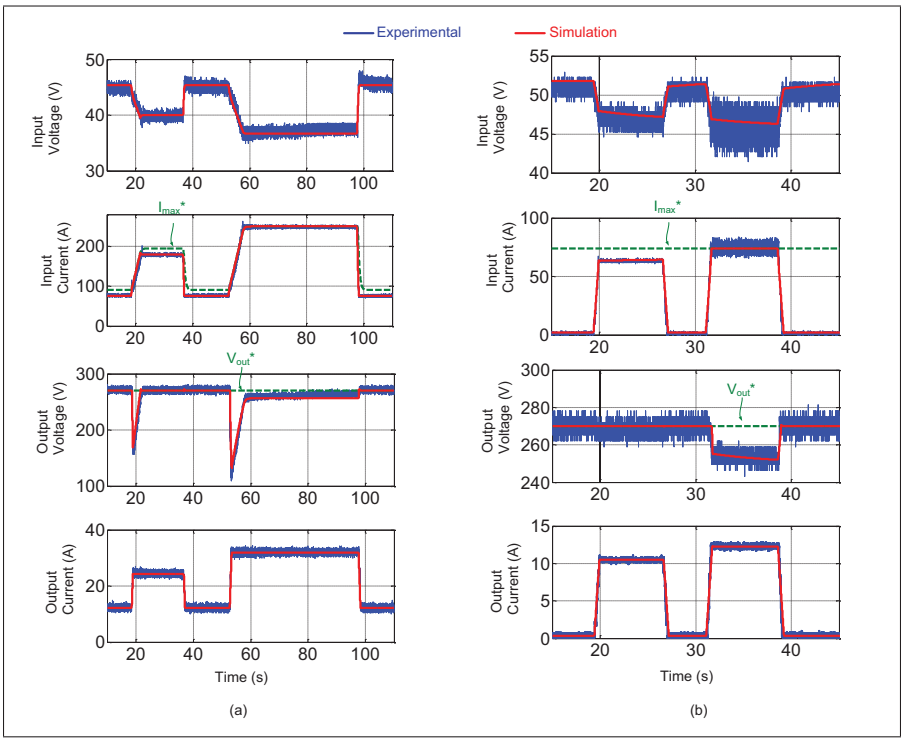

Figure 3.17 DC/DC boost converter validation:
(a) Fuel cell converter (b) Battery converter

3.3.2 The DC-DC buck converter model and control

Similar to the model of the DC/DC boost converter, the DC/DC buck converter is modelled assuming a standard transformer-less DC/DC buck converter topology. Its circuit is shown in Figure 3.18 along with its averaged-value switch model equivalent.

For the buck converter, the steady state equations are given by:

$$V_L = DV_H \tag{3.38}$$

$$I_H = \frac{DI_L}{\eta} \tag{3.39}$$

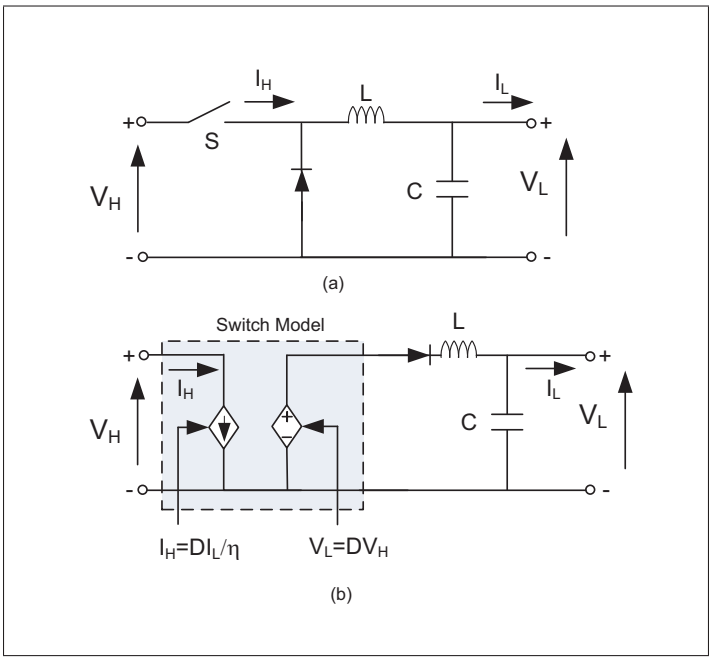

Figure 3.18 DC/DC buck converter: (a) standard transformer-less buck circuit (b) equivalent averaged-value switch model

The converter is a regulated output voltage with output current limitation. Similar to the boost converter, the model uses an inner current control loop and an outer voltage control loop to represent these features. This is shown in Figure 3.19.

3.3.2.1 Design of buck converter control loops

From the average-value equivalent circuit (Figure 3.18 (b)), the inductor (L) current and capacitor (C) voltage can be expressed in Laplace domain as:

$$I_L(s) = \frac{DV_H - V_L}{Ls} \tag{3.40}$$

$$V_C(s) = V_L(s) = \frac{I_L - \eta\left(\frac{V_H}{V_L}\right) I_H}{Cs} \tag{3.41}$$

Similar to the boost converter control, PI controllers are used as shown in Figure 3.20. The PI controllers gains are also determined using Equations 3.32 - 3.37.

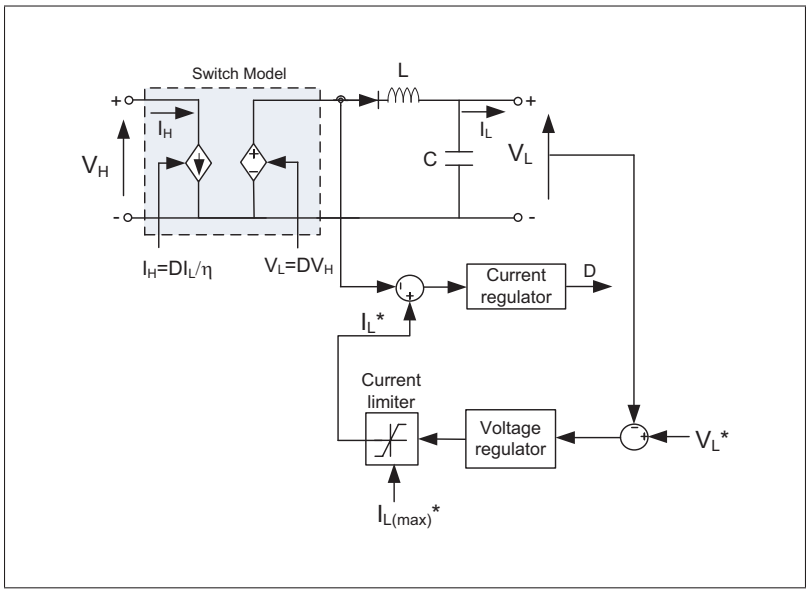

Figure 3.19 Control of the DC/DC buck converter

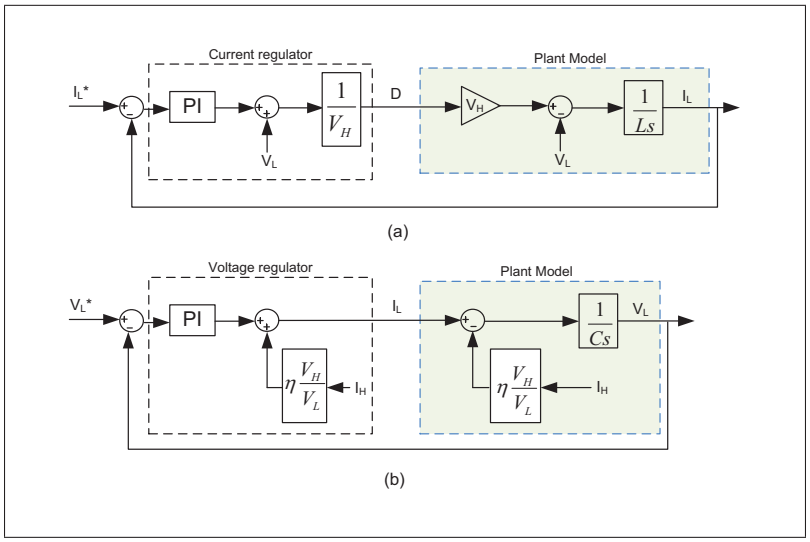

Figure 3.20 The DC/DC buck converter regulators:
(a) current regulator (b) voltage regulator

The model parameters for the buck converter are summarized in Figure 3.21. The efficiencies at 10% and 100 % full load are obtained from experiments along with the voltage regulator response time.

BATTERY BUCK CONVERTER MODEL INPUT PARAMETERS	
Full load current (A)	20
Efficiency @ 100% and 10% Full load (%) [n1, n2]	[80, 88]
Voltage regulator response time (s)	0.1
Load capacitance (F)	0.1

Figure 3.21 buck converter model input parameters

The performances of the buck converter model is shown in Figure 3.22. As observed, the model behaves as the real converter with similar responses to changes in output voltage reference and output current limits.

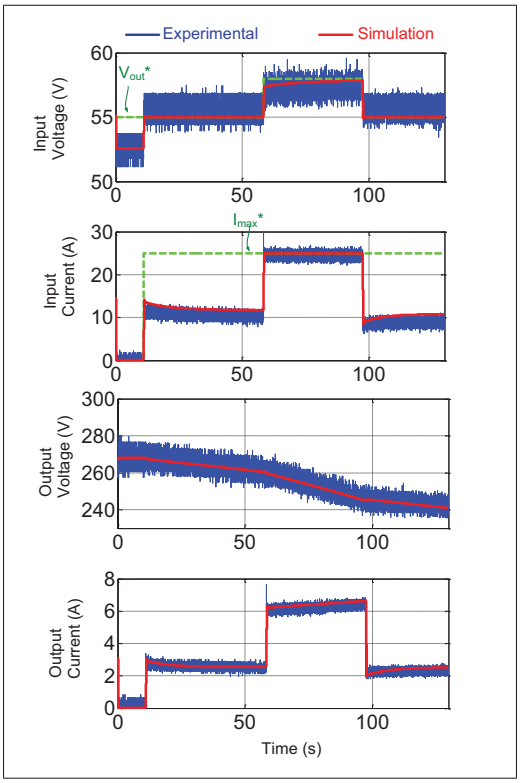

Figure 3.22 Buck converter model validation

3.3.3 The DC-AC converter model

Similar to the DC/DC converter model, the DC/AC converter is represented by an average value model shown in Figure 3.23. A 3-phase 200 V, 400 Hz voltage signal is the reference for the voltage controlled sources. The input current is obtained from the generated output power and DC bus voltage. A fixed efficiency is assumed, as for inverters, the efficiency does not varies much with load.

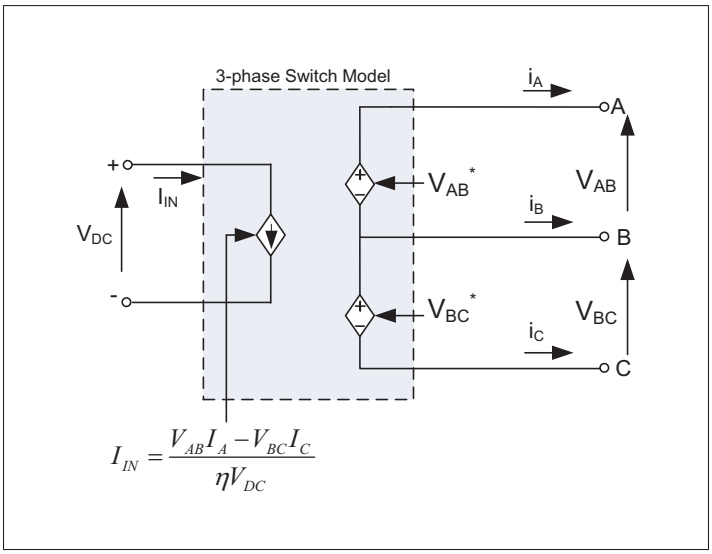

Figure 3.23 DC/AC converter model

The performances of the DC/AC converter model is shown in Figure 3.24. As observed, the model behaves as the real converter with similar response during a load step.

3.4 Modelling of the emergency load

The load is represented by a 3-phase controlled current source, where the load current is obtained from the 3-phase apparent power (kVA) load profile, the power factor and the nominal line voltage.

The model equations are as follows:

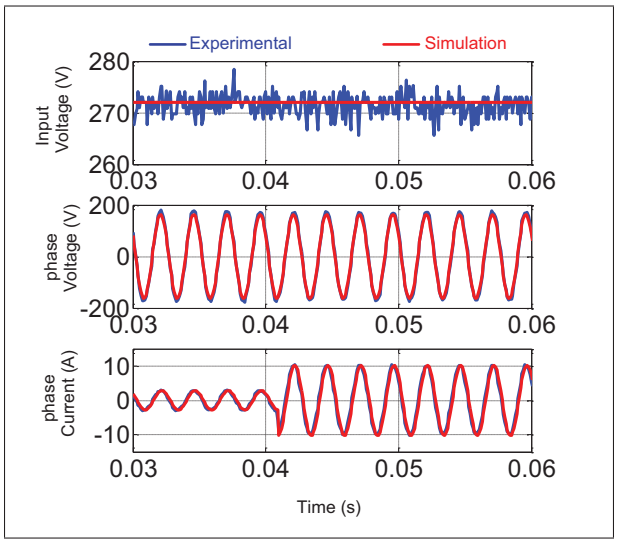

Figure 3.24 DC/AC converter model validation

The load impedance vector is given by:

$$Z = \left(\frac{Vp_{nom}^2}{P_p + jQ_p} \right)^* \tag{3.42}$$

With,

$$P_p = (S/3)cos\theta \tag{3.43}$$

$$Q_p = \sqrt{(S/3)^2 - P_p^2} \tag{3.44}$$

Where Vp_{nom} is the nominal rms phase voltage (115 V). P_p and Q_p are the phase active and reactive power (W) respectively. S and $cos\theta$ are the provided 3-phase apparent power(VA) and power factor.

The phase voltage vector is obtained from the 3-phase voltage using the Park transformation (T) as:

$$V_s = T \cdot [V_{AN}, V_{BN}, V_{CN}]' \tag{3.45}$$

Finally, the phase currents can be determined as:

$$[I_A, I_B, I_C]' = T^{-1} \cdot \frac{V_s}{Z} \tag{3.46}$$

The load model implemented in SPS is shown in Figure 3.25, where Block A represents Equations 3.42 - 3.44.

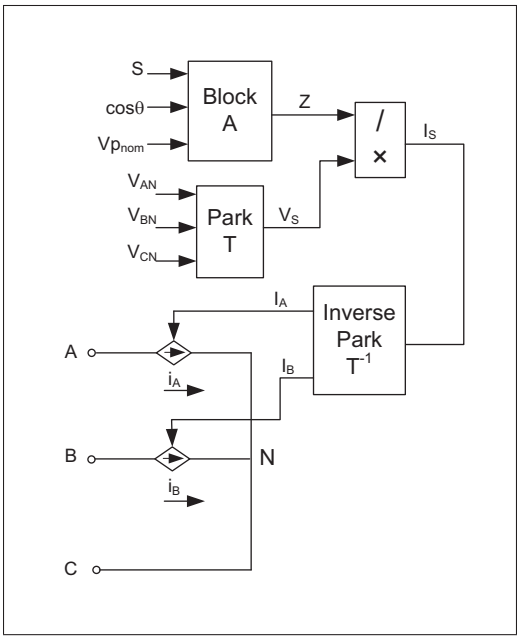

Figure 3.25 Emergency load model

3.5 Conclusion

In this chapter, the model of each component of the hybrid power system was developed. The models of the fuel cell, battery and supercapacitor available in SPS were selected for this study due to the fact that the model parameters could easily be determined from specifications or simple experiments. The model performances were compared to experiments and a maximum error of $\pm$ 2 % was obtained, which confirms the validity of the models.

As for the power converter models, an average-value modelling approach was selected to reduce the simulation time, while keeping the converter dynamics. The models included the

impact of converter efficiency and the voltage/current controllers dynamics were designed to match with the real system. The performances of the fuel cell and battery converter models were compared to experiments and the results obtained were as expected.

The emergency load were modelled using controlled current sources, where the load currents were obtained from the provided 3-phase apparent power (kVA) load profile and the power factor.

With the model of each component of the hybrid system completed, different energy management schemes can be implemented and simulated, with the goal to obtain the scheme which best fits with MEA load profile. This topic is addressed in the next chapter.

CHAPTER 4

DESIGN OF THE ENERGY MANAGEMENT SCHEMES

4.1 Introduction

To ensure the fuel cell, battery and supercapacitor systems operate efficiently and within their respective constraints, an energy management system is necessary. This chapter focuses on the design and simulation of the energy management schemes. The most common strategies, which can be easily realisable using standard microprocessors-based solutions, are selected for performance comparison. Moreover, a new cost function based optimization strategy is proposed, with the objective to minimize the fuel consumption. Also, an off-line optimization strategy is developed, which will serve as a baseline for comparison in terms of fuel consumption.

The performance of each EMS is simulated with the same initial conditions and the main criteria for comparison are: the hydrogen consumption, the state of charges of the batteries/supercapacitors and the overall system efficiency.

4.2 Design of the energy management schemes

The main objectives of an energy management system are to guarantee the following:

- low hydrogen consumption;
- high overall system efficiency;
- narrow scope of the battery/supercapacitor SOC;
- long life cycle.

This is achieved by controlling the power response of each energy source with load demand through their associated converters, using a given energy management strategy (EMS).

The energy management schemes addressed are state-of-the-art, most commonly used energy management techniques in fuel cell vehicle applications and include:

- the state machine control strategy (Fernandez *et al.* (2010)) , (Fernandez *et al.* (2011));
- the rule based fuzzy logics strategy (Caux *et al.* (2010));
- the classical PI control strategy (Thounthong *et al.* (2011));
- the frequency decoupling-fuzzy logics strategy (Ates *et al.* (2010)), (Erdinc *et al.* (2009)), (Vural *et al.* (2010));
- the equivalent consumption minimization strategy (ECMS) (García *et al.* (2012)), (Torreglosa *et al.* (2011)), (Rodatz *et al.* (2005)).

In addition, a novel strategy based on H_2 consumption minimization is proposed. The strategy consists on maximizing the energy delivered by the batteries and supercapacitors at any given instant while meeting their operating constraints. The main advantage of the proposed strategy over the ECMS and other H_2 consumption minimization strategies is its non sensitivity to the load profile as the cost function to be optimized does not include the equivalent fuel consumption, which strongly depends on the whole mission profile. This improves the performance of the energy management system and a near optimal solution can be obtained. To ascertain the validity of the proposed strategy in terms of fuel consumption, an off-line optimization based strategy is also developed.

For fair comparison, all the EMS are designed based on the same requirements (given in Table 4.1). To prevent reactants starvation, the fuel cell current slope (when positive) is limited to the maximum slope of 40 A/s. Also to operate the battery system efficiently, it is required to keep the battery SOC above 40 % at all time.

The DC bus voltage (or supercapacitor SOC) is regulated through the battery converters for all EMS strategies as shown in Figure 4.1 (f). The voltage regulator consists of a simple PI controller. The main difference between the EMS relies on the approach to obtain the fuel cell reference power. The following sections describe the EMS considered in details.

Table 4.1 Energy management design requirements

DESIGN REQUIREMENTS	Value
Fuel cell power [Pfc_{min} - Pfc_{max}] (kW)	[1 - 10]
Battery power [$Pbatt_{min}$ - $Pbatt_{max}$] (kW)	[-1.2 - 4]
Battery state of charge [SOC_{min} - SOC_{max}] (%)	[60 - 90]
DC bus voltage [Vdc_{min} - Vdc_{max}] (V)	[250 - 280]
Fuel cell current maximum slope (A/s)	40

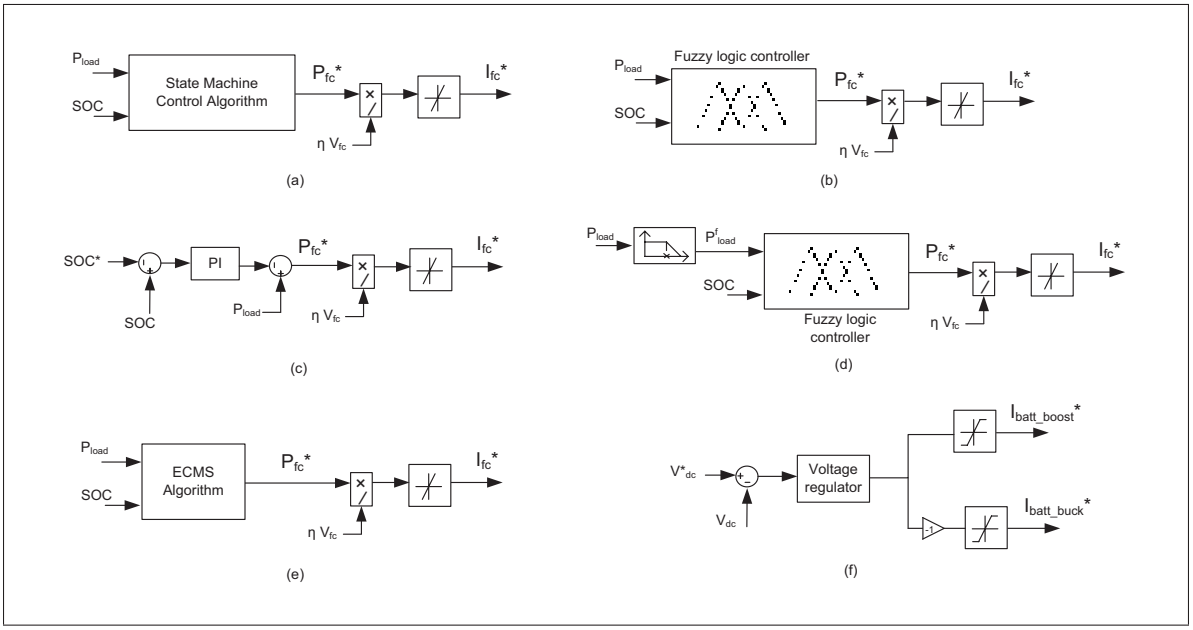

Figure 4.1 Classical energy management schemes:(a) state machine control (b) rule-based fuzzy logic (c) classical PI control (d) frequency decoupling and fuzzy logic (e) ECMS (e) DC bus voltage control common to all EMS

4.2.1 The state machine control strategy

The state machine control strategy implemented consists of eight states as shown in Figure 4.2 (a). These states are derived using the same approach proposed in (Fernandez *et al.* (2011)). The fuel cell power is determined based on the battery SOC range and load power (P_{load}). The EMS scheme is depicted in Figure 4.1 (a). One drawback of this method is the fact that an hysteresis control (shown in Figure 4.2 (b)) is required when switching the states, which affects the response of the EMS to changes in load demand. As shown, the output of the algorithm is the fuel cell reference power, which is divided by the fuel cell voltage and the DC/DC converter efficiency to get the fuel cell reference current.

STATE MACHINE CONTROL DECISIONS

If SOC High	& $P_{load} < Pfc_{min}$	state=1	$Pfc^* = Pfc_{min}$
If SOC High	& $P_{load} \in [Pfc_{min}, Pfc_{max}]$	state=2	$Pfc^* = P_{load}$
If SOC High	& $P_{load} \geq Pfc_{max}$	state=3	$Pfc^* = Pfc_{max}$
If SOC Normal	& $P_{load} < Pfc_{opt}$	state=4	$Pfc^* = Pfc_{opt}$
If SOC Normal	& $P_{load} \in [Pfc_{opt}, Pfc_{max}]$	state=5	$Pfc^* = P_{load}$
If SOC Normal	& $P_{load} \geq Pfc_{max}$	state=6	$Pfc^* = Pfc_{max}$
If SOC Low	& $P_{load} < Pfc_{max}$	state=7	$Pfc^* = P_{load} + P_{char}$
If SOC Low	& $P_{load} \geq Pfc_{max}$	state=8	$Pfc^* = Pfc_{max}$

SOC High → $SOC > SOC_{max}$ $P_{char} = -Pbatt_{min}$

SOC Normal → $SOC \in [85, 65]$ $Pfc_{opt} = Pfc|_{max.\ efficiency}$

SOC Low → $SOC < SOC_{min}$

(a)

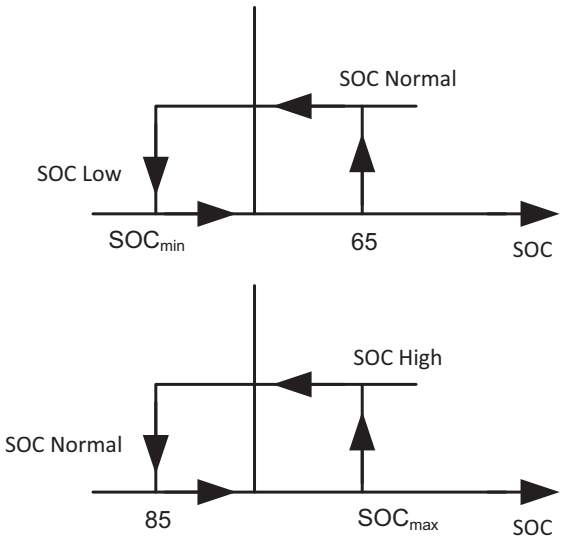

(b)

Figure 4.2 (a) State machine control decisions and (b) Hysteresis control

The state machine control strategy is implemented in SPS using a Simulink S-function block, to facilitate the code transfer from the simulation environment to the LabVIEW real time environment. The S-function consists essentially of sets of if-else statements derived from Table 4.1 and Figure 4.2. The full code is given in Appendix 1.

4.2.2 The rule based fuzzy logic strategy

This scheme has a faster response to load change compared to state machine control and is more robust to measurement imprecisions. The fuel cell power is obtained based on the load power and SOC membership functions and the set of if-then rules. The scheme is shown in Figure 4.1 (b). The design is made following an approach similar to (Caux *et al.* (2010)) where trapezoidal membership functions are used as shown in Figure 4.3. The fuzzy logic rules are derived from the state machine control decisions as shown in Figure 4.4 (a). The Mamdani's fuzzy inference approach is used along with the centroid method for defuzzification. The fuzzy logic control surface obtained is shown in Figure 4.4 (b).

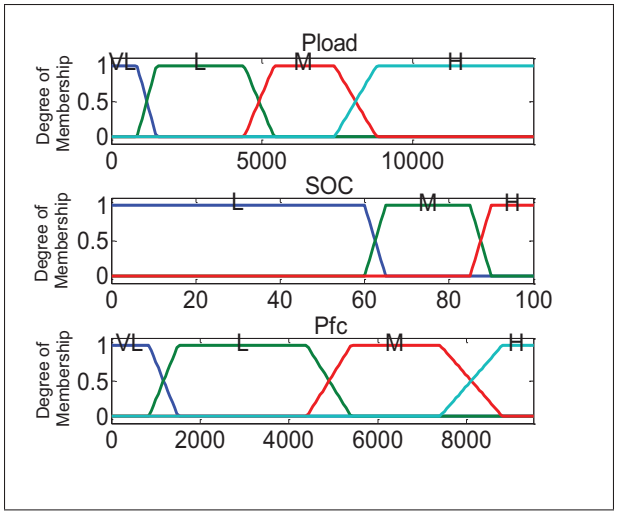

Figure 4.3 Membership functions

The rule based fuzzy logics strategy is implemented in SPS using a Simulink Fuzzy Logic Controller block from the Fuzzy logic Toolbox. The design of this Fuzzy Logic controller is made with the help of the FIS (Fuzzy Inference System) Editor GUI (Graphical user interface) tool of Matlab. This tool allows to create input/output variables, membership functions and rules in a very convenient fashion, without having to develop complicated fuzzy logic system code.

FUZZY LOGIC RULES

If SOC H	&	P_{load} VL	Pfc* = VL
If SOC H	&	P_{load} L	Pfc* = L
If SOC H	&	P_{load} M	Pfc* = M
If SOC H	&	P_{load} H	Pfc* = H
If SOC M	&	P_{load} VL	Pfc* = VL
If SOC M	&	P_{load} L	Pfc* = L
If SOC M	&	P_{load} M	Pfc* = M
If SOC M	&	P_{load} H	Pfc* = H
If SOC L	&	P_{load} VL	Pfc* = L
If SOC L	&	P_{load} L	Pfc* = M
If SOC L	&	P_{load} M	Pfc* = H
If SOC L	&	P_{load} H	Pfc* = H

H → High M → Medium L → Low VL → Very Low

(a)

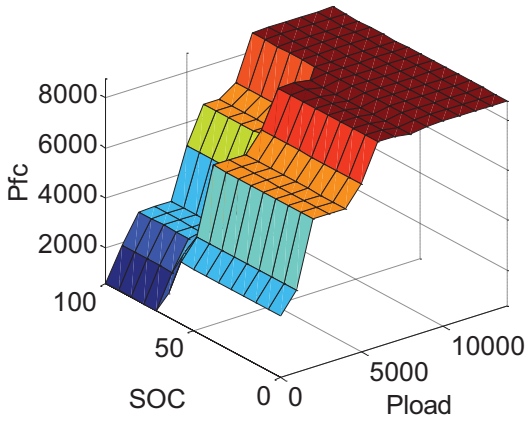

(b)

Figure 4.4 (a) Fuzzy logic rules and (b) Fuzzy logic control surface

4.2.3 The classical PI control strategy

This scheme controls the battery SOC using a PI regulator (Thounthong *et al.* (2011)) as shown in Figure 4.1 (c). The output of the PI regulator is the battery power, which is afterwards removed from the load power to obtain the fuel cell reference power. When the battery SOC

is above the reference (SOC_{min}), the fuel cell power is low and the battery provides its full power. When the SOC is below the reference, the fuel cell provides almost the load power. This scheme is easy to implement compared to previous strategies and the PI gains are tuned on line for better response. The Simulink block diagrams are shown in Appendix 1.

4.2.4 The frequency decoupling and fuzzy logic strategy

The frequency decoupling and fuzzy logic strategy allows the fuel cell system to provide a low frequency load demand while the other energy sources deal with the high frequency demands (Vural *et al.* (2010)). The main advantage with this method is the fact that the mean energy of the battery is close to zero, which ensures a narrow scope of the battery SOC. Nevertheless, a fuzzy logic controller is required to control the battery SOC around a minimum limit. The scheme is shown in Figure 4.1 (d), where a low pass filter is used for frequency decoupling. The cut-off frequency of the filter is set to 8 mHz, which allows the fuel cell to provide a nearly constant power. The fuzzy logic controller is the same as in the rule based fuzzy logic strategy.

The scheme is implemented exactly as in the rule based fuzzy logic case, with the exception of a low pass filter which filters out the high frequency component of the load power. The simulink block diagrams are shown in Appendix 1.

4.2.5 The Equivalent Consumption Minimization Strategy (ECMS)

The ECMS is a well known instantaneous cost function based optimization strategy used by several authors (Zheng *et al.* (2012)), (García *et al.* (2012)), (Torreglosa *et al.* (2011)), (Rodatz *et al.* (2005)), (Sciarretta *et al.* (2004)), (Liangfei *et al.* (2009)). The goal is to achieve a minimum fuel consumption by minimizing the fuel consumed by the fuel cell and the equivalent fuel required to maintain the battery SOC. The approach proposed in (Rodatz *et al.* (2005)) is used in this study. Here, instead of using two constant equivalence factors, a variable equivalence factor which depends on the battery SOC is used (as proposed in (García *et al.* (2012)), (Torreglosa *et al.* (2011)) and (Liangfei *et al.* (2009))). Also, to make the algorithm less sensible to the SOC balance coefficient (μ), the equivalence factor is part of the cost function to be optimized. That is, for different values of μ, an optimum value of the equivalence factor

is obtained. The scheme is shown in Figure 4.1 (e). The optimization problem is defined as follows:

Find an optimal solution $x = [P_{fc}, \alpha_p, P_{batt}]$

Which minimizes

$$F = [P_{fc} + \alpha_p P_{batt}] \cdot \Delta T \tag{4.1}$$

Under the equality constraints

$$P_{load} = P_{fc} + P_{batt} \tag{4.2}$$

$$\alpha_p = 1 - 2\mu \frac{(SOC - 0.5\,(SOC_{max} + SOC_{min}))}{SOC_{max} + SOC_{min}} \tag{4.3}$$

Within the boundary conditions

$$P_{fcmin} \leq P_{fc} \leq P_{fcmax}$$
$$P_{battmin} \leq P_{batt} \leq P_{battmax}$$
$$0 \leq \alpha_p \leq 100$$

Where P_{fc}, P_{batt} and P_{load} are the fuel cell power, battery power and load power respectively (referred to the DC bus, that is considering the converter losses). α_p is the penalty coefficient. ΔT is the sampling time. P_{fcmin} and P_{fcmax} are the minimum and maximum fuel cell power. $P_{battmin}$ and $P_{battmax}$ are the minimum and maximum battery power. SOC_{min} and SOC_{max} are the minimum and maximum battery SOC. μ is the SOC balance coefficient (equal to 0.6 as in (García *et al.* (2012)) and (Liangfei *et al.* (2009))).

The supercapacitor power is not considered in the optimization problem as the DC bus voltage (V_{dc}) is controlled by the battery converters. That is, as soon as the supercapacitors discharge, they are recharged with the same energy from the battery system. Therefore the total load energy is shared only between the fuel cell and battery over a given load cycle.

For the implementation, a Simulink S-function along with the «fmincon» function from the Matlab optimization toolbox are used to solve the optimization problem. The full code is given in Appendix 1.

4.2.6 The proposed H_2 consumption minimization strategy

The ECMS and most of other real time, H_2 consumption minimization strategies are based on the concept of equivalent fuel consumption, where the cost function consists of two parts: the fuel cell H_2 consumption and an equivalent battery/supercapacitor H_2 consumption. The latter being represented by a penalty or equivalence factor of the battery/supercapacitor energy delivered at any given instant. This equivalent consumption is defined as the fuel consumption required to maintain the battery/supercapacitor state of charge (SOC) within its limit, over the whole load profile. Therefore, by definition, the performance of the energy management strategy is sensitive to the load profile and an optimal load sharing can not be ensured, considering the stochastic nature of the load.

This problem was tackled in (Zheng *et al.* (2012)), where the equivalence factor was replaced by a constant value, derived from a predetermined load profile. Similarly, in (Rodatz *et al.* (2005)) and (Sciarretta *et al.* (2004)), the equivalence factor is expressed in terms of two equivalence factors (for battery charge and discharge), which were both derived from mission profiles. In (García *et al.* (2012)), (Torreglosa *et al.* (2011)) and (Liangfei *et al.* (2009)), the equivalence factor is obtained using an empiric expression which depends on the battery SOC and the SOC balance coefficient (μ), the latter is tuned on-line to ensure better control of the battery SOC, throughout the whole load profile. In (Musardo *et al.* (2005)), the equivalence factor is designed to adapt to any mission profile (A-ECMS) using a time ordered prediction of future power demand. The performance of the energy management controller was greatly improved, but at the expense of excessive computations and complexity.

In this study, a new real time H_2 consumption minimization algorithm is proposed. Instead of minimizing the fuel consumption, which requires the evaluation of the equivalent fuel consumption, the proposed strategy aims at maximizing the battery and supercapacitor energies at

any given instant (external energy maximization strategy or EEMS), while keeping the battery SOC and DC bus voltage (or supercapacitor SOC) within their operating limits. The scheme is shown in Figure 4.5.

The optimization problem is defined as follows:

Find an optimal solution $x = [P_{batt}, \Delta V]$

Which minimizes

$$F = -\left[P_{batt}\Delta T + \frac{1}{2}C_r \cdot \Delta V^2\right] \tag{4.4}$$

Under the inequality constraint

$$P_{batt}\Delta T \leq (SOC - SOC_{min})\, V_{battr} Q \tag{4.5}$$

Within the boundary conditions

$$P_{battmin} \leq P_{batt} \leq P_{battmax}$$
$$V_{dcmin} - V_{dc} \leq \Delta V \leq V_{dcmax} - V_{dc}$$

Where ΔV is the supercapacitor charge/discharge voltage and C_r is the rated capacitance of the supercapacitor. V_{dcmin} and V_{dcmax} are the minimum and maximum DC bus voltage. V_{battr} is the rated battery voltage.

As shown in Figure 4.5, the outputs of the EEMS algorithm are the battery reference power and the supercapacitor charge/discharge voltage. The battery reference power is afterwards removed from the load power to get the fuel cell reference power. The supercapacitor charge/discharge voltage is added to the DC bus voltage reference to force the supercapacitor system to charge or discharge. Similar to the ECMS, the DC bus voltage is controlled by the battery converters.

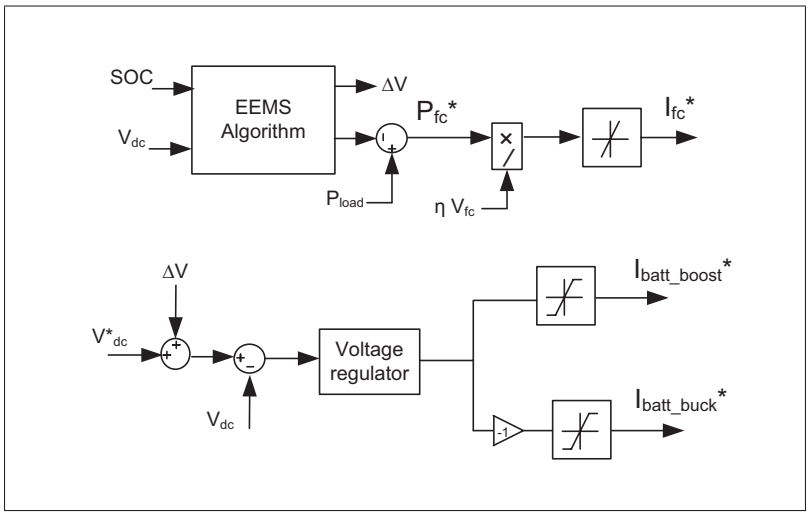

Figure 4.5 External energy maximization strategy (EEMS)

The EEMS is also implemented using the «fmincon» function and a Simulink S-function. The full code is provided in Appendix 1.

4.2.7 H_2 consumption minimization based on off-line optimization

To compare the performance of the proposed scheme with respect to fuel economy, an off-line optimization algorithm similar to (Bernard *et al.* (2006)) is developed. This algorithm gives the minimum fuel consumption that can be achieved for a given load profile, while keeping the battery SOC within its limits. As shown in Figure 4.6, the algorithm takes as inputs the load profile along with the initial and minimum battery SOC. The output is the minimum fuel consumption required.

The optimization problem is defined as follows:

Find an optimal solution

$x = [P_{fc}(1), P_{fc}(2), P_{fc}(3), ..., P_{fc}(n)]$

Which minimizes

$$F = \sum_{k=1}^{n} P_{fc}(k) \cdot \Delta T \tag{4.6}$$

Under the inequality constraints (with k=1, 2, 3, ..., n)

$$y(k+1) \leq (SOC_0 - SOC_{min})\, V_{battr} Q \tag{4.7}$$

$$\sum_{k=1}^{n} P_{fc}(k) \geq n \times P_{fcmin} \tag{4.8}$$

With,

$$y(k+1) = y(k) + (P_{load}(k) - P_{fc}(k))\, \Delta T \tag{4.9}$$

Within the boundary condition

$$P_{fcmin} \leq P_{fc} \leq P_{fcmax}$$

Where n is the number of samples (n = $T_p/\Delta T$), with T_p being the load profile duration.

The minimum fuel consumption is obtained from the nominal fuel consumption ($ConsH2_{nom}$) as:

$$ConsH2^{opt} = \frac{F^{opt} \cdot ConsH2_{nom}}{\sum_{k=1}^{n} P_{fcnom} \cdot \Delta T} \tag{4.10}$$

Where P_{fcnom} is the nominal fuel cell power.

The algorithm is implemented on a M-file using the «fmincon» function. The full code is provided in Appendix 1.

4.3 Simulation results

The energy management schemes are first tested through simulation to ensure they are properly designed prior to implementation in the real system. This section compares the simulated performance obtained from each EMS, using a 30 min. emergency load profile ((Figure 2.2)). To guarantee the same conditions for comparison, the simulations are started with the same initial

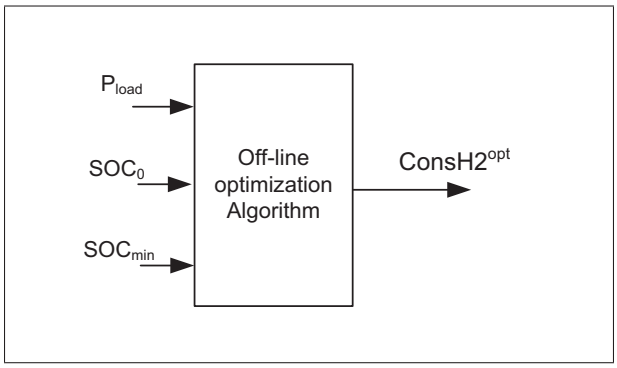

Figure 4.6 Off-line optimization inputs/output

conditions for the battery and supercapacitor system (battery SOC = 70 %, supercapacitor voltage = 270 V). The main criteria for performance comparison are: the hydrogen consumption, the state of charges of the batteries/supercapacitors and the overall system efficiency

Figure 4.7 shows the full system model of the whole hybrid system. As shown, the energy management system block outputs the control signals (output voltage and input/output current references) required by the DC/DC converters. In addition, two ON/OFF signals are used to control the protecting resistor and the load respectively. The resistor or the load are turned ON/OFF depending on the supercapacitor (or DC bus) voltage to avoid overvoltage or undervoltage situations that could occur during system starts or sudden decrease in load.
The inputs to the energy management system block are the load, fuel cell, battery and supercapacitor voltage and current, along with the battery SOC and the output current of each DC/DC converter.

4.3.1 Power distribution, battery SOC and supercapacitor voltage

The power distribution between the energy devices is shown in Figures 4.8, 4.9, 4.10 and 4.11, where the fuel cell power (W), battery power (W), supercapacitor power (W) and load power (W) are all referred to the 270 V DC bus. The battery SOC (%) and supercapacitor voltage (V) are also shown.

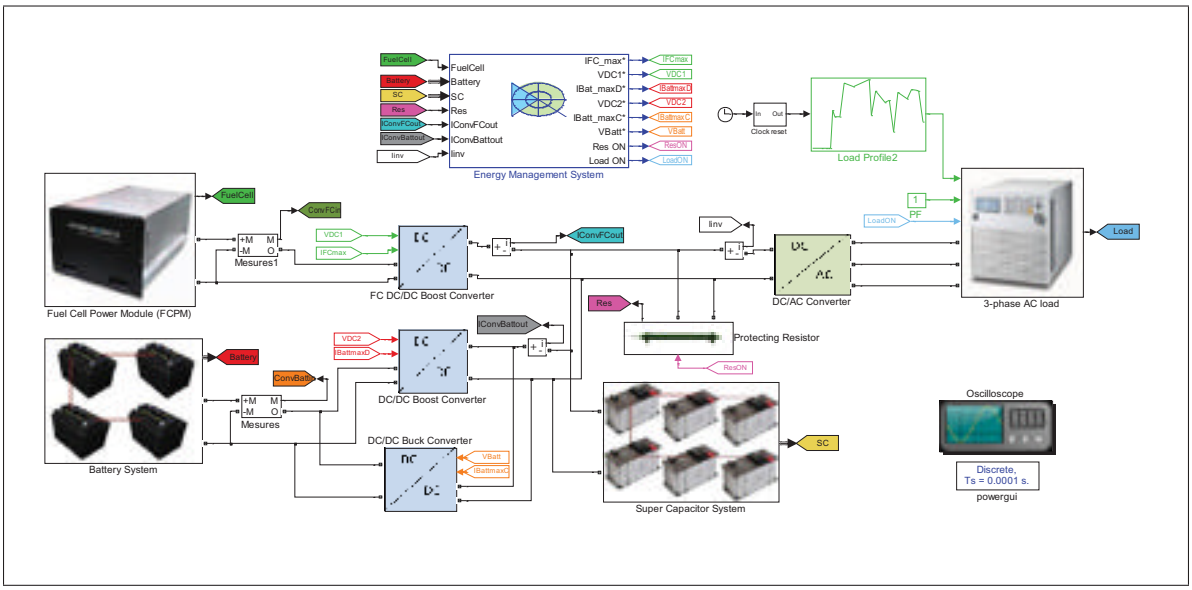

Figure 4.7 The fuel cell hybrid power system model in SPS

As observed, for the state machine control scheme (Figures 4.8 (a) and 4.9 (a)), the fuel cell follows the load till the battery SOC reaches its minimum, then it tries to recharge the battery afterwards. When the battery SOC reaches it minimum, the supercapacitors are charged more often by the fuel cell above their reference voltage (270 V), which forces the DC bus voltage regulator to request a negative current to recharge the battery.

In the rule based fuzzy logic scheme (Figures 4.8 (b) and 4.9 (b)), as expected, the fuel cell response is faster and smooth as the battery SOC gets close to its minimum. When the battery SOC reaches its minimum, the fuel cell behave as in the state machine control.

In the case of the classical PI control scheme (Figure 4.8 (c) and 4.9 (c)), the battery discharges faster to get to the SOC reference (60 %), afterwards the fuel cell tries to provide the load power and recharge the battery. At starting, the fuel cell reference power is low and the supercapacitors discharge to help the battery, consequently the DC bus voltage goes below the reference voltage. This can be avoided if the SOC reference is set to the initial battery SOC, but then the comparison with other schemes will not be fair.

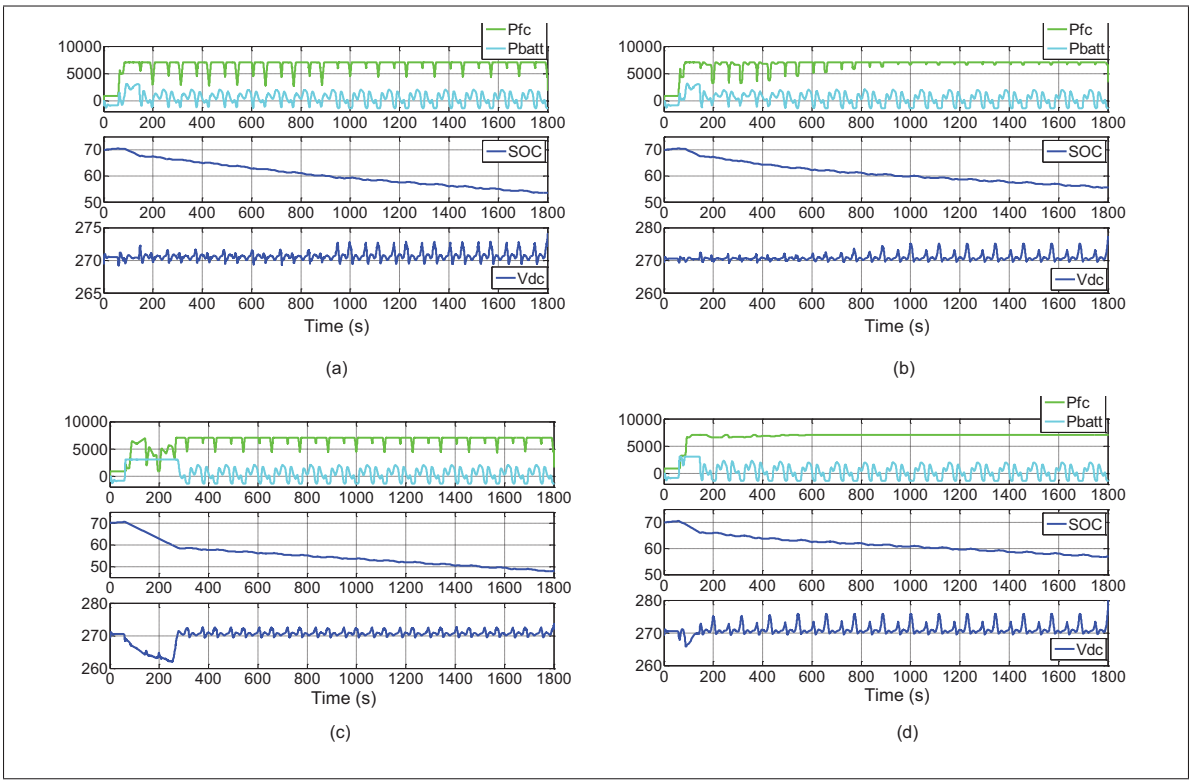

Figure 4.8 Simulation results of EMSs, fuel cell and battery power:
(a) State machine control (b) Rule based fuzzy logic (c) Classical PI control
(d) Frequency decoupling and fuzzy logic

The frequency decoupling and fuzzy logic (Figures 4.8 (d) and 4.9 (d)) forces the fuel cell to provide a nearly constant power, which allows the battery to recharge more often than the previous schemes. As observed, this scheme provides the lowest use of the battery energy (SOC between 70-57.5 %). A higher cut-off frequency (close to the air compressor response) can be used, which will make this scheme behaves as others. But due to the fact that the high frequency component of the load is shared between the battery and supercapacitor system, it is more beneficial in term of the system life time, to put less stress on the fuel cell system and achieve a nearly zero battery energy.

For the ECMS (Figures 4.10 (a) and 4.11 (a)), as soon as the fuel cell is under loaded, it tries to recharge the battery, even when the battery SOC is above its minimum. Hence in this scheme, the supercapacitors are charged more often by the fuel cell above their reference voltage (270 V), to allow the DC bus voltage regulator to request a negative current to recharge the battery.

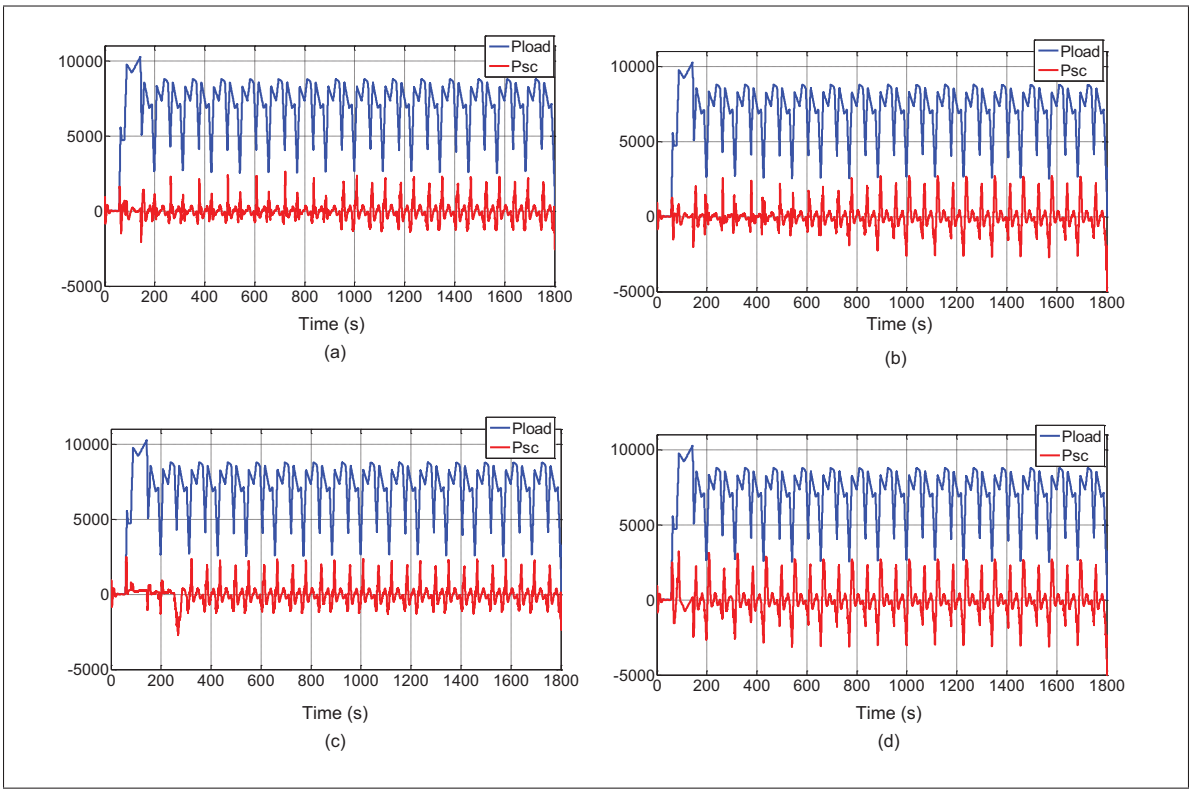

Figure 4.9 Simulation results of EMSs, load power and supercapacitor power: (a) State machine control (b) Rule based fuzzy logic (c) Classical PI control (d) Frequency decoupling and fuzzy logic

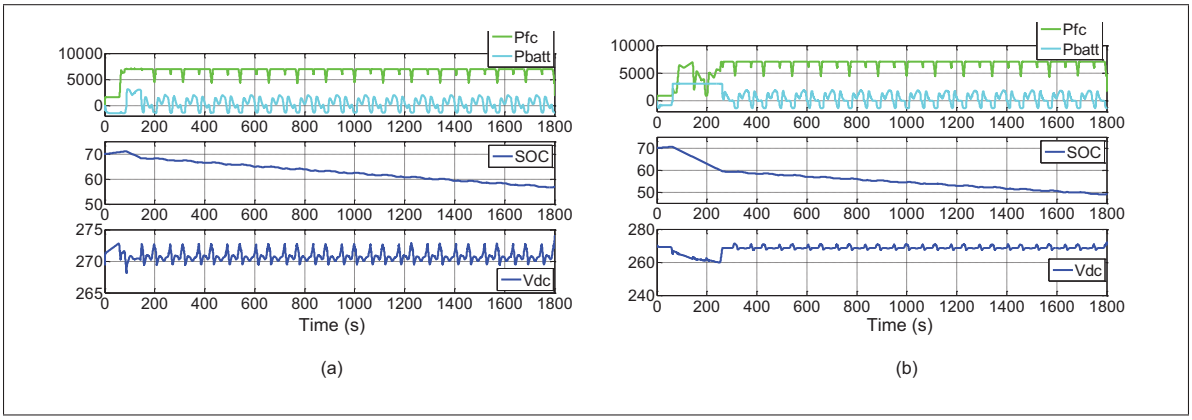

Figure 4.10 Simulation results of EMSs, fuel cell and battery power: (a) ECMS (b) EEMS

In the case of the EEMS (Figures 4.10 (b) and 4.11 (b)), the battery discharges faster to get to its minimum SOC (60 %), afterwards the fuel cell tries to provide the load power and recharge

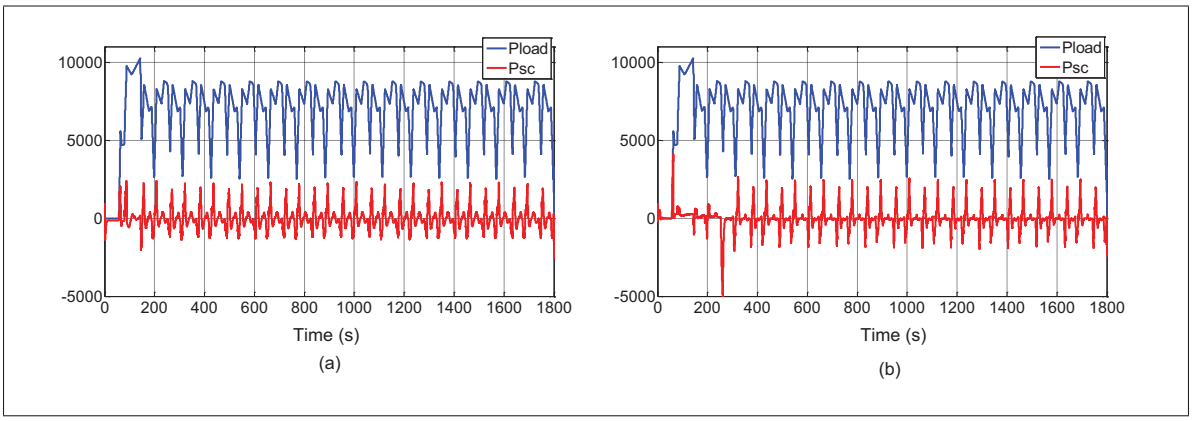

Figure 4.11 Simulation results of EMSs, load power and supercapacitor power: (a) ECMS (b) EEMS

the battery. At starting, the fuel cell reference power is low and the supercapacitors discharge to help the battery, consequently the DC bus voltage goes below the reference voltage (but still well above the minimum DC bus voltage). Compared to the ECMS, more battery energy is used (SOC between 70-49.1 %).

4.3.2 Hydrogen consumption and overall efficiency

The hydrogen consumption and overall efficiency obtained from all schemes are calculated as follows:

The hydrogen consumption (g) is given by:

$$ConsH2 = \frac{N}{F} \int_{0}^{1800} i_{fc} dt \tag{4.11}$$

Where F is the Faraday constant (A s/mol).

The overall efficiency is given by:

$$efficiency = \frac{P_{load}}{P_{fc}^{in} + P_{batt}^{in} + P_{cap}^{in}} \tag{4.12}$$

Where P_{fc}^{in}, P_{batt}^{in} and P_{cap}^{in} are the fuel cell power (input to the DC/DC converter), battery power (input to the DC/DC converters) and supercapacitor power, respectively.

Figures 4.12 and 4.13 shows the hydrogen consumption and efficiency obtained for all schemes from simulation.

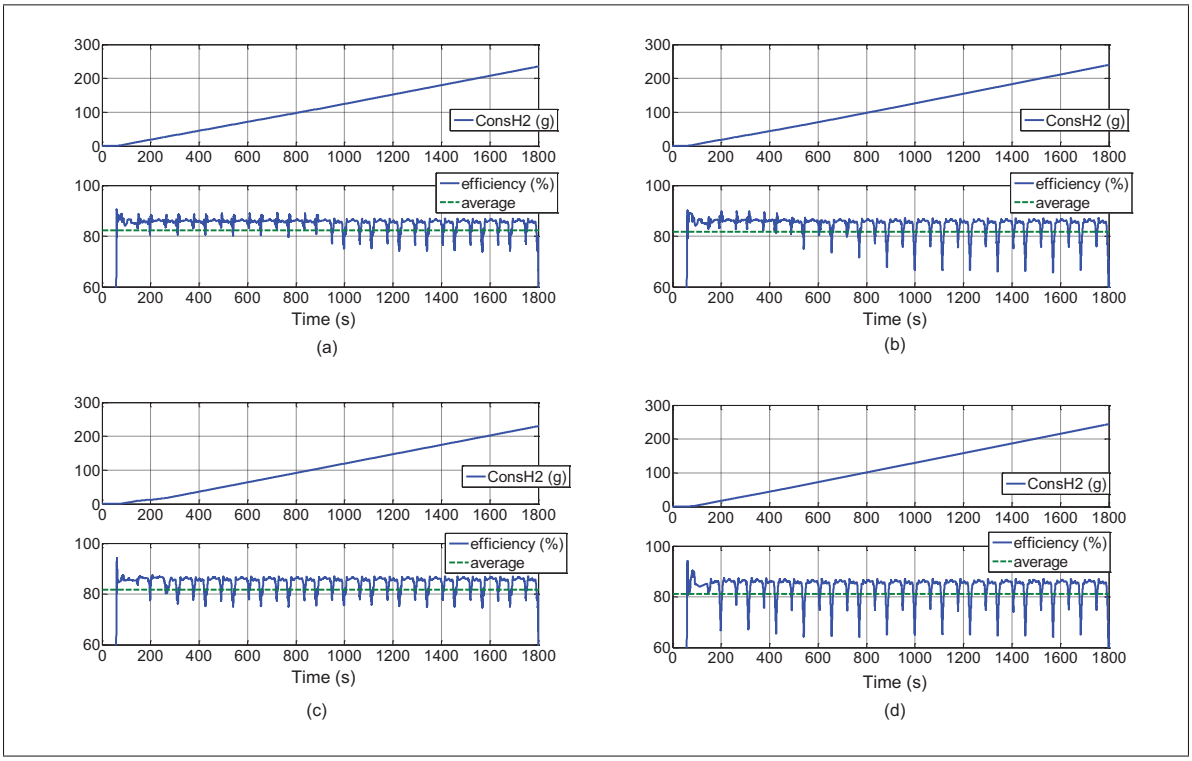

Figure 4.12 Simulation results of EMSs, H_2 consumption and overall efficiency: (a) State machine control (b) Rule based fuzzy logic (c) Classical PI control (d) Frequency decoupling and fuzzy logic

It can be noted that the state machine control (Figure 4.12 (a)) is slightly more efficient than the other schemes, while the classical PI regulator has the lowest fuel consumption (Figure 4.12 (c)). Also the frequency decoupling scheme has the lowest overall efficiency and the highest fuel consumption (Figure 4.12 (d)). As expected, the proposed strategy (EEMS) is slightly more efficient than the ECMS, Moreover the fuel economy with the EEMS is increased by 4.7 % compared to the ECMS. Tables 4.2 and 4.3 summarise the results obtained for each scheme along with the result obtained from the off-line optimization.

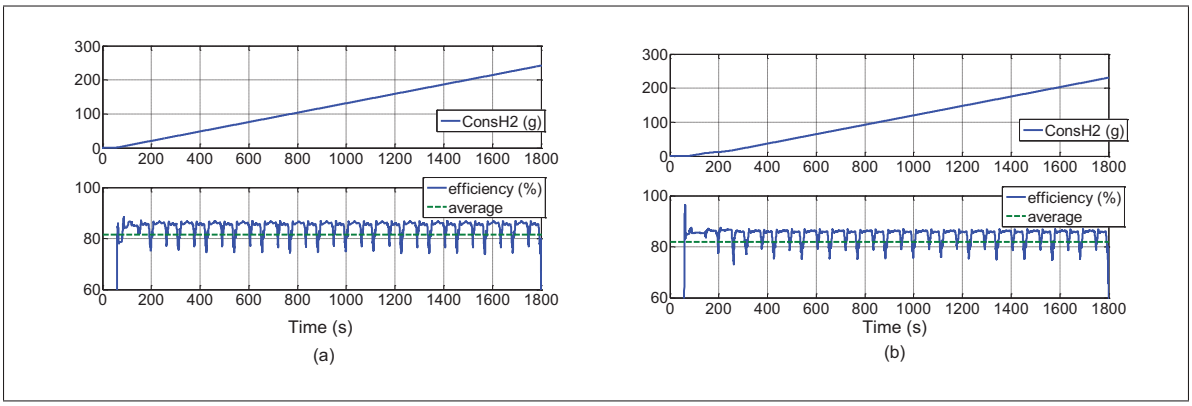

Figure 4.13 Simulation results of EMSs, H_2 consumption and overall efficiency: (a) ECMS (b) EEMS

Table 4.2 Simulation results: overall performance of the EMS

Criteria	State machine control	Rule based fuzzy logic	Classical PI control	Frequency decoupling & rule base fuzzy logic
Battery SOC (%)	70 – 53.5	70 – 55.5	70 – 48	70 – 57.5
H2 Consumption (g)	235	240	230	245
Overall efficiency (%)	82.26	81.75	81.77	81.09

Table 4.3 Simulation results: overall performance of the optimization based EMS

Criteria	ECMS	Off-line optimization	EEMS	Off-line optimization
Battery SOC (%)	70 – 56.8	70 – 56.8	70 – 49.1	70 – 49.1
H2 Consumption (g)	242	227.58	230.6	217.5
Overall efficiency (%)	81.6	- -	81.91	- -

As observed from Table 4.3, in terms of fuel economy, the ECMS and EEMS are both close to the optimal fuel consumption by 6 %, which confirms the validity of the proposed strategy.

4.4 Conclusion

In this chapter, the most common energy management schemes are selected for implementation and comparison. To ensure a fair comparison, the energy management schemes were designed following the same requirements. The strategies included: the state machine control

strategy, the rule based fuzzy logic strategy, the classical PI control strategy, the frequency decoupling/fuzzy logic control strategy and the equivalent consumption minimization strategy (ECMS).

A new strategy (external energy maximization strategy or EEMS) is proposed as an alternative to strategies based on fuel equivalent consumption. The strategy is based on maximizing the energy delivered by the batteries and supercapacitors at any given instant while meeting their operating constraints.

The proposed strategy is simple, straightforward and more robust to change in load profile compared to existing H_2 consumption minimization strategies. An off-line optimization based approach was developed to ascertain the validity of the strategy in terms of fuel consumption.

The energy management schemes were compared through simulation using the same initial conditions and a 30 min. emergency load profile. The criteria for performance comparison were the hydrogen consumption, the battery state of charge and the overall efficiency. Compared to the other schemes, the state machine control scheme performed better in terms of efficiency. The classical PI control scheme had the lowest fuel consumption and more use of the battery energy. As expected, the lowest use of the battery energy was achieved with the frequency decoupling and fuzzy logic scheme, but at the expense of more fuel consumption and lower overall efficiency. The proposed strategy performed slightly better compared to the ECMS in terms of efficiency and fuel consumption, with an increase in fuel economy by 4.7 %. The DC bus or supercapacitor voltage was maintained nearly constant for all the schemes.

To confirm the validity of the proposed strategy, its performance in term of fuel consumption is compared to an off-line optimization approach and the results obtained are close by 6 %.

The next chapter deals with the implementation of these schemes in the real system and presents experimental results of their performance. The impact of each EMS on the life cycle is also addressed by evaluating the stress seen by each energy source over the load profile.

CHAPTER 5

EXPERIMENTAL VALIDATION

5.1 Introduction

This chapter describes briefly the implementation of the energy management schemes in the real system and presents some experimental results to ascertain the validity of the hybrid power system model. The test bench consists of a 14 kW fuel cell hybrid power system, with its control and monitoring software developed using an NI PXI 8108 embedded controller and LabVIEW real time. At first, the test bench setup is briefly described. Then energy management schemes are implemented in the controller exactly as in the simulation and their performances are tested using a 30 min. emergency load profile.

5.2 Description of the test bench

Figures 2.6 and 5.1 show the overall system schematic and the test bench setup respectively. The main characteristics of each component are provided below:

a. The fuel cell power module (FCPM): it is a 12.5 kW, liquid cooled, PEM fuel cell power module with in-built balance of plant (air blower, filter, H_2 recirculation pump, H2 pressure regulator and valves, coolant pump and fans, etc.). The FCPM also has an internal controller (engine control unit or ECU), which communicates with the NI-PXI controller through CAN (controller area network) interface. All the commands and operating modes of the module are programmed in the NI-PXI controller following the "CAN specifications" provided by the manufacturer. The FCPM is connected to the DC/DC converter through contactors which are controlled by the ECU. The ECU shutdown the FCPM and open the contactors in case of faults (such as H_2 low pressure fault, system heartbeat fault, coolant high temperature fault, over current fault, etc.). Also a high power diode is used to prevent reverse currents from flowing into the FCPM (this is per manufacturer's requirement and normally not needed as the FCPM is connected to a boost converter);

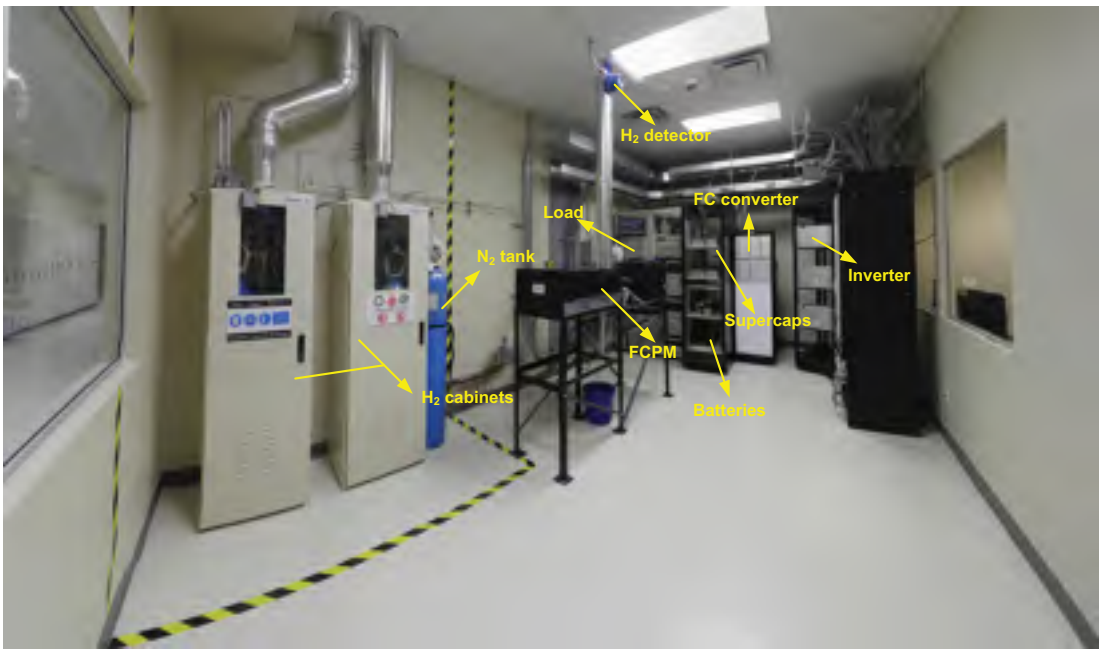

Figure 5.1 Test bench setup

b. The battery system: It consists of 4, 12.8 V, 40 Ah Li-ion battery module connected in series. Each module is equipped with an internal controller for: cell-to-cell balancing (or intra module balancing), cell temperature and voltage/current sensing, SOC calculation and communication with overall battery management system (BMS) through RS485. The BMS is in charge of inter-module balancing and monitoring of the voltage, current and temperature of all 4 modules. Contactors are also required at the output of the battery system, which are opened by the BMS in case of faults (over temperature, over voltage, over current, under voltage, communication loss, sensor failure, etc.). The BMS and the NI PXI also communicate through CAN bus and all the commands are programmed following the BMS "CAN specifications". The modules are also equipped with LED indicators to indicate their status (normal, fault, warning);

c. Supercapacitor system: It consists of 6, 48.6 V, 88 F, super capacitor modules connected in series. Each module is also equipped with an internal controller (ultracapacitor management unit or UMU) for cell-to-cell balancing, voltage and temperature sensing. An

output high or low signal is used to detect an overvoltage and the temperature information is obtained from the thermistor resistance;

d. The fuel cell DC/DC converter system: It consists of 5, (40-64 V) DC in, 270 V DC (adjustable 243-297 V), 9.2 A out, DC/DC isolated boost converters connected in parallel. The system is equipped with overload and overvoltage protection for each module. Redundant operation is possible with the use of decoupling diode. Current balancing required for parallel operation is achieved by active current sharing. A relay is used to indicate converter failure. The output voltage and input current are adjusted by external signals (0-10V). Also, low pass filters are used at both the input and output of each converter to ensure the input current ripple is below 5 %, as required by the FCPM manufacturer;

e. The battery DC/DC converter system: It consists of 2, (40-58.4V) DC in, 270 V DC (adjustable 243-297 V), 7 A out, DC/DC isolated boost converter connected in parallel. Together with 1, (243-297 V) DC in, 48 V DC (adjustable 0-58.4 V), 20 A (max.) out, DC/DC isolated buck converter. All converters feature overload and overvoltage protection, redundant and parallel operation. The output voltage and input/output current are adjusted by external signals (0-10V);

f. The inverter system: It consists of 3, (160-320 V) DC in, 200 VAC, 400 Hz, 5 kVA, DC/AC isolated converters connected in parallel. The system is equipped with overload, overvoltage and short circuit protection. Each converter output voltage is regulated to the nominal voltage with a THD (total harmonic distortion) of less than 3 %;

g. The programmable DC/AC load: It consists of 6, 4.5kW/45 A/350 V electronically programmable load. Each load is equipped with a DSP (digital signal processor) to emulate non-linear/ linear AC (45-440 Hz) or DC load. The load can operate in constant power/ current/voltage/impedance mode with variable power factor (0-1) inductive or capacitive. Each load also features overload, overvoltage and over temperature protections. The load can be controlled locally or remotely via RS232 or GPIB interface;

h. The protecting resistor: It consists of a 15kW, 300 V DC, resistor with a relay. The relay is controlled with a 12 V signal generated from the NI-PXI depending on the supercapacitor (or DC bus) voltage;

i. The NI-PXI embedded controller: it is a 2.53 GHz dual-core processor with integrated hard drive and 4GB of RAM. The controller communicates with a standard PC over Ethernet and has in-built GPIB and RS232 interfaces. The 14 slots NI-PXI 1044 chassis is used to connect the controller to NI data acquisition (NI DAQ) and CAN interface cards. All voltage/current/temperature/pressure sensors data are accessed through NI DAQs. A LabVIEW real time software is required for programming the controller and all data acquisition and interface cards;

j. H_2 supply system: It consists of 2 cabinets, each with 2 H_2 high pressure (2000 psi) tanks. Each tank holds around 0.5 Kg of H_2 and the system is equipped with a low pressure alarm to indicate a low H_2 threshold. Also, when a low H_2 threshold is reached, there is a automatic switch between cabinet to allow continuous FCPM operation;

k. The H_2 leak detector: There are 3 H_2 detectors, 1 in each cabinet and 1 above the FCPM. Each detector output data are connected to the main security/alarm system to allow rapid intervention of the fire and security department in case of an unlikely event of H_2 leak above recommended limit;

l. The ventilation system: the FCPM system is well ventilated during operation to ensure proper operation of the air supply system. Also, each cabinet and the FCPM cathode/anode outputs are ventilated 24/7 without interruption, so that any H_2 leak is rapidly cleared.

5.3 Energy management implementation

The energy management is achieved by controlling the DC/DC converters using analog control signals (0-10 V) generated from NI DAQs. All data (load power, battery SOC, DC bus voltage, fuel cell voltage, etc.) required for the implementation of the energy management strategy are

obtained from the CAN bus, the RS 232 or data acquisition cards. The software for the control and monitoring of the hybrid system is developed in LabVIEW and described in Appendix 2.

Based on the EMS models presented in the previous chapter, a LabVIEW programming VI (virtual instrument) of each EMS is developed. The sections below briefly describe each EMS implementation. The same voltage regulator, based on a PI controller is used for all scheme. All the LabVIEW programming VI diagrams are provided in Appendix 2.

5.3.1 The state machine control strategy

The state machine control strategy is implemented in LabVIEW using the Formula Node VI from the Programming/Structures Toolbox. The if-else statements from the Simulink S-function are essentially copied and pasted in the LabVIEW formula node. To check if the implemented EMS corresponds to simulation, the input (load power and battery SOC) are varied and the output of the block (fuel cell reference power) is compared to simulation.

5.3.2 The rule based fuzzy logics strategy

The rule based fuzzy logics strategy is implemented in LabVIEW using a Fuzzy Logic Controller VI from the Control design and simulation/Fuzzy logic Toolbox. Similar to Matlab, LabVIEW has an integrated Fuzzy system design tool (Fuzzy system designer, under Tools–> Control Design and Simulation), with the same features as the FIS Editor GUI. This tool allows to create input/output variables, membership functions and rules using the same approach as in Matlab. The same defuzzification method is selected as in simulation and the fuzzy logic surface are plotted and compared with Matlab results.

5.3.3 The classical PI control strategy

The implementation of this strategy is straightforward, just as in the simulation using a PI controller VI from the LabVIEW Control design and simulation/PID Toolbox . The performance of the regulator was tested and tuned to achieve better control of the battery SOC.

5.3.4 The frequency decoupling & rule based fuzzy logics strategy

This strategy is implemented as the rule based fuzzy logics strategy, with a low pass filter of the same cut-off frequency as in simulation, added to remove the high frequency component of the load power.

5.3.5 The ECMS

The ECMS is implemented using the Constrained Nonlinear Optimization VI from LabVIEW Mathematics/Optimization Toolbox. The VI algorithm uses the sequential quadratique programming (sqp) approach similar to the Matlab «fmincon» function. The parameters (initial conditions, boundaries and constraints) required by the algorithm are the same as in the simulation. The VI is tested to ensure it converges to the same optimal solution as obtained using «fmincon».

5.3.6 The EEMS

The EEMS is also implemented using the Constrained Nonlinear Optimization VI with the same initial conditions, boundaries and constraint as in the simulation. The same optimal solutions were obtained in both LabVIEW and SPS.

5.4 Experimental results

Using the same load profile as in the simulation, the performance of the energy management schemes were tested. To ensure a fair comparison, the tests are started with the same initial conditions (battery SOC = 70 %, battery temperature = 30 ^oC; supercapacitor voltage = 270 V, supercapacitor temperature = 25 ^oC, fuel cell voltage = 52 V, fuel cell temperature = 40 ^oC).

5.4.1 Power distribution, battery SOC and supercapacitor voltage

The power distribution between the energy devices is shown in Figures 5.2, 5.3, 5.4 and 5.5, where the fuel cell power (W), battery power (W), supercapacitor power (W) and load power

(W) are all referred to the 270 V DC bus. The battery SOC (%) and supercapacitor voltage (V) are also shown.

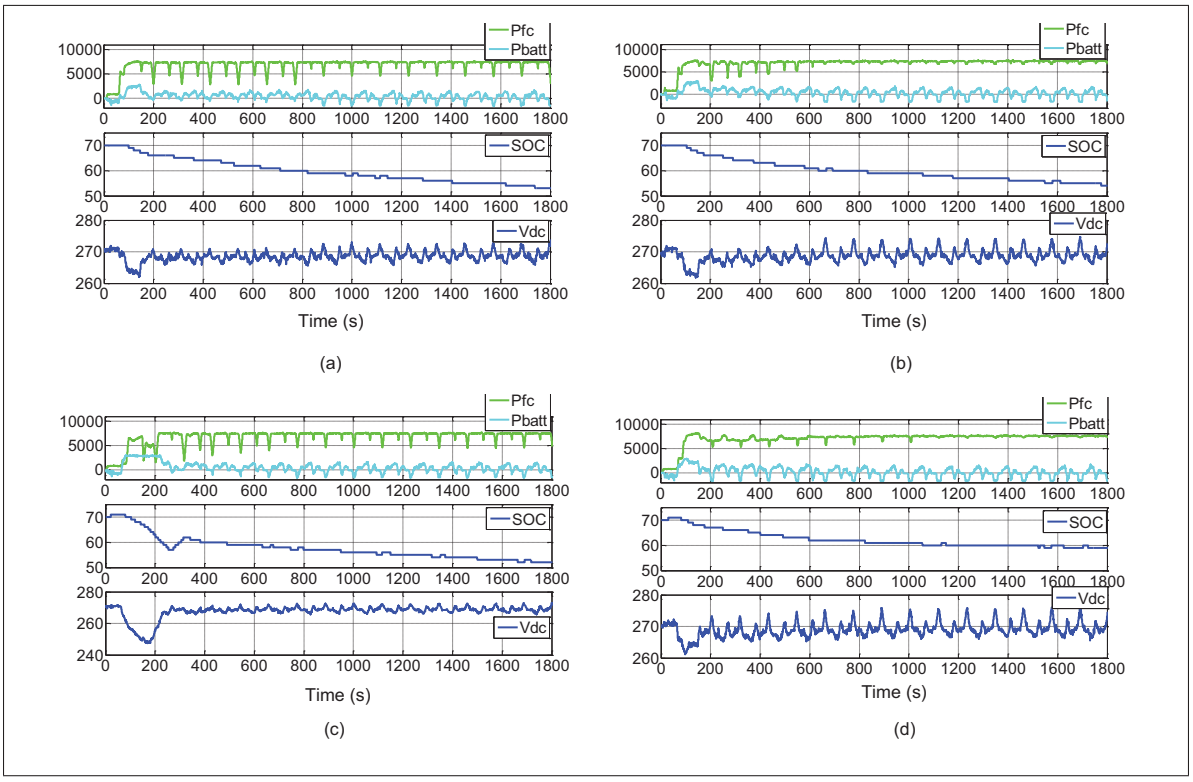

Figure 5.2 Experimental results of EMSs, fuel cell and battery power:
(a) State machine control (b) Rule based fuzzy logic (c) Classical PI control
(d) Frequency decoupling and fuzzy logic

As observed from Figures 4.8-4.11 and Figures 5.2-5.5, the performances obtained from experiments correspond with the simulation, for the state machine control scheme (Figures 5.2 (a) and 5.3 (a)), the fuel cell behave as expected, it follows the load till the battery SOC reaches its minimum, then it tries to recharge the battery afterwards. The use of the battery energy (SOC between 70-54 %) is close to simulation by less than 1 % (SOC between 70-53.5 % in simulation).

In the rule based fuzzy logic scheme (Figures 5.2 (b) and 5.3 (b)), the same behavior as in simulation is also obtained, the fuel cell response is faster and smooth as the battery SOC gets close to its minimum. When the battery SOC reaches its minimum, the fuel cell provides more

than the load power to recharge the batteries. Here also, the battery energy used is as expected.

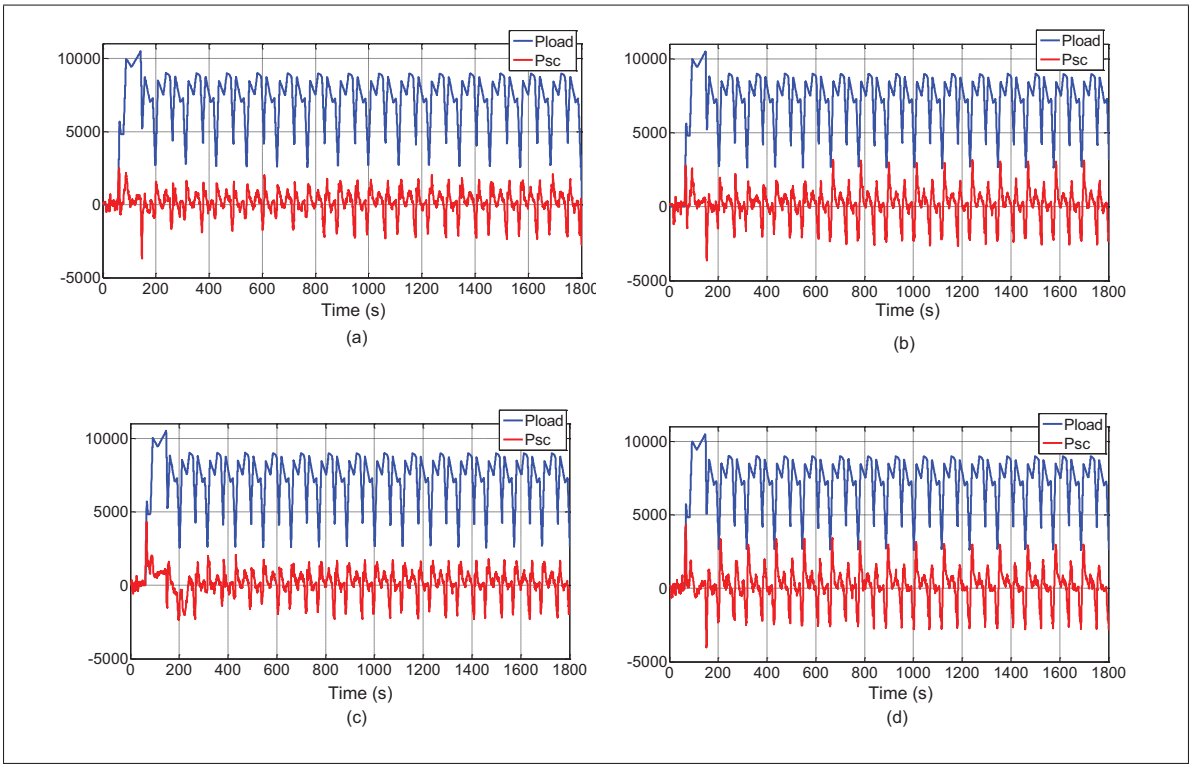

Figure 5.3 Experimental results of EMSs, load power and supercapacitor power: (a) State machine control (b) Rule based fuzzy logic (c) Classical PI control (d) Frequency decoupling and fuzzy logic

In the case of the classical PI control scheme (Figure 5.2 (c) and 5.3 (c)), at starting, as the battery SOC is above its reference (60 %), the battery provides its full power. As expected, when the SOC goes below the reference, the fuel cell power increases while the battery power reduces. As in simulation, more battery energy is used compared to the previous schemes.

Just as simulated, the fuel cell provides a nearly constant power in the frequency decoupling and fuzzy logic strategy (Figures 5.2 (d) and 5.3 (d)), which allows the battery to recharge more often than the previous schemes. As expected, the lowest use of the battery energy (SOC between 70-59 %) is obtained.

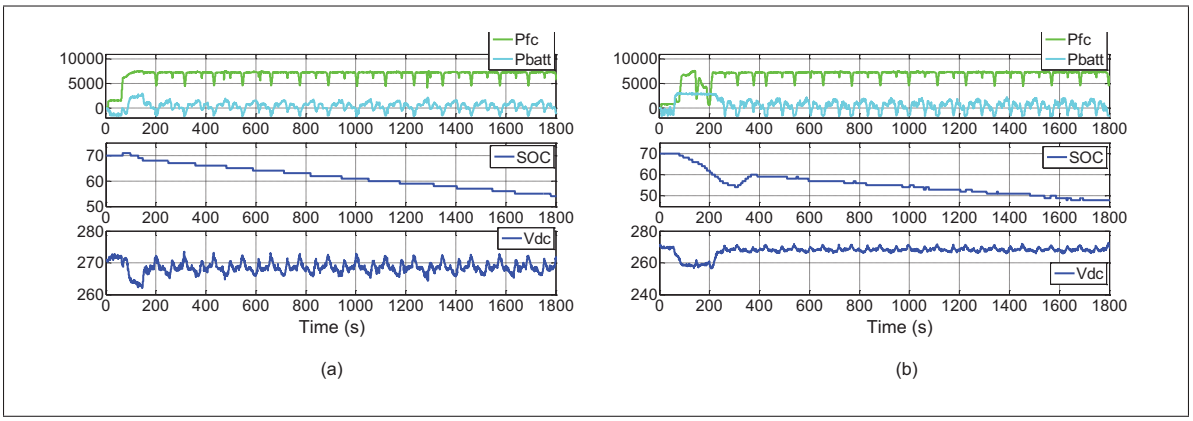

Figure 5.4 Experimental results of EMSs, fuel cell and battery power: (a) ECMS (b) EEMS

For the ECMS (Figures 5.4 (a) and 5.5 (a)), the fuel cell tries to recharge the battery more often to prevent the battery SOC to reach to its minimum. The battery mainly provides power to maintain the DC bus voltage to the required value. A similar behavior is also obtained in simulation.

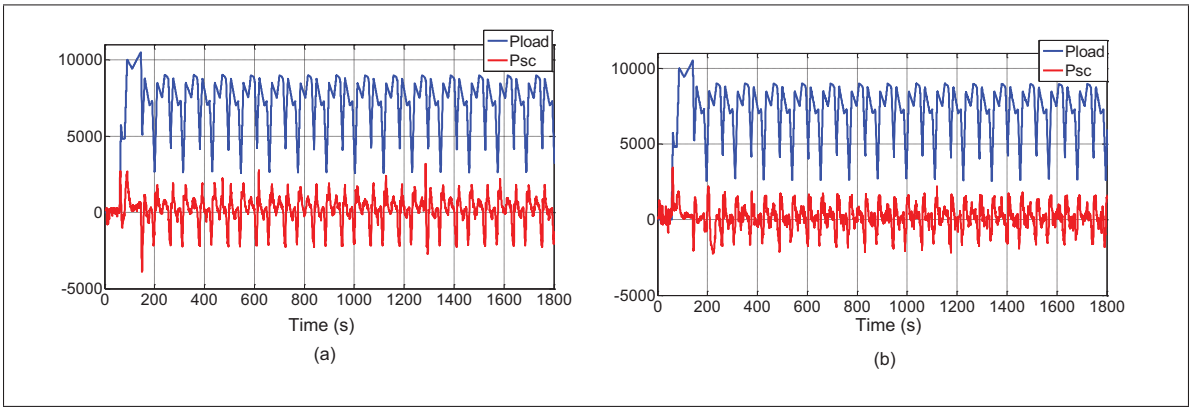

Figure 5.5 Experimental results of EMSs, load power and supercapacitor power: (a) ECMS (b) EEMS

In the case of the EEMS (Figures 5.4 (b) and 5.5 (b)), the strategy works like the classical PI controller, the battery discharges faster to get to its minimum SOC (60 %), afterwards the fuel cell tries to provide the load power and recharge the battery. As expected, more battery energy is used (SOC between 70-48 %) compared to the ECMS.

5.4.2 Hydrogen consumption and overall efficiency

Figures 5.6 and 5.7 shows the hydrogen consumption and efficiency obtained for all schemes from experiments.

As obtained in simulation, the state machine control (Figure 5.6 (a)) is slightly more efficient than the other schemes, while the classical PI regulator and the proposed scheme have the lowest fuel consumption (Figure 5.6 (c)) and more used of the battery energy. Also, as expected, the frequency decoupling scheme has the lowest overall efficiency and the highest fuel consumption (Figure 5.6 (d)). The proposed strategy (EEMS) performs similar to simulation with an increase in fuel economy by 3 % and a slightly high efficiency compared to the ECMS. A summary (in tabular form) showing the results obtained for each scheme is provided in the next section, after the stress analysis of each device is addressed.

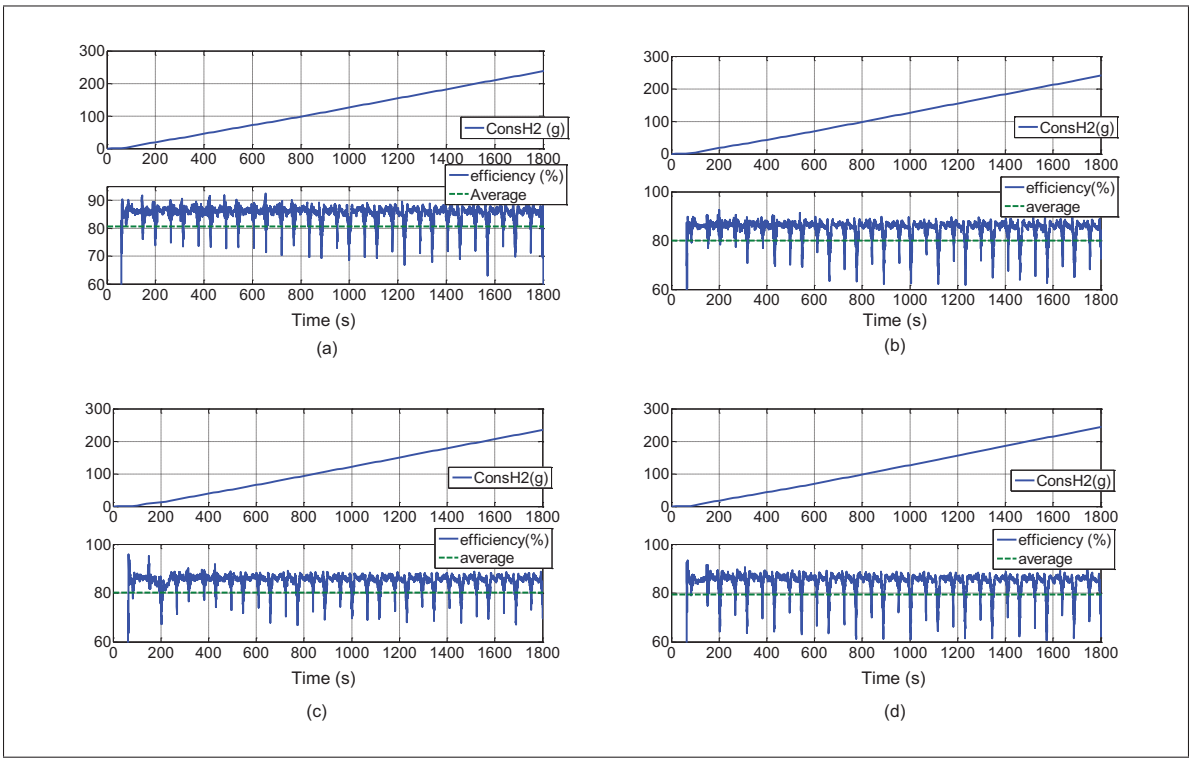

Figure 5.6 Experimental results of EMSs, H_2 consumption and overall efficiency: (a) State machine control (b) Rule based fuzzy logic (c) Classical PI control (d) Frequency decoupling and fuzzy logic

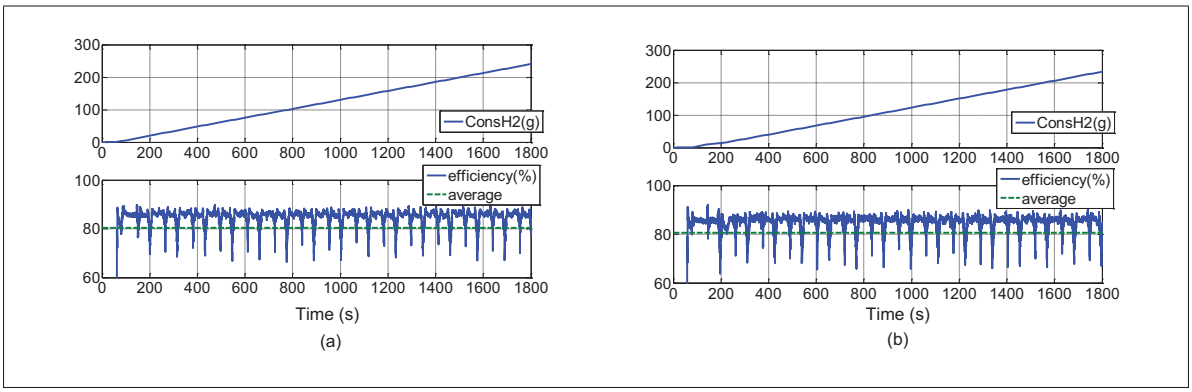

Figure 5.7 Experimental results of EMSs, H_2 consumption and overall efficiency: (a) ECMS (b) EEMS

5.4.3 Stress analysis

The stress on each energy source is determined with a new approach based on the wavelet transform of the fuel cell power, battery power and supercapacitor power referred to the 270 V DC bus. Each power is decomposed in a low and high frequency components using the Haar wavelet decomposition, available in the Matlab wavelet toolbox. The high frequency component of each power has a mean value of zero and the histogram or standard deviation (SD or σ) of this component gives a good indication of how often each energy source is solicited.

Figures 5.8, 5.9 and 5.10 shows the experimental results obtained for each scheme.
It is observed that the state machine control scheme has the lowest battery and supercapacitor stresses (Figure 5.8(a)), while the frequency decoupling and fuzzy logic scheme provides the lowest stress on the fuel cell system (Figure 5.9(b)). As expected, the proposed stragegy (EEMS) has the highest battery and supercapacitor stresses (Figure 5.10 (b)). As new technology Li-ion batteries and supercapacitors are designed to handle more stress compared to NiCd, NiMH or lead acid batteries, this feature will be beneficial for the proposed strategy.

The overall performance of all schemes based on the comparison criteria is summarized in Tables 5.1 and 5.2 .

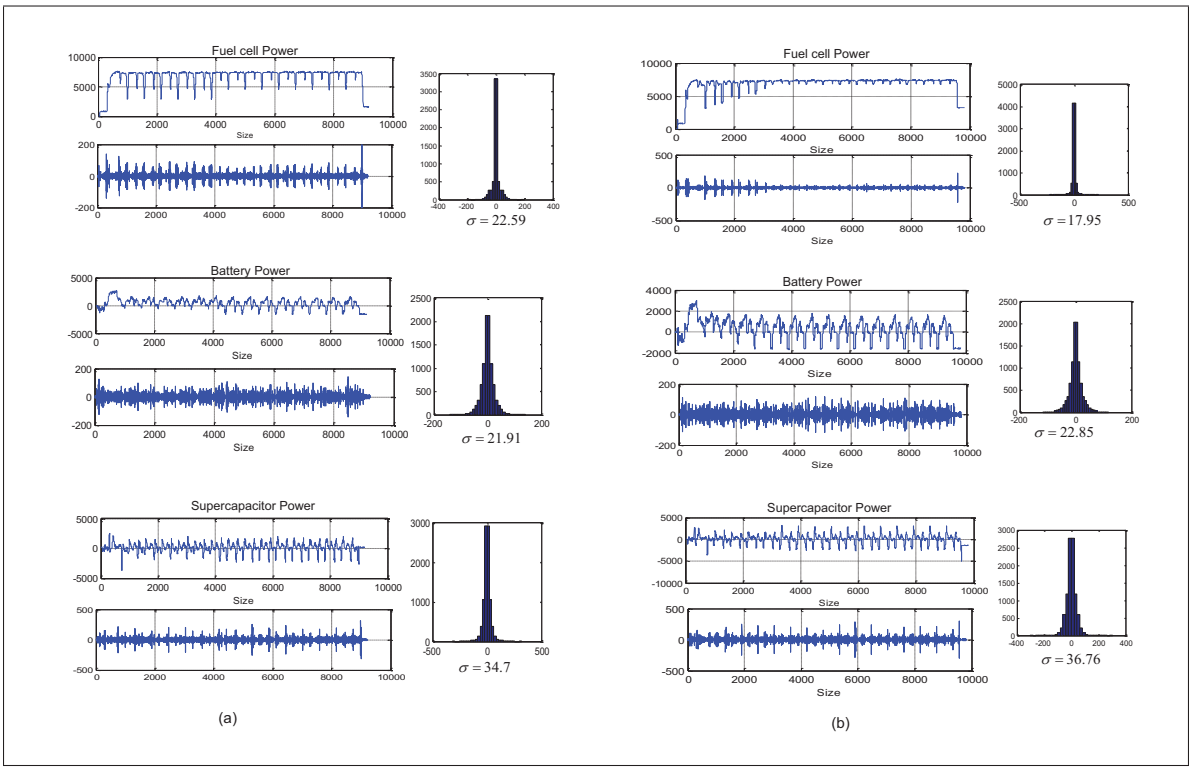

Figure 5.8 Experimental results of EMSs, stress analysis:
(a) State machine control (b) Rule based fuzzy logic

Table 5.1 Experimental results: overall performance of the EMS

Criteria	State machine control	Rule based fuzzy logic	Classical PI control	Frequency decoupling & Fuzzy logic
Battery SOC (%)	70 – 54	70 – 54	70 – 51	70 – 59
H2 Consumption (g)	238	240.6	235	245
Overall efficiency (%)	80.72	80.1	80.28	79.32
Fuel cell stress SD	22.59	17.95	23.42	12.04
Battery stress SD	21.91	22.85	22	24.6
Supercap. Stress SD	34.7	36.76	35.92	37.84

5.5 Conclusion

In this chapter, the performances of the energy management schemes considered in this study are experimentally validated. The test bench setup was briefly described along with the implementation of these schemes in the real system using LabVIEW real time software. The

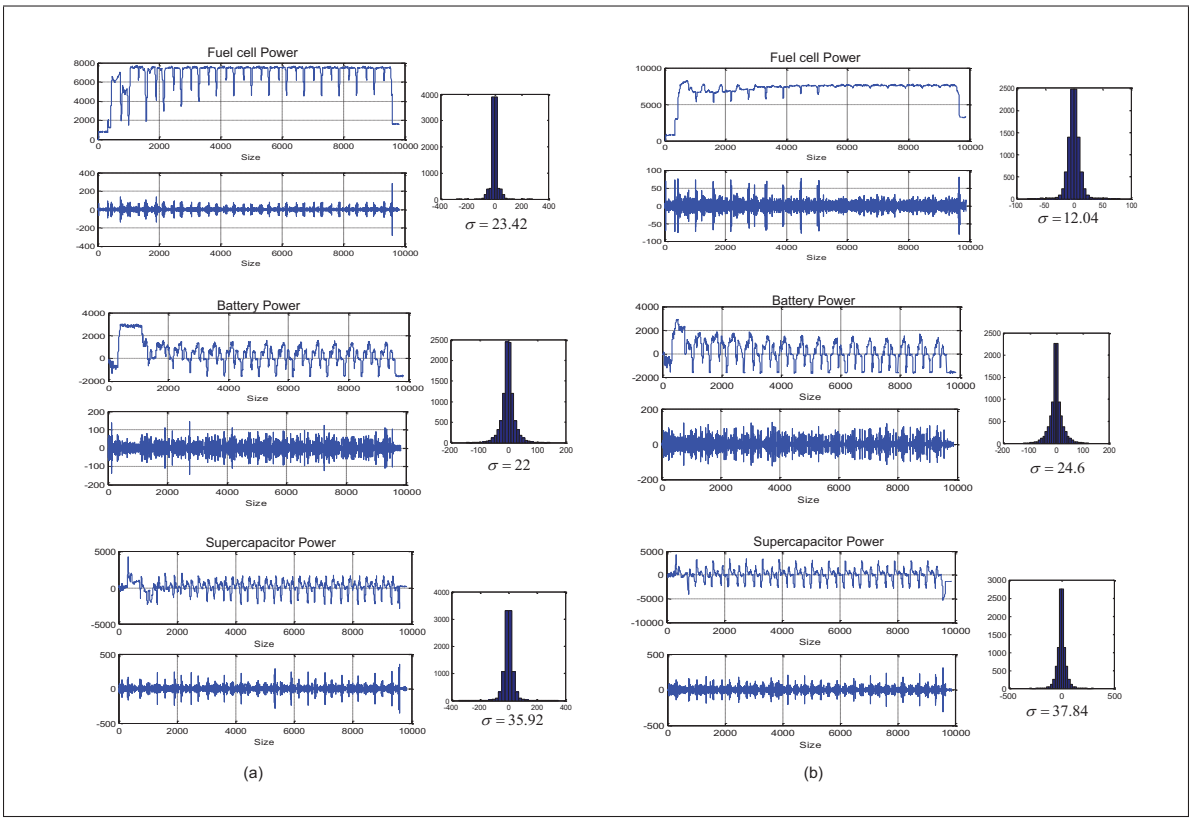

Figure 5.9 Experimental results of EMSs, stress analysis:
(a) Classical PI control (b) Frequency decoupling and fuzzy logic

Table 5.2 Experimental results: overall performance of the optimization based EMS

Criteria	ECMS	Off-line optimization	EEMS	Off-line optimization
Battery SOC (%)	70 – 54	70 – 54	70 – 48	70 – 59
H2 Consumption (g)	240	224	233	216
Overall efficiency (%)	80.47	- -	80.55	- -
Fuel cell stress SD	22.04	- -	22.61	- -
Battery stress SD	24.44	- -	35.92	- -
Supercap. Stress SD	38.64	- -	44.98	- -

bench consisted of a 14 kW fuel cell hybrid power system and the same initial conditions were maintained for all the schemes, to ensure a fair comparison.

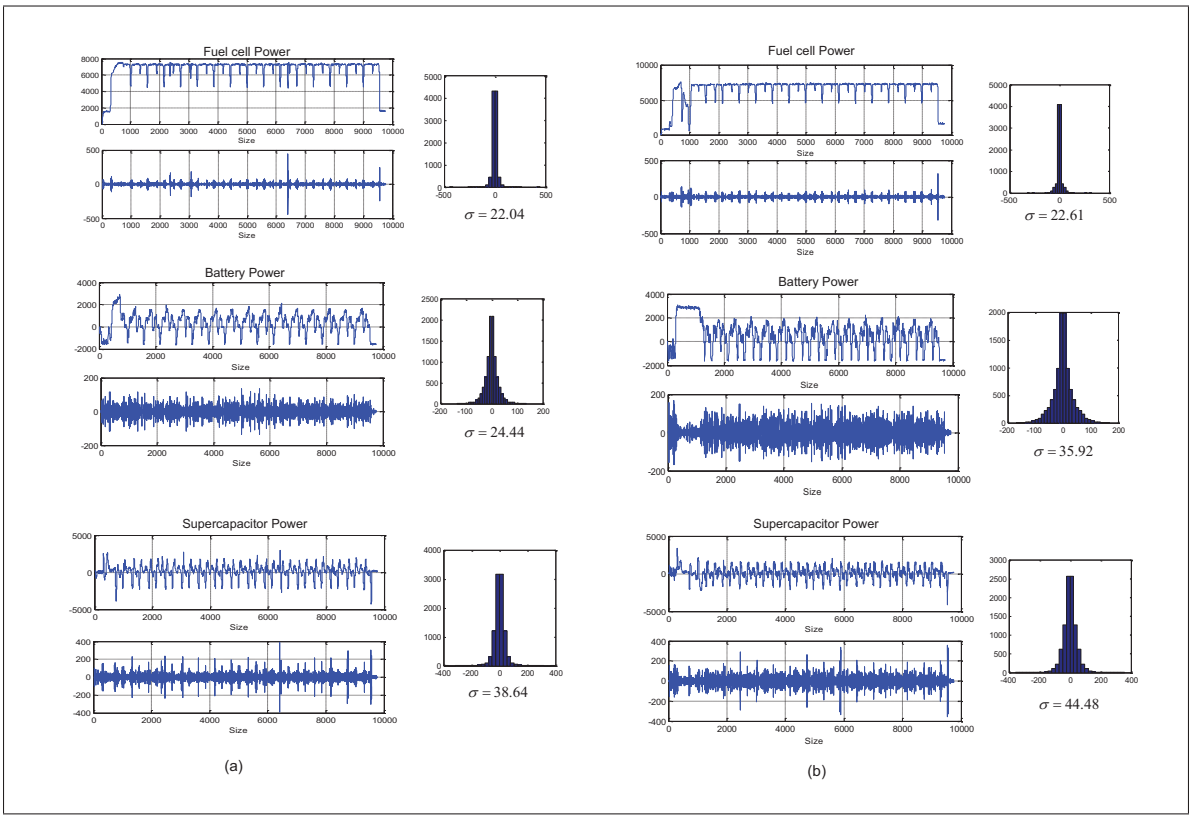

Figure 5.10 Experimental results of EMSs, stress analysis:
(a) ECMS (b) EEMS

The results obtained from the experiments were very close to simulations, which confirm the validity of the hybrid power system model. Beside the criteria such as the fuel consumption, state of charge of batteries/supercapacitors and overall efficiency, considered during the simulations, the stress seen by each energy source was also evaluated to observe the impact of the EMS on the life cycle of the hybrid power system. This stress was measured using a new approach based on the wavelet transform of each device instantaneous power.

As expected, the state machine control scheme performed better than the other schemes, in terms of efficiency and stresses on the batteries and supercapacitors. Also, as in simulation, the classical PI control and the proposed schemes had the lowest fuel consumption and more use of the battery energy. The lowest fuel cell stress and lowest use of the battery energy was achieved with the frequency decoupling and fuzzy logic scheme, but at the expense of more

fuel consumption and lower overall efficiency. Also similar to simulation, the DC bus voltage was maintained nearly constant for all the schemes.

Compared to the ECMS, the proposed strategy performed slightly better in terms of efficiency and fuel consumption, with an increase in fuel economy by 3 %. But, as expected this schemes had the highest batteries and supercapacitors stresses, which is not a major concern as new technology Li-ions batteries and supercapacitors are designed to handle more stress compared to other type of batteries. To confirm the validity of the proposed strategy, its performance in term of fuel consumption is compared to an off-line optimization approach and the results obtained are close by 7 %.

CONCLUSION

Environmental emissions policy along with recent advancements in fuel cell technology with regards to cost, weight and performance have made Fuel cell very attractive for automotive and aircraft applications. Hence most aircraft manufacturers are moving toward replacing some of their gas turbine based power source with fuel cell systems.

Due to its high maintenance cost and poor performance at low aircraft speed, the aircraft emergency power system, which consists of an air driven generator (ADG) or ram air turbine (RAT), is potentially to be replaced by a fuel cell hybrid system as a first step toward greener aircraft. This replacement will be beneficial particularly for more electric aircraft (MEA) which require higher peak electrical load during landing compared to their conventional counterparts.

To ensure the fuel cell hybrid system will be able to meet the load demand, it must be properly designed and an effective energy management strategy must be tested with real situations load profile. The main objective of this study was to design a fuel cell emergency power system of a more electric aircraft and evaluate different energy management schemes; with the goal to ensure the load demand is fully satisfied within the constraints of each energy source.

Using a typical emergency load profile of a MEA, the fuel cell hybrid system was designed based on the energy/power requirements. It consisted of Fuel cell, lithium-ion batteries and supercapacitors, along with associated DC-DC and DC-AC converters. Based on the efficiency, cost, weight and power controllability, the topology of the hybrid system was selected. This topology consisted of using a separate DC/DC converter for the fuel cell and battery systems and connecting the supercapacitor system directly on the DC bus.

Each component of the hybrid system was modelled. The fuel cell, battery and supercapacitor models available in SPS were selected for this study due to the fact that the model parameters could easily be determined from specifications or simple experiments. The model performances were compared to experiments and a maximum error of $\pm$ 2 % was obtained, which confirms the validity of the models. The power converters were modeled using average-value modelling approach, which greatly reduced the simulation time. The models included

the impact of converter efficiency and the voltage/current controllers dynamics were designed to match with the real system. The performances of the fuel cell and battery converter models were compared to experiments and the results obtained were as expected.

Five state-of-the-art commonly used energy management schemes were selected for implementation and comparison. To ensure a fair comparison, the energy management schemes were designed following the same requirements. The strategies included: the state machine control strategy, the rule based fuzzy logic strategy, the classical PI control strategy, the frequency decoupling/fuzzy logic control strategy and the equivalent consumption minimization strategy (ECMS). A new strategy (external energy maximization strategy or EEMS) is proposed as an alternative to strategies based on fuel equivalent consumption. The strategy is based on maximizing the energy delivered by the batteries and supercapacitors at any given instant while meeting their operating constraints.

The proposed strategy is simple, straightforward and more robust to change in load profile compared to existing H_2 consumption minimization strategies. An off-line optimization based approach was developed to ascertain the validity of the strategy in terms of fuel consumption.

The energy management schemes were compared through simulation and experiments, using the same initial conditions and a 30 min. emergency load profile. For all schemes, the simulation and experimental results were very close. The schemes were evaluated based on the following criteria: the hydrogen consumption, the battery state of charge, the overall efficiency and the stress seen by each energy source. The latter is measured using a new approach based on wavelet transform.

Compared to the other schemes, the state machine control scheme provided a slightly better efficiency (80.72%) and stresses on the batteries and supercapacitors (σ of 21.91 and 34.7 respectively). The classical PI control and the proposed scheme had the lowest fuel consumption (235 g and 233 g of H_2 consumed respectively) and more use of the battery energy (SOC between 70 - 51 % and 70 - 48 % respectively). As expected, the lowest fuel cell stress (σ of 12.04) and lowest use of the battery energy (SOC between 70 - 59 %) was achieved with the

frequency decoupling and fuzzy logic scheme, but at the expense of more fuel consumption (245 g of H_2 consumed) and lower overall efficiency (79.32 %). The DC bus or supercapacitor voltage was maintained nearly constant ($\approx$ 270 V DC) for all the schemes.

The proposed strategy (EEMS) performed slightly better than the ECMS in terms of efficiency and fuel consumption, with an increase in fuel economy by 3 %. But, as expected this schemes had the highest batteries and supercapacitors stresses, which is not a major concern as new technology Li-ions batteries and supercapacitors are designed to handle more stress compared to other type of batteries.

To confirm the validity of the proposed strategy, its performance in term of fuel consumption is compared to an off-line optimization approach and the results obtained are close by 7 %.

To conclude, the energy management scheme suitable for a MEA emergency system should be a multi-scheme EMS such that each scheme is chosen based on a specific criterion to prioritize. As an example, depending on the operating life of each energy source, the energy management strategy can be chosen to either minimise the stress on the fuel cell system, the battery system or supercapacitor system, hence maximizing the life cycle of the hybrid power system. Also if the target is to reduce the fuel consumption, the strategy based on the classical PI or EEMS could be selected. An alternative is to design a multi-objective optimization EMS to optimize all the performance criteria, which is the next topic for further studies

Future work

One of the main reasons which explains the slow pace of aircraft manufacturers toward greener aircraft, powered by a fuel cell system resides on its non competitive weight compared to actual gas turbines engines or RAT systems. With a solid knowledge on the system operation and energy management strategies for better fuel economy and longer life cycle at hands, the next part of this project could be to optimize the size and weight of the hybrid power system to further improve the fuel economy. Starting from DC/DC converters, bipolar transformer-less topologies could be investigated. Also different hybrid system topologies such as direct integration topology or topology with one DC/DC converter could be investigated.

Some requirements on fuel cell systems for aircraft application such as, the operation with different stack inclinations, impact of vibrations and altitudes on the fuel cell system performance must be tested in the next part of this project. The same applies to batteries and supercapacitors, in terms of vibrations, temperature, humidity and safety.

There are still more work to be done on energy management strategies and optimal design of the hybrid power system. An interesting approach which requires more attention could be to size the components of the hybrid power system using a multi-objective global optimization approach, where the variables such as weight, efficiency and life cycle are simultaneously optimized. In the optimization process, the parameters of a real time multi-objective optimal energy management scheme could also be determined. This approach will ensure the system is optimal in sizing as well as in operation.

APPENDIX I

HYBRID POWER SYSTEM MODEL IN SPS

The hybrid power system is modelled in Simulink/SimPowerSystems (SPS). This section presents the block diagram of each component model. Also the models of the energy management schemes considered are presented.

1 Energy source models

The models of the fuel cell, battery, supercapacitor are shown in Figures-A I-1, I-2 and I-3 respectively. Their interfaces are also shown.

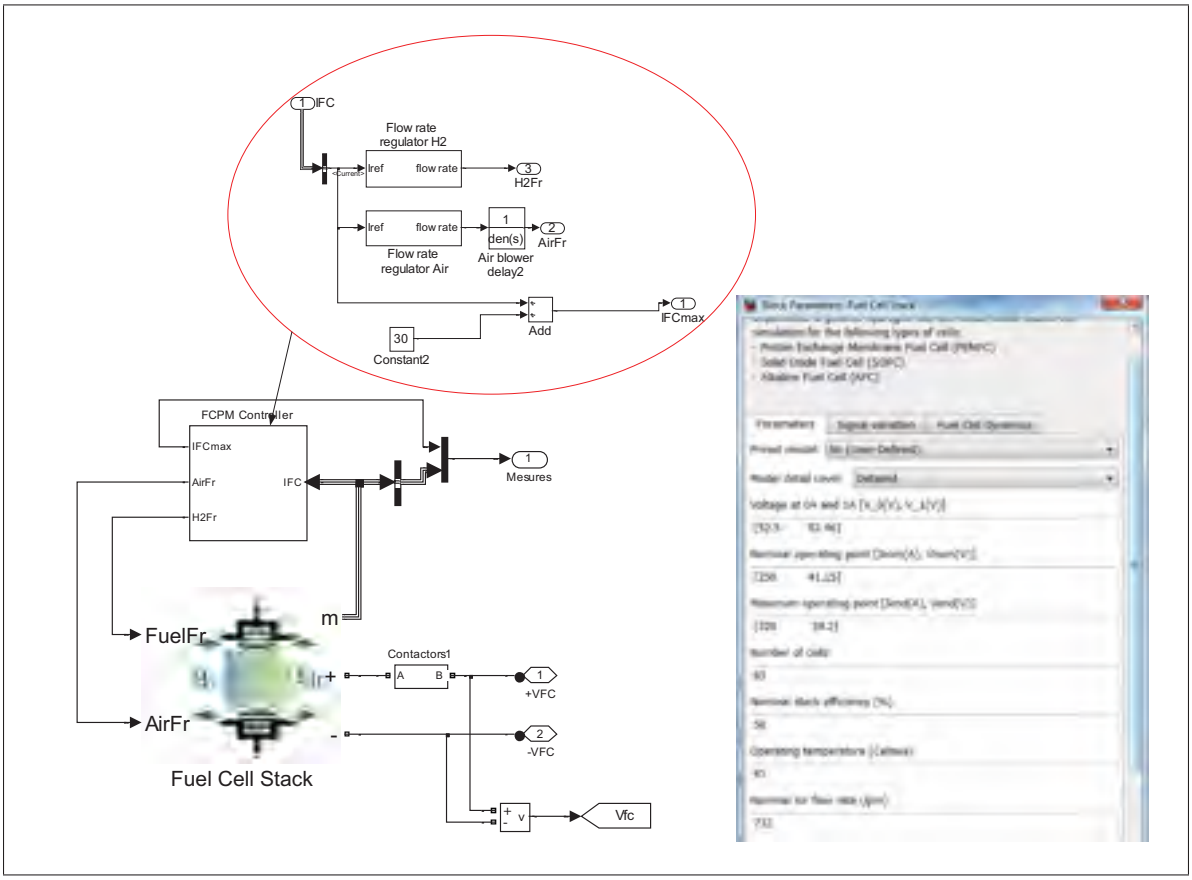

Figure-A I-1 The fuel cell model in SPS and interface

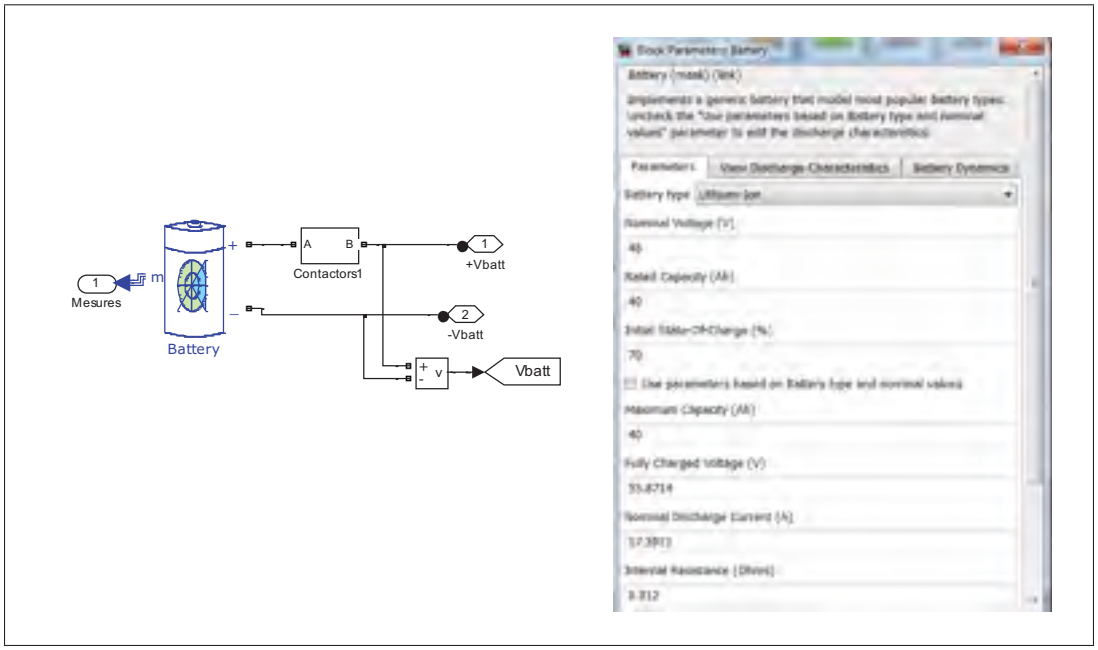

Figure-A I-2 The battery model in SPS and interface

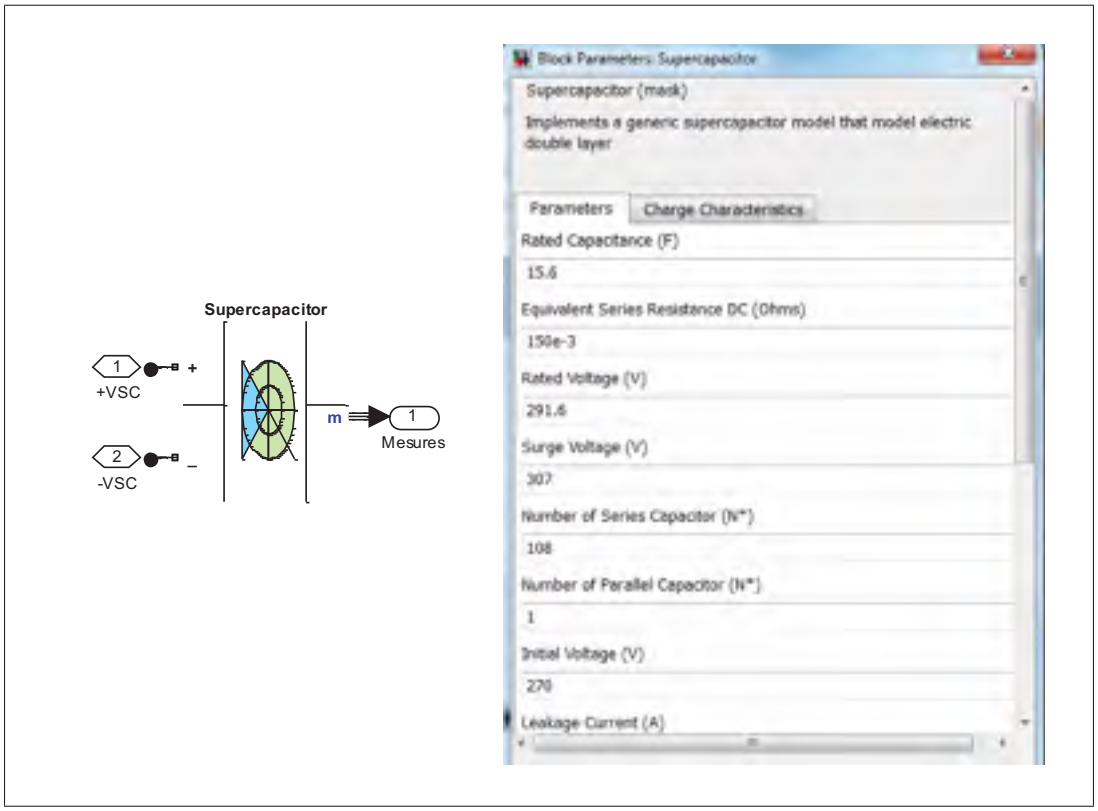

Figure-A I-3 The supercapacitor model in SPS and interface

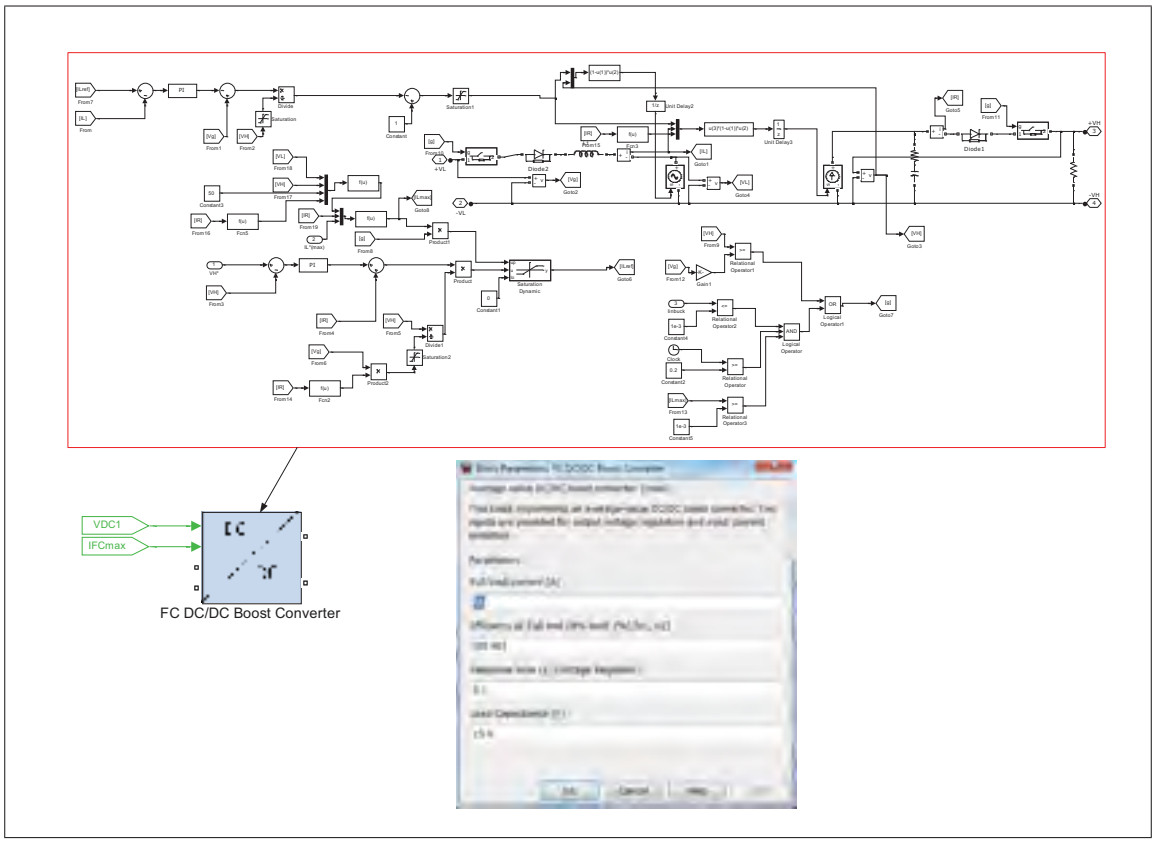

Figure-A I-4 The DC/DC boost converter model in SPS and interface

2 Power converter models

The model of the boost DC/DC converter, buck DC/DC converter and inverter are shown in Figures-A I-4, I-5 and I-6 respectively. Their interfaces are also shown.

3 Emergency load model

The load model is shown in Figure-A I-7. A large resistor (10 KΩ) is used in parallel to improve the simulation stability.

4 Energy management schemes models

The EMS models are shown in the following sections.

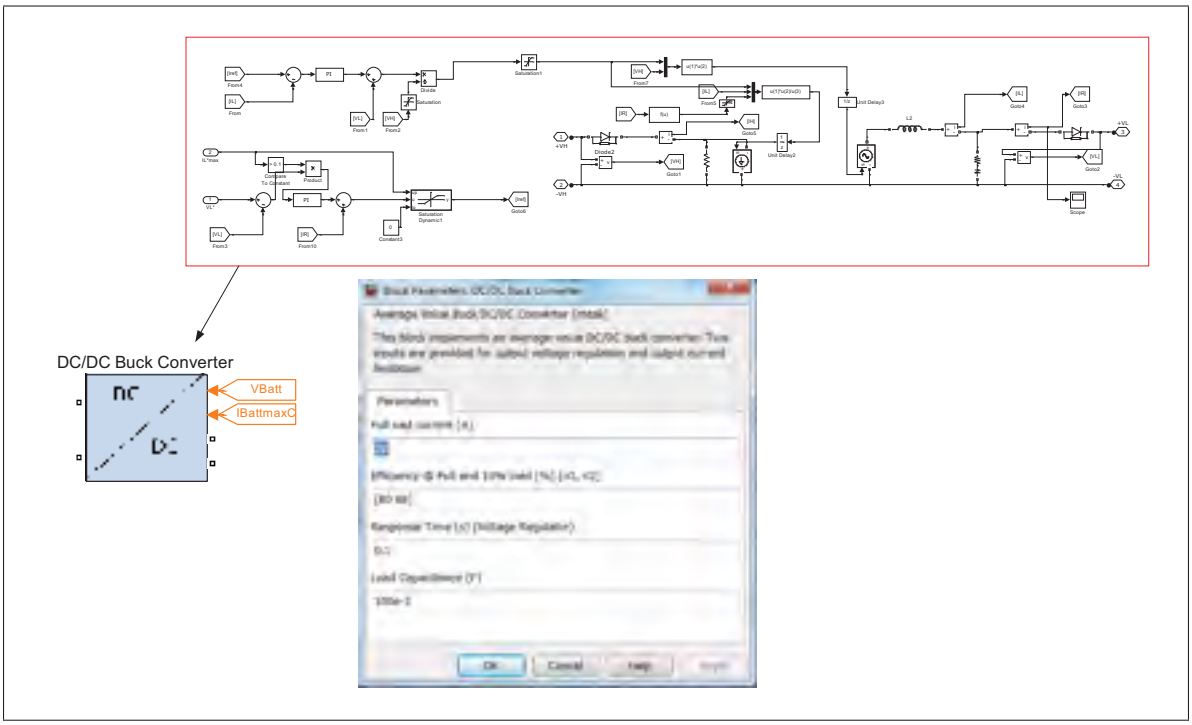

Figure-A I-5 The DC/DC buck converter model in SPS and interface

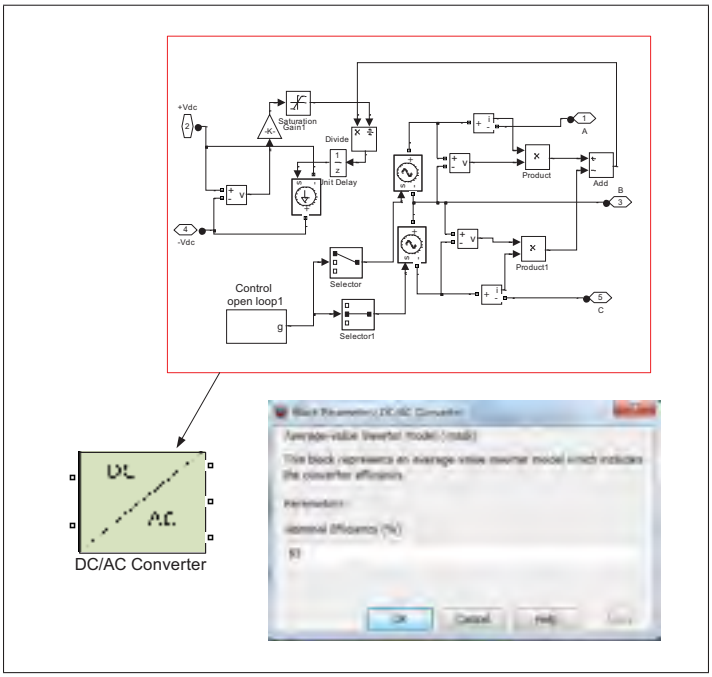

Figure-A I-6 The DC/AC converter model in SPS and interface

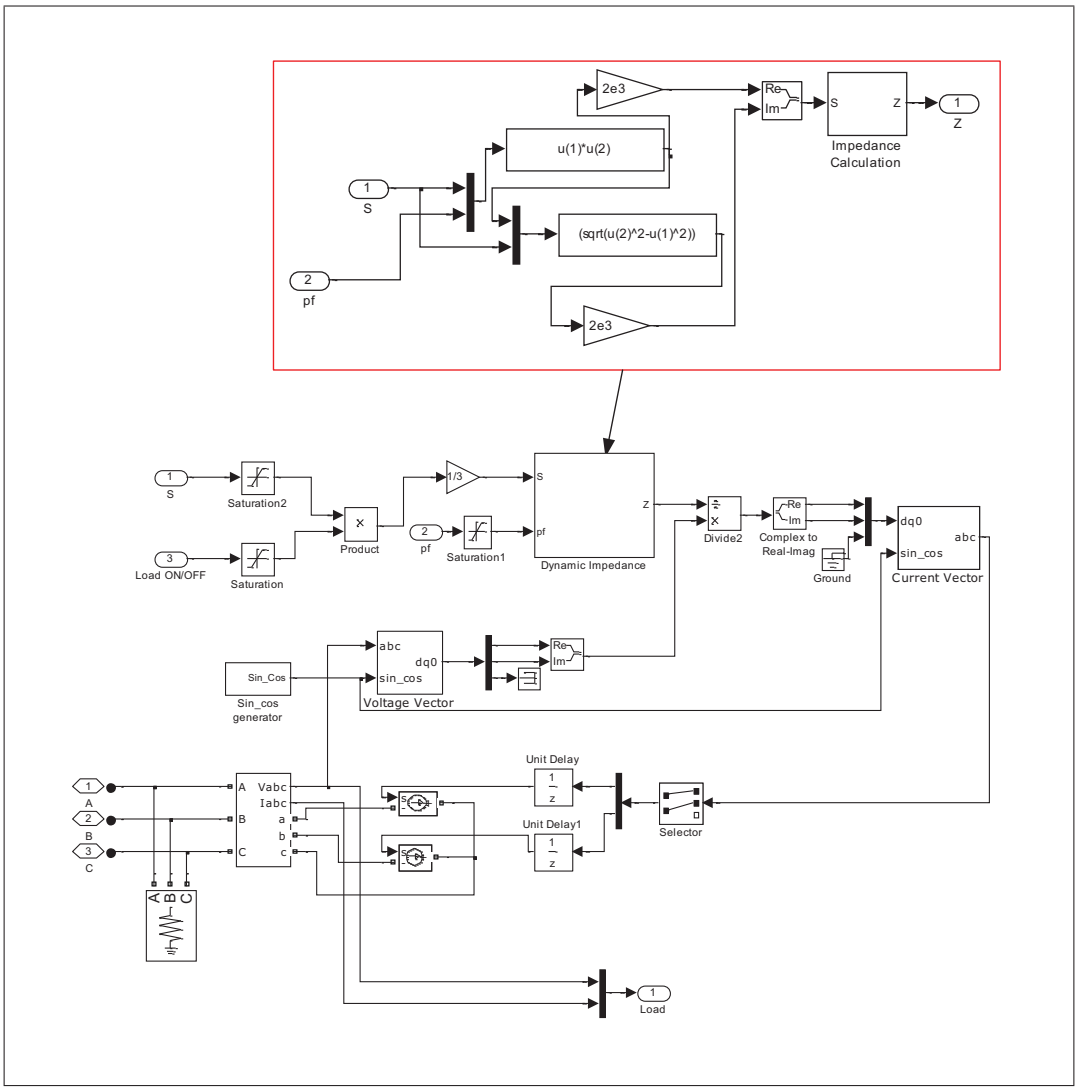

Figure-A I-7 The load model in SPS

4.1 State machine control strategy EMS model

The state machine control EMS model is shown in Figure-A I-8. The algorithm implemented is shown in Figure-A I-9. The third input to the control algorithm is the actual state, which is required for the implementation of the hysteresis control.

4.2 Rule based fuzzy logic strategy EMS model

The rule based fuzzy logic EMS model is shown in Figure-A I-10.

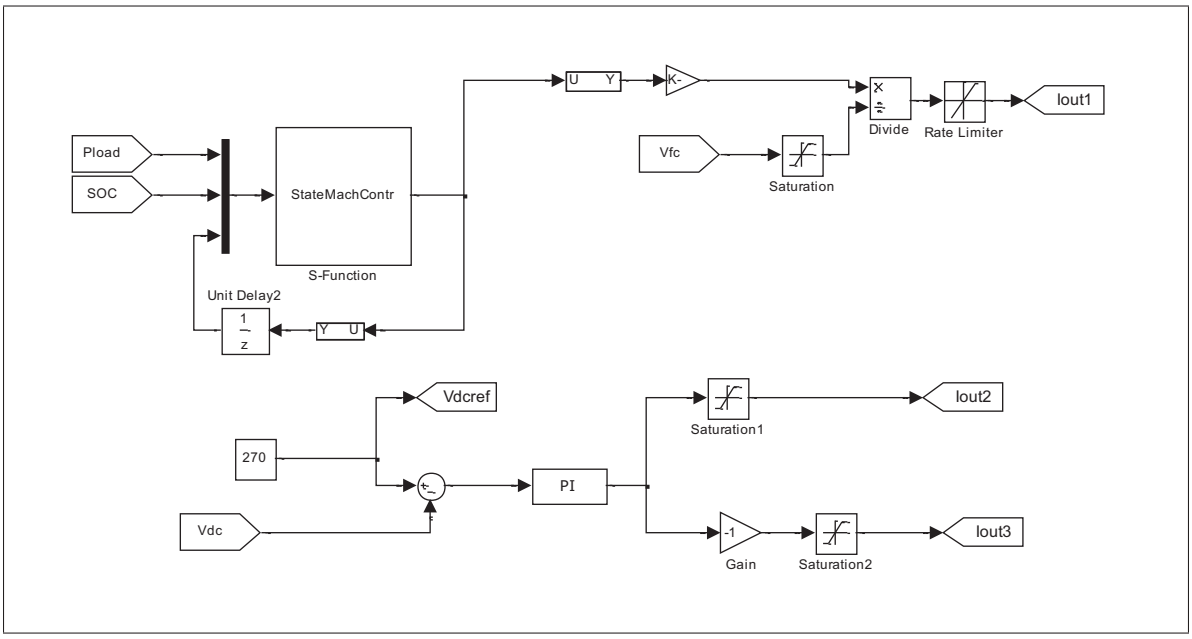

Figure-A I-8 State machine control EMS model

4.3 Classical PI control strategy EMS model

The classical PI control EMS model is shown in Figure-A I-11.

4.4 Frequency decoupling and fuzzy logic strategy EMS model

The frequency decoupling and fuzzy logic EMS model is shown in Figure-A I-12.

4.5 ECMS EMS model

The ECMS EMS model is shown in Figure-A I-13. The algorithm implemented is shown in Figure-A I-14.

4.6 EEMS EMS model

The EEMS EMS model is shown in Figure-A I-15. The algorithm implemented is shown in Figure-A I-16.

```
function sys=mdlOutputs(t,x,u)
%constants initialization
Pbatt_char=1500;
SOC_min=60; SOC_max=90;
SOC_nom1=85;SOC_nom2=65;Pfc_min=850;Pfc_max=8800;
Pfc_opt=1500;Pbatt_max=3400;

if(u(2)>SOC_max)
    state=1;
end
if(u(2)>=SOC_nom2 && u(2)<=SOC_nom1)
    state=2;
end
if(u(2)>SOC_nom1 && u(2)<=SOC_max)
    state=u(3);
end
if(u(2)<SOC_min)
    state=3;
end
if(u(2)>=SOC_min && u(2)<SOC_nom2)
    state=u(3);
end

%state 1
if(state==1 && u(1)<Pfc_min)
            Pfc=Pfc_min;

end


%state 2

if(state==1 && u(1)>=Pfc_min && u(1)<Pfc_max)
            Pfc=u(1);

end

%state 3

if(state==1 && u(1)>=Pfc_max)
            Pfc=Pfc_max;

end
if(state==2 && u(1)<Pfc_min)
            Pfc=Pfc_min;

end

%state 4
if(state==2 && u(1)>=Pfc_min && u(1)<Pfc_opt)
            Pfc=Pfc_opt;
end

%state 5

if(state==2 && u(1)>=Pfc_opt && u(1)<Pfc_max)
            Pfc=u(1);

end
%state 6

if(state==2 && u(1)>=Pfc_max)
            Pfc=Pfc_max;

end


if(state==3 && u(1)<Pfc_min)
            Pfc=u(1)+Pbatt_char;

end
%state 7

if(state==3 &&  u(1)>=Pfc_min && u(1)<Pfc_opt)
            Pfc=max(u(1)+Pbatt_char,Pfc_opt);

end

%state 8

if(state==3 && u(1)>=Pfc_opt && u(1)<Pfc_max)
            Pfc=u(1)+Pbatt_char;
            %Pfc=Pfc_max;

end

%state 9

if(state==3 && u(1)>=Pfc_max)
            Pfc=Pfc_max;

end


sys = [Pfc state];
```

Figure-A I-9 State machine control algorithm

4.7 The off-line optimization algorithm

The off-line optimization algorithm is shown in Figure-A I-17.

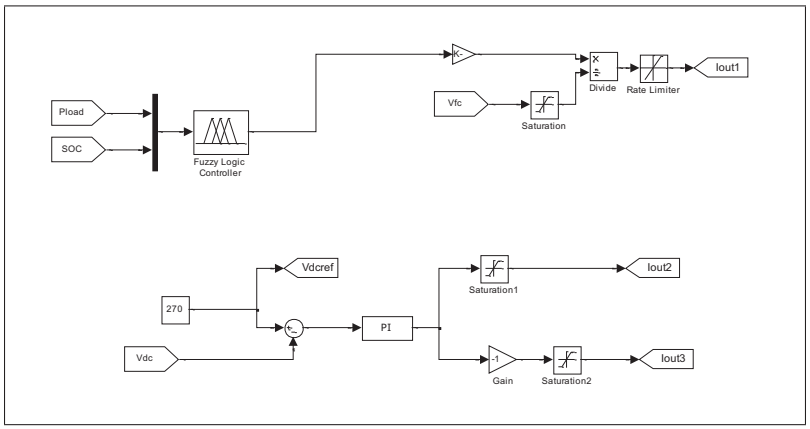

Figure-A I-10 Rule based fuzzy logic EMS model

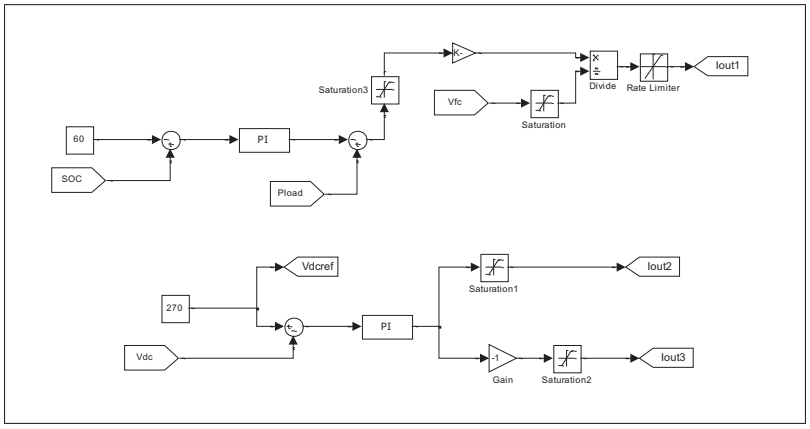

Figure-A I-11 Classical PI control EMS model

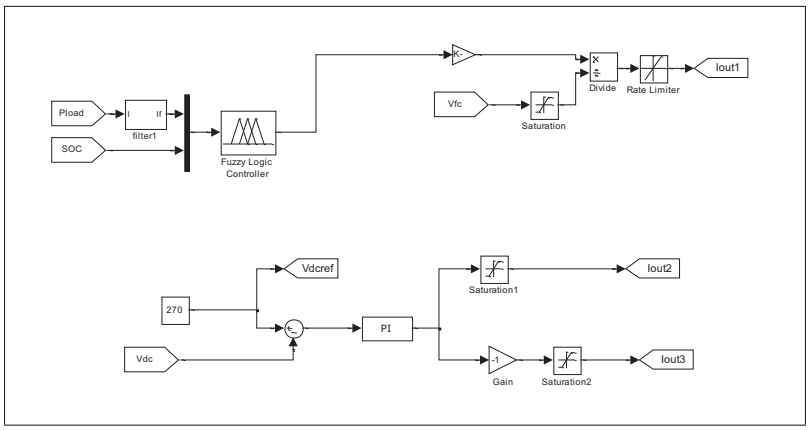

Figure-A I-12 Frequency decoupling and fuzzy logic EMS model

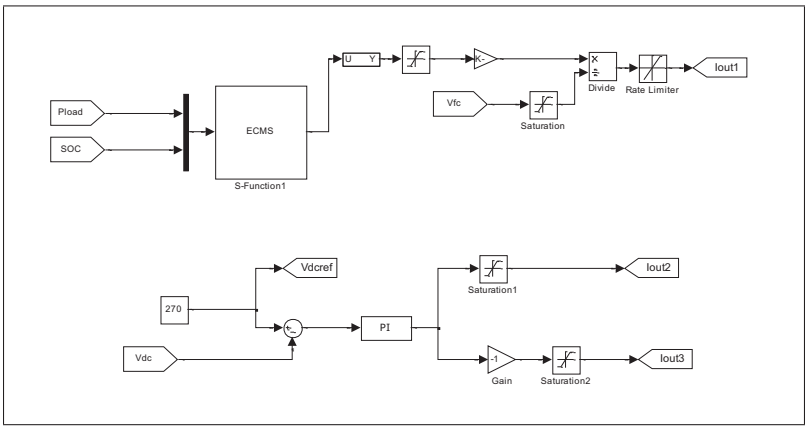

Figure-A I-13 ECMS EMS model

```
function sys=mdlOutputs(t,x,u)
%constants initialization
Pbatt_char=1500;
SOC_min=60; SOC_max=90; Pfc_min=850;Pfc_max=8800;
Pbatt_max=3400;

%define Matrix Aeq

Aeq=[0 1 0;1 0 1];

%define Matrix beq
mu=0.6;
beq=[1-2*mu*((u(2)-0.5*(SOC_max+SOC_min))/
(SOC_max+SOC_min)); u(1)];

%define boundary conditions
lb=[Pfc_min, 0, -Pbatt_char];
ub=[Pfc_max, 100, Pbatt_max];

%define initial conditions
%x0=[Pfc_min, 0, 0];
x0=[3000, 0.1, 3000];
[y,fval] =
fmincon(@myfun3,x0,[],[],Aeq,beq,lb,ub);

Pfc=y(1); Pbatt=y(3); alpha=y(2);


sys = [Pfc Pbatt alpha];
```

```
function f = myfun3(x)
DT=200e-3;
f = (x(1)+x(2)*x(3))*DT;
```

Figure-A I-14 ECMS control algorithm

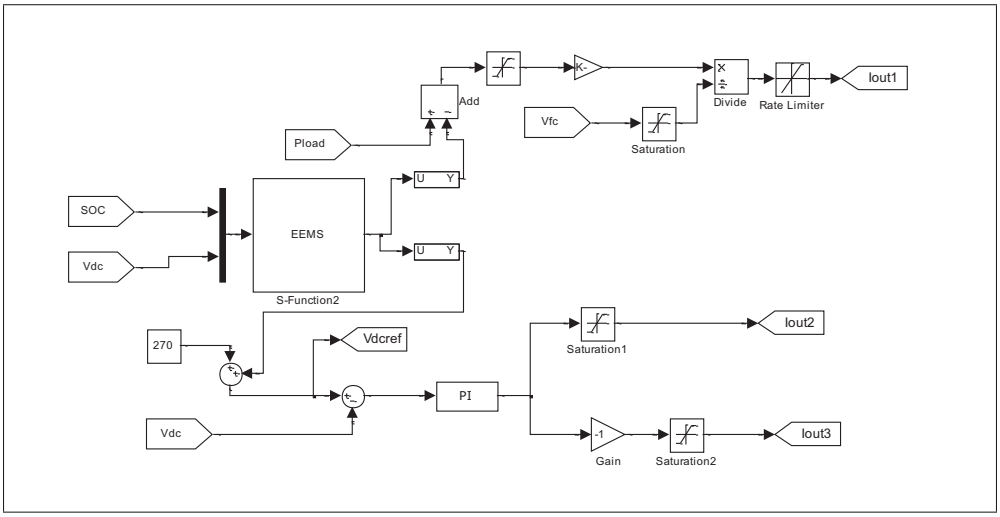

Figure-A I-15 EEMS EMS model

```
function sys=mdlOutputs(t,x,u)
%constants initialization
Pbatt_char=1500; Pbatt_max=3400;
SOC_min=60; Q=36*40;DV_min=-2; DV_max=2;
DT=200e-3; Vbatt_nom=48;Vdc_min=268;
% define matrix A

A = [DT 0;0 -1];

%define matrix b

b =[(u(1)-SOC_min)*Vbatt_nom*Q; u(2)-Vdc_min];
%define boundary conditions
lb=[-Pbatt_char, DV_min];
ub=[Pbatt_max, DV_max];
%define initial conditions
x0=[Pbatt_max, DV_min];
[y,fval] = fmincon(@myfun,x0,A,b,[],[],lb,ub);
Pbatt=y(1); DV=y(2);
sys = [Pbatt DV];
```

```
function f = myfun(x)
DT=200e-3;C=15.6;
f = -x(1)*DT- 0.5*C*x(2)^2;
```

Figure-A I-16 EEMS control algorithm

```
Tp=1800;
DT=1;
N=1:DT:1800;
Pfc_min=850; Pfc_max=8800;
x0=Pfc_min*ones(1,length(N));
%defining matrix A
A=zeros(length(N),length(N));
Ab=zeros(length(N),length(N));
for i=1:length(N)
    for j=1:i
        A(i,j)=-DT;
        Ab(i,j)=1;
    end
end

%defining matrix b
b=zeros(length(N),1);
y=zeros(length(N),1);
Pload=load('Pload.txt');
Pload=Pload'*1e3;
SOC0=70; SOC_min=56.9;Q=40*36; Vbatt_nom=48;

y=Ab*Pload';
for i=1:length(N)
    b(i,1)=(SOC0-SOC_min)*Vbatt_nom*Q-y(i)*DT;
end
% add the energy constraint
%Fuel cell minimum energy s
Efc_min=sum(x0)*DT;
b(length(N),1)=-Efc_min;
lb=Pfc_min*ones(1,length(N));
ub=Pfc_max*ones(1,length(N));
%options=optimset('MaxIter', 10);
[x,fval] = fmincon(@myfun2,x0,A,b,[],[],lb,ub);
SOC=SOC0-(A*x'+y)/(Vbatt_nom*Q);
ConsH2=fval*242/(7100*1800);
```

```
function f = myfun2(x)
DT=1;
f = sum(x)*DT;
```

Figure-A I-17 Off-line optimization algorithm

APPENDIX II

CONTROL AND MONITORING SOFTWARE DESCRIPTION

The control and monitoring software is implemented in LabVIEW real time and its main interface is shown in Figure-A II-1. It includes menu to send commands to the FCPM, the load, the DC/DC converters and the protecting resistor relay. Also, a menu is provided to select the energy management scheme to be tested. The load profile can be provided either in tabular form or from an external file. Indicators are used for warning in case of any device fault or H_2 leaks. Windows are provided to view more information on the FCPM (Figure-A II-2), battery system (Figure-A II-3) and the DC/AC programmable load. This section briefly presents the LabVIEW block diagrams developed for the communication, control and data acquisition. Also the top level LabVIEW block diagrams for the EMS implemented are presented.

5 Drivers for communication/data acquisition

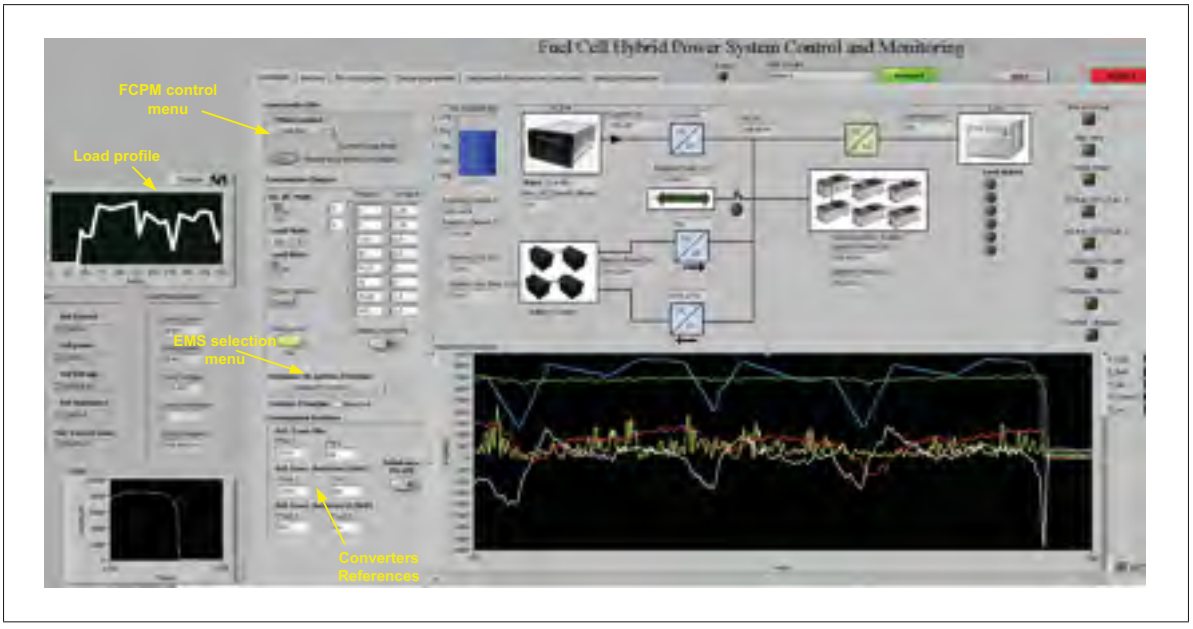

Figure-A II-1 Control and monitoring software main interface

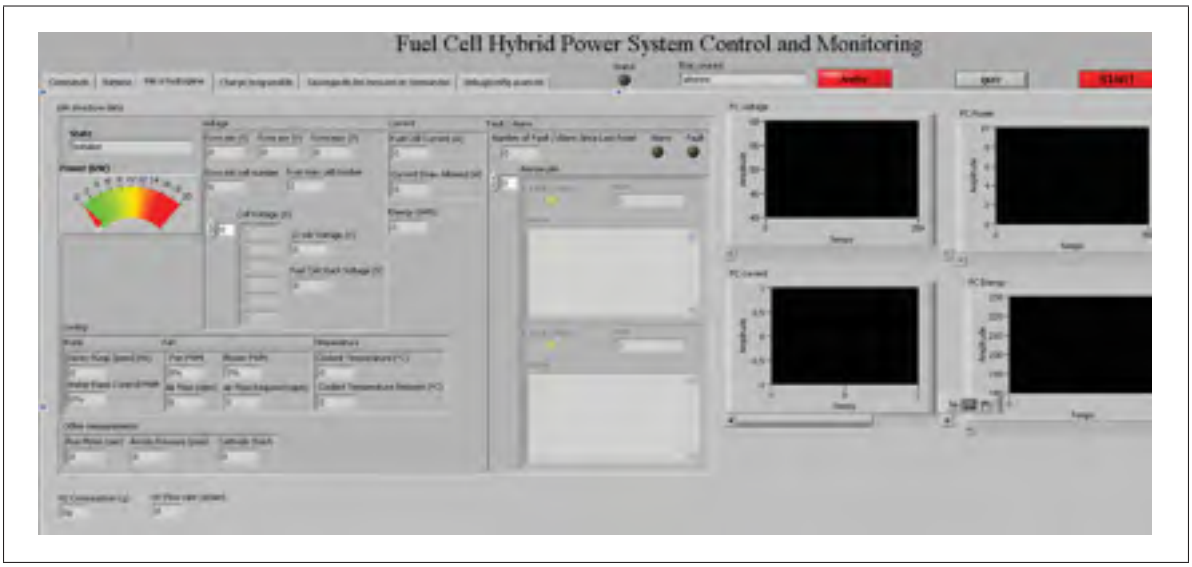

Figure-A II-2 FCPM interface

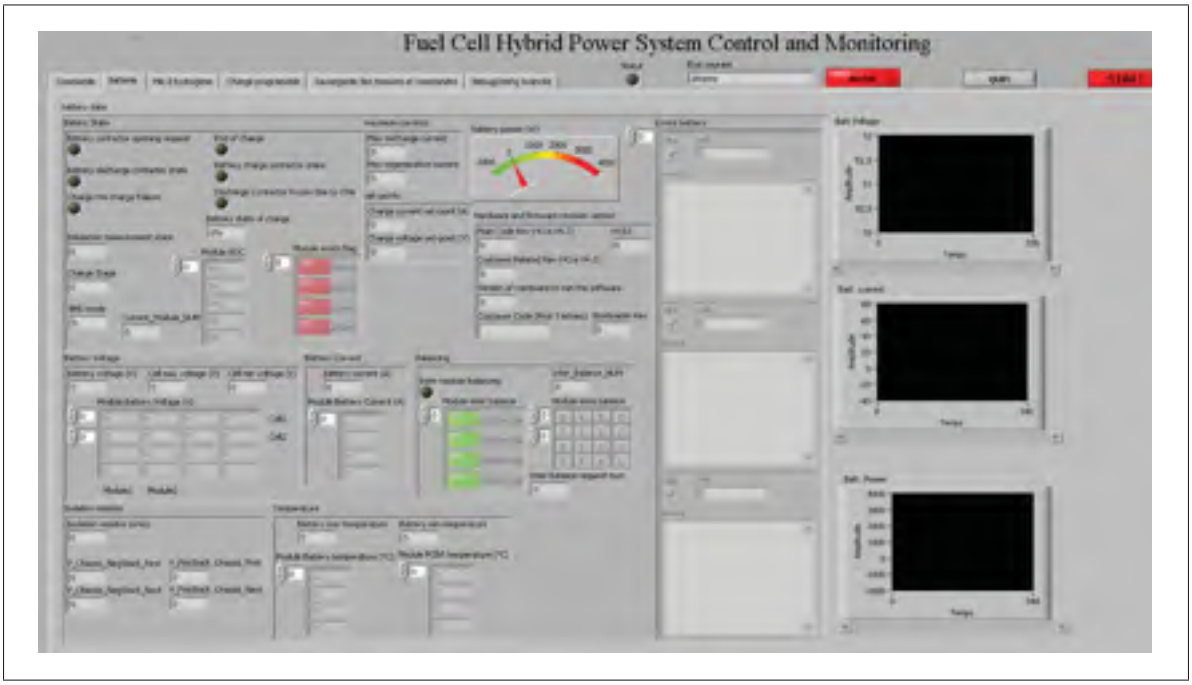

Figure-A II-3 Battery modules interface

Using the “CAN specifications” for the FCPM and the BMS, and “GPIB specifications” for the DC/AC programmable load, the drivers required for communication and control of each device were developed. The LabVIEW block diagram of these drivers are shown in Figures-A

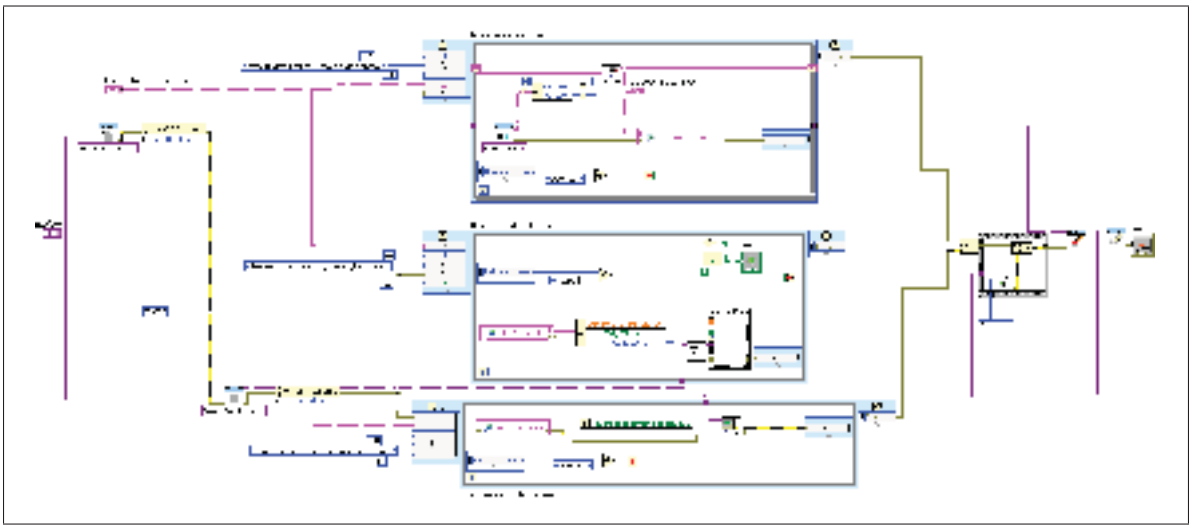

Figure-A II-4 FCPM communication and control LabVIEW code

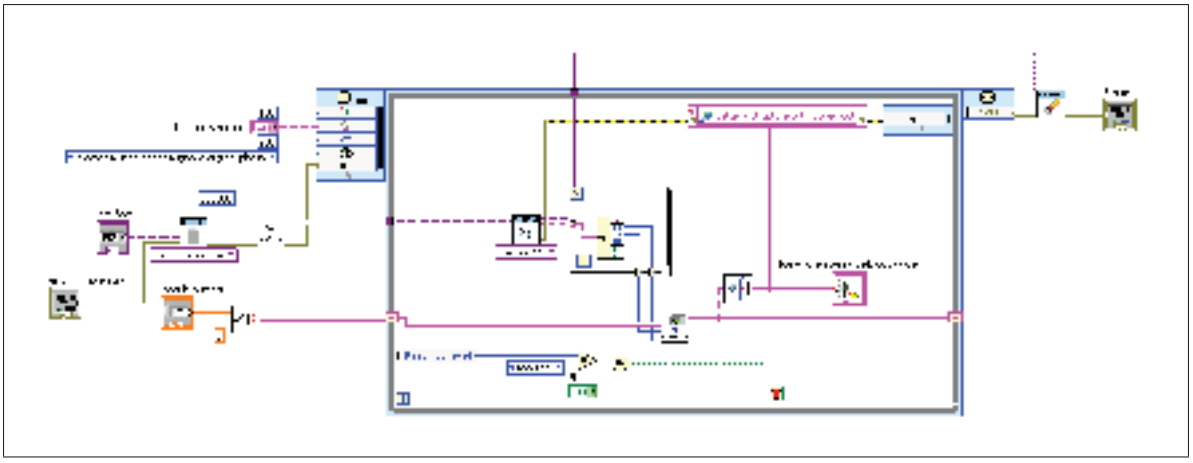

Figure-A II-5 BMS communication LabVIEW code

II-4, II-5 and II-6 for the FCPM, BMS and load respectively. The data acquisition drivers for the NI-DAQs were also developed as shown in Figure-A II-7.

6 EMS LabVIEW block diagram

The EMS LabVIEW VI block diagrams are presented in the following sections (for simplification, only top level diagrams are shown).

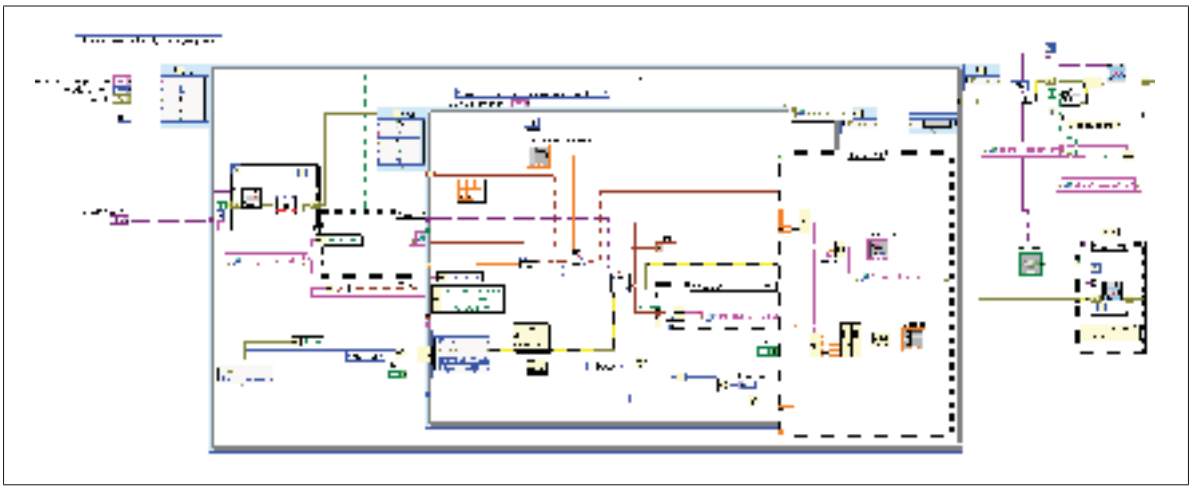

Figure-A II-6 DC/AC programmable load communication and control LabVIEW code

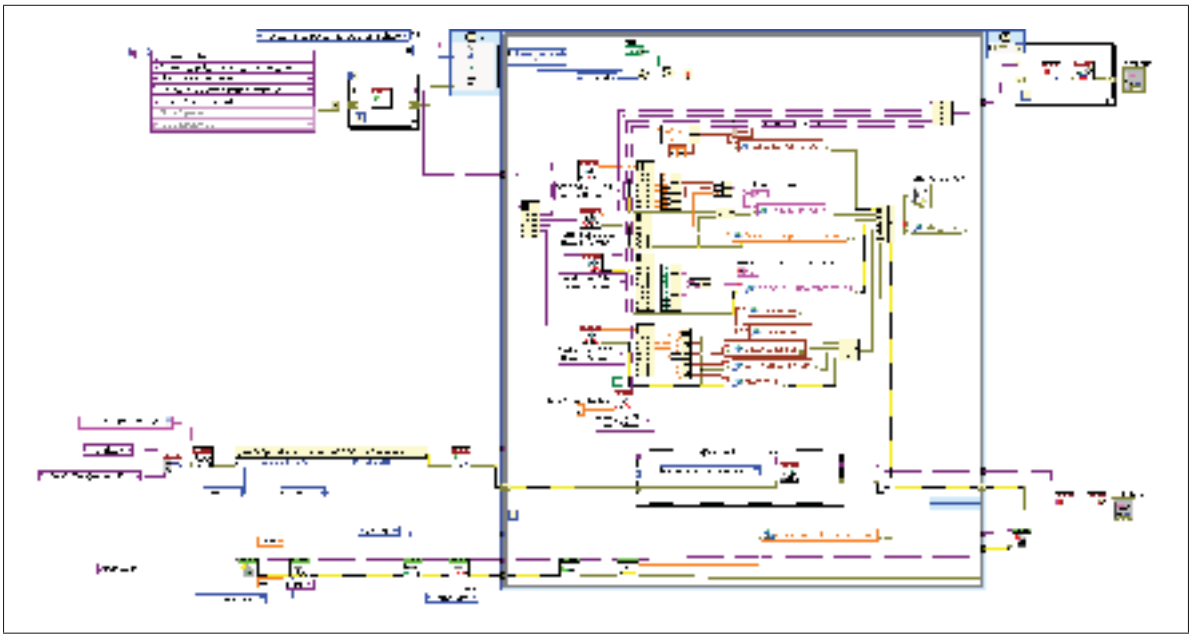

Figure-A II-7 Data acquisition for NI-DAQs LabVIEW code

6.1 State machine control EMS LabVIEW code

The state machine control EMS LabVIEW code is shown in Figure-A II-8.

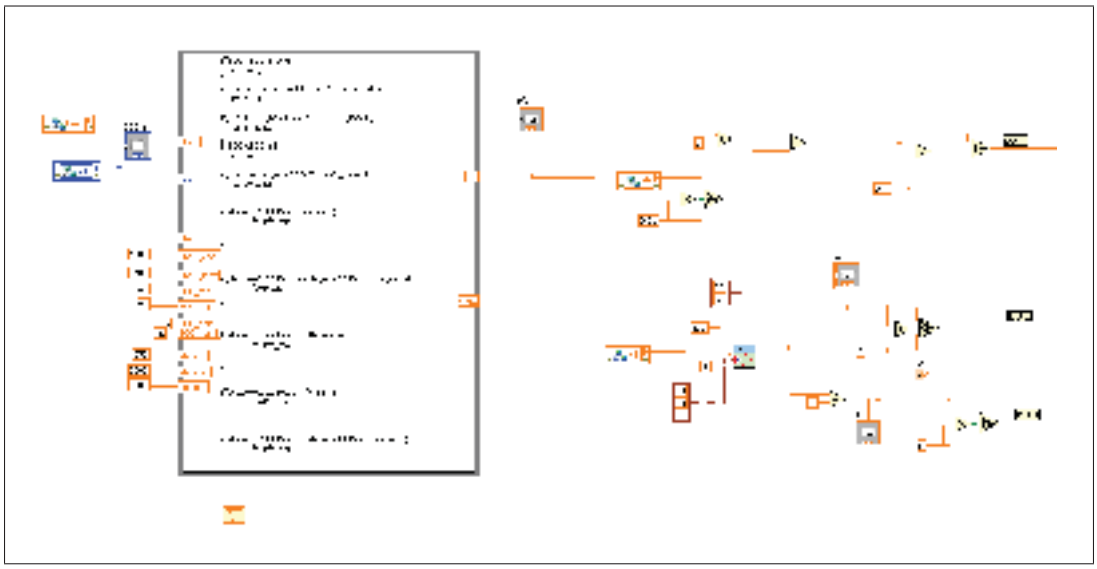

Figure-A II-8 State machine control EMS LabVIEW code

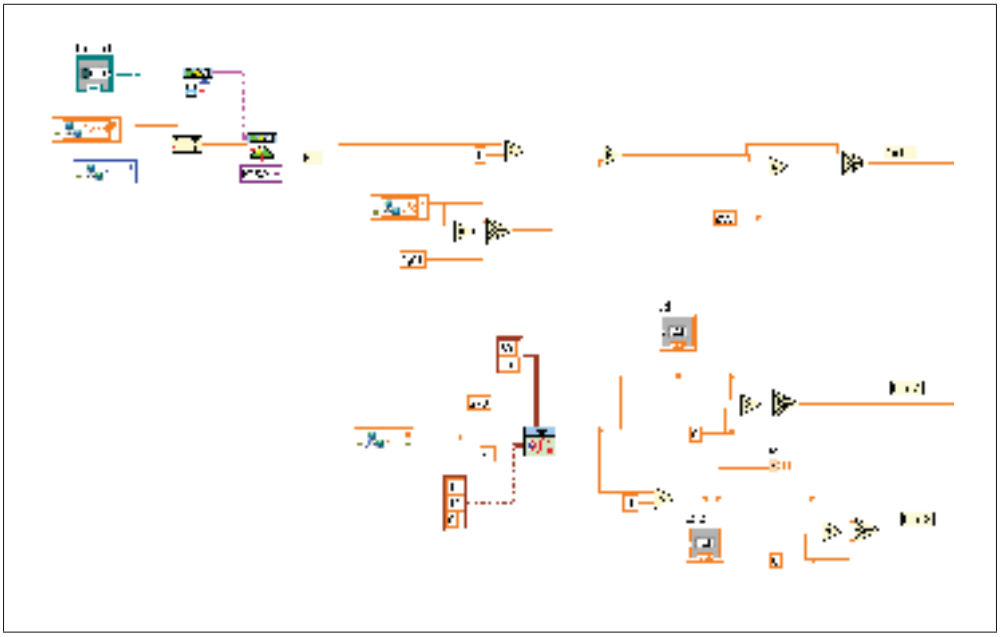

Figure-A II-9 Rule based fuzzy logic EMS LabVIEW code

6.2 Rule based fuzzy logic EMS LabVIEW code

The rule based fuzzy logic EMS LabVIEW code is shown in Figure-A II-9.

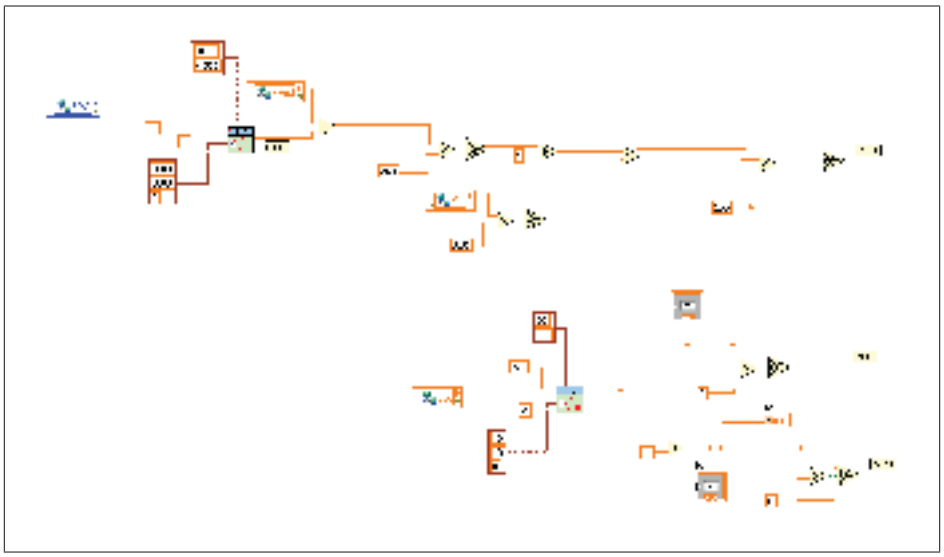

Figure-A II-10 Classical PI control EMS LabVIEW code

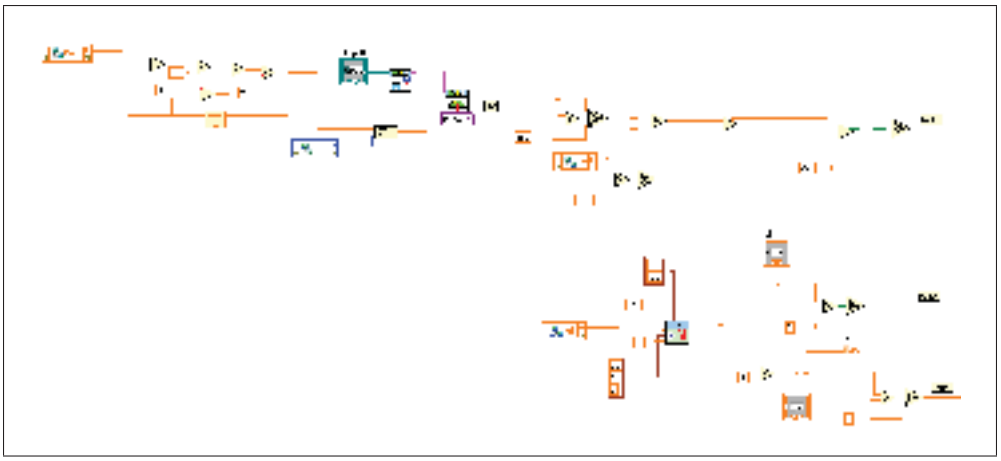

Figure-A II-11 Frequency decoupling and fuzzy logic EMS LabVIEW code

6.3 Classical PI control EMS LabVIEW code

The classical PI control EMS LabVIEW code is shown in Figure-A II-10.

6.4 Frequency decoupling and fuzzy logic EMS LabVIEW code

The frequency decoupling and fuzzy logic EMS LabVIEW code is shown in Figure-A II-11.

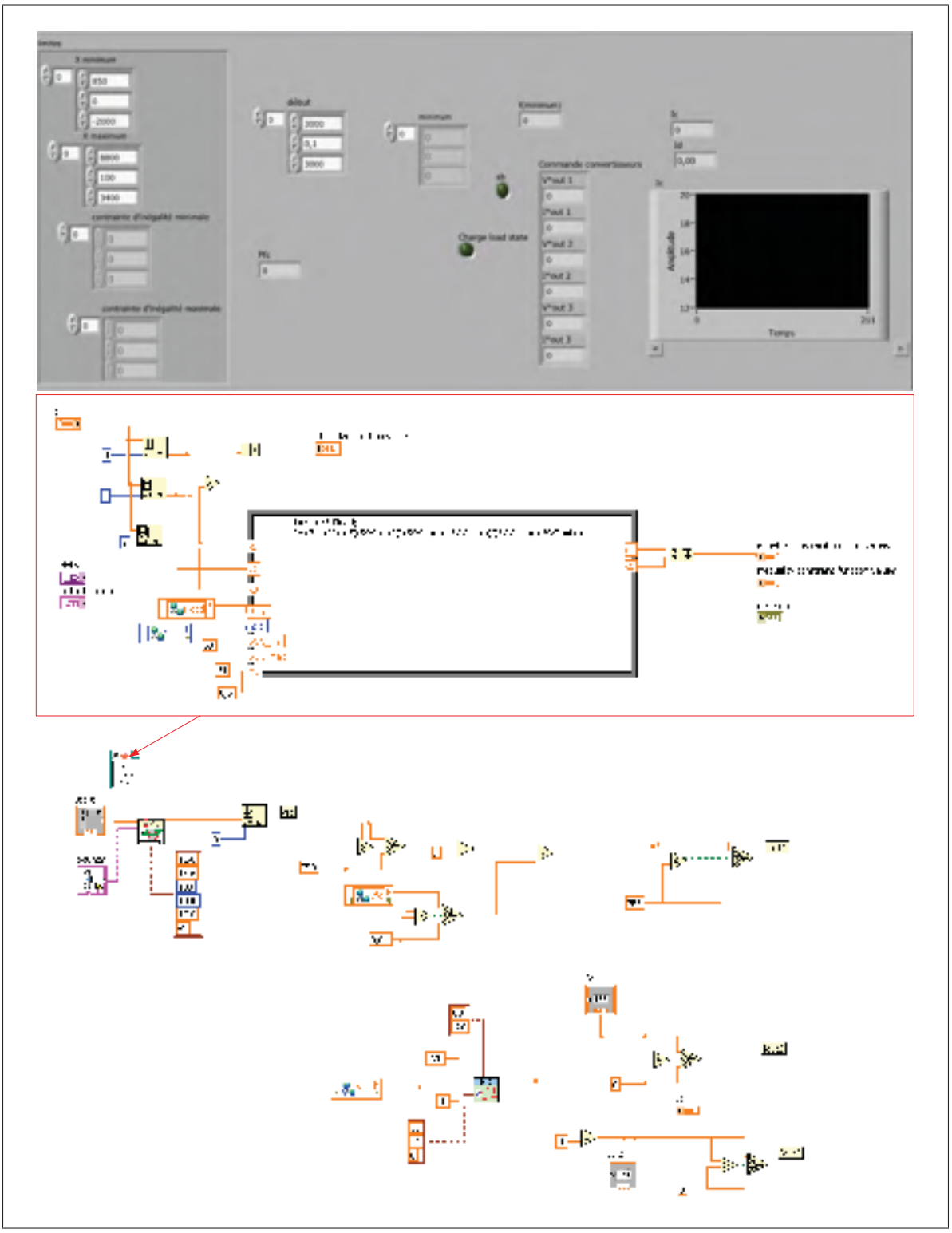

Figure-A II-12 ECMS EMS LabVIEW code

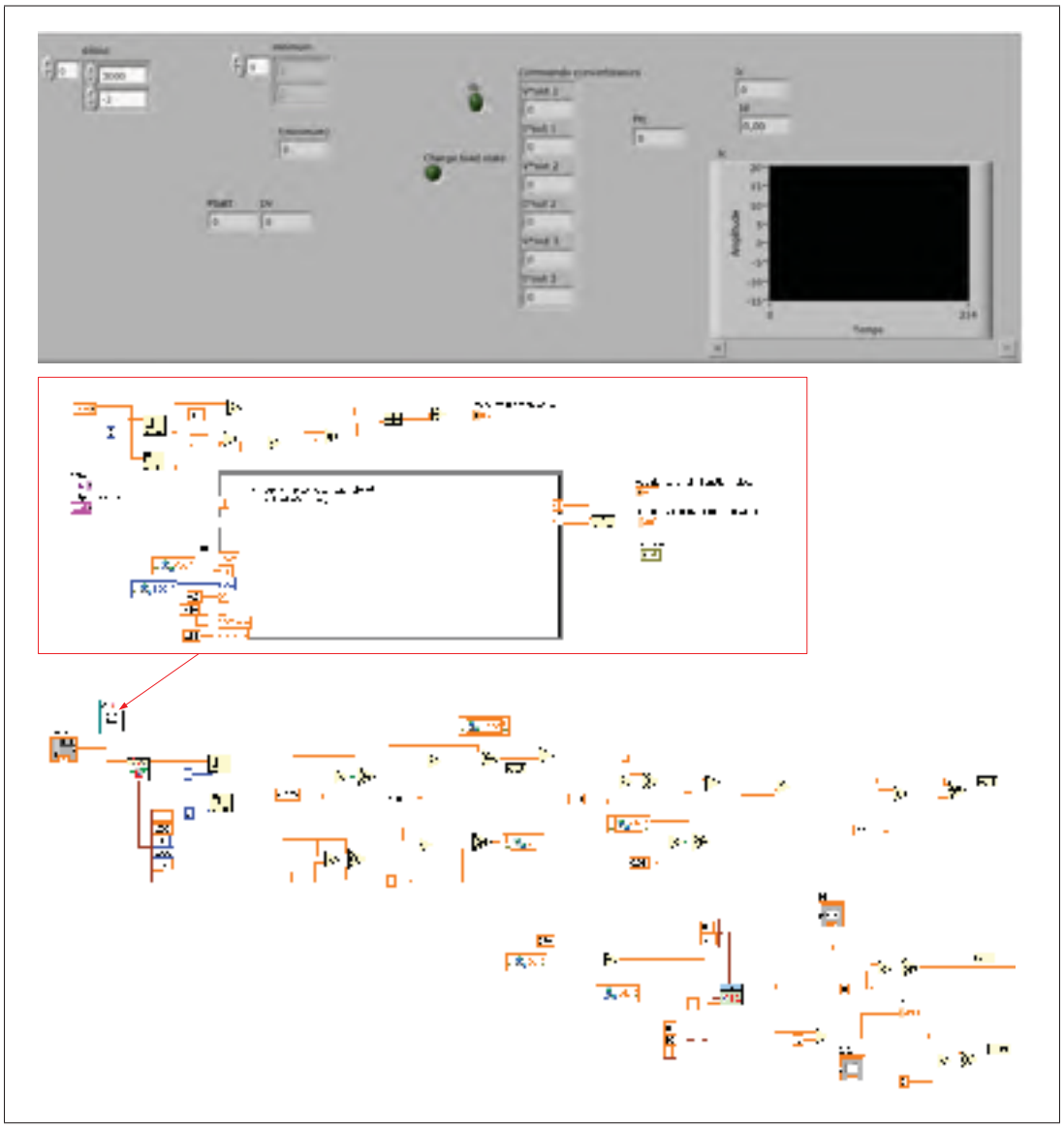

Figure-A II-13 EEMS EMS LabVIEW code

6.5 ECMS EMS LabVIEW code

The ECMS EMS LabVIEW code is shown in Figure-A II-12.

6.6 EEMS EMS LabVIEW code

The EEMS EMS LabVIEW code is shown in Figure-A II-13.

APPENDIX III

COMPONENTS SPECIFICATIONS

This section presents the specifications of the energy source devices used in this study.

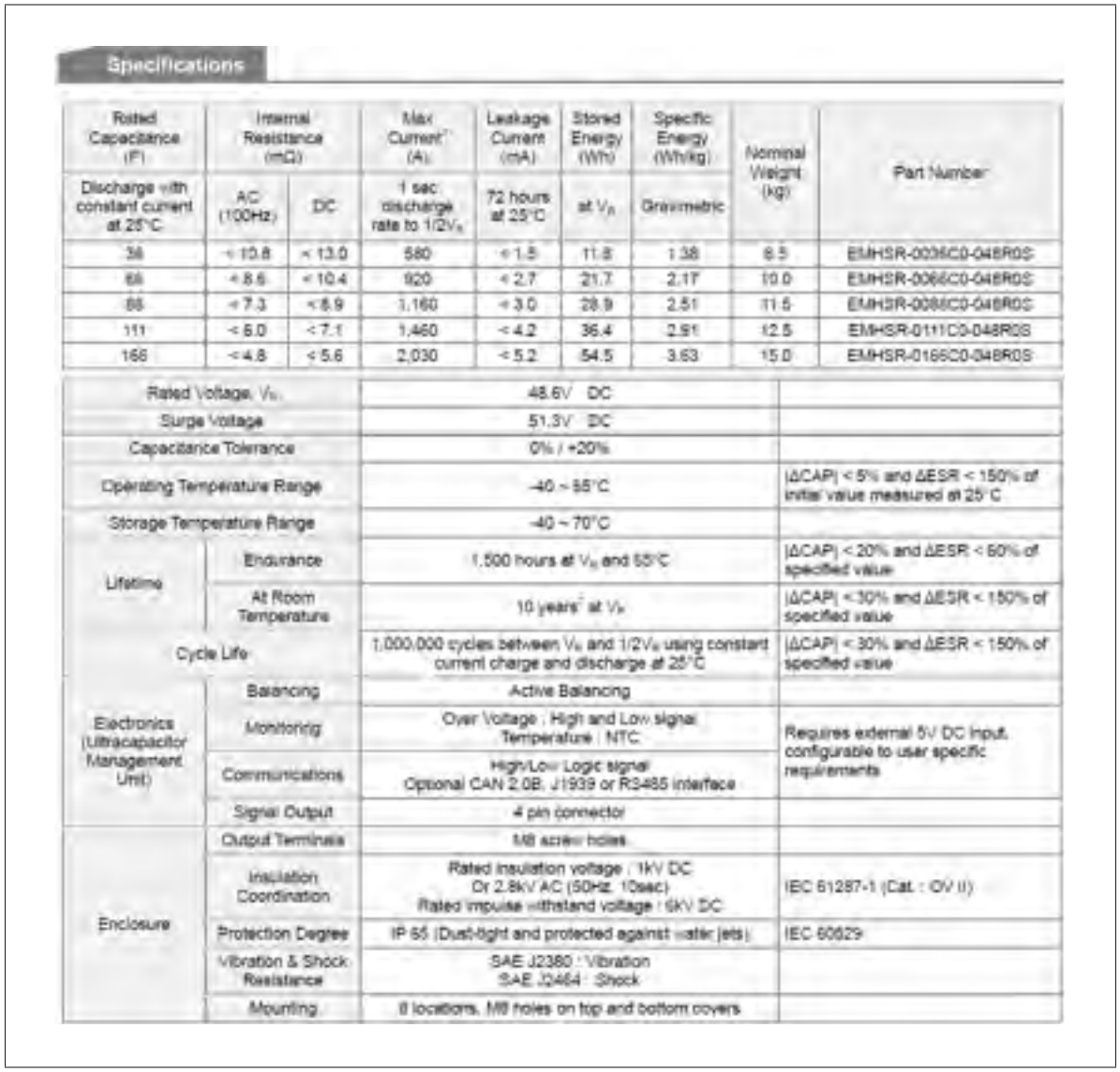

Specifications

Rated Capacitance (F)	Internal Resistance (mΩ)		Max Current* (A)	Leakage Current (mA)	Stored Energy (Wh)	Specific Energy (Wh/kg)	Nominal Weight (kg)	Part Number
Discharge with constant current at 25°C	AC (100Hz)	DC	1 sec discharge rate to 1/2V_R	72 hours at 25°C	at V_R	Gravimetric		
36	< 10.8	< 13.0	580	< 1.5	11.8	1.38	8.5	EMHSR-0036C0-048R0S
63	< 8.6	< 10.4	920	< 2.7	21.7	2.17	10.0	EMHSR-0063C0-048R0S
88	< 7.3	< 8.9	1,160	< 3.0	28.9	2.51	11.5	EMHSR-0088C0-048R0S
111	< 6.0	< 7.1	1,460	< 4.2	36.4	2.91	12.5	EMHSR-0111C0-048R0S
166	< 4.8	< 5.6	2,030	< 5.2	54.5	3.63	15.0	EMHSR-0166C0-048R0S

Rated Voltage, V_R		48.6V DC	
Surge Voltage		51.3V DC	
Capacitance Tolerance		0% / +20%	
Operating Temperature Range		-40 ~ 65°C	|ΔCAP| < 5% and ΔESR < 150% of initial value measured at 25°C
Storage Temperature Range		-40 ~ 70°C	
Lifetime	Endurance	1,500 hours at V_R and 65°C	|ΔCAP| < 20% and ΔESR < 60% of specified value
	At Room Temperature	10 years* at V_R	|ΔCAP| < 30% and ΔESR < 150% of specified value
Cycle Life		1,000,000 cycles between V_R and 1/2V_R using constant current charge and discharge at 25°C	|ΔCAP| < 30% and ΔESR < 150% of specified value
Electronics (Ultracapacitor Management Unit)	Balancing	Active Balancing	
	Monitoring	Over Voltage : High and Low signal Temperature : NTC	Requires external 5V DC input, configurable to user specific requirements
	Communications	High/Low Logic signal Optional CAN 2.0B, J1939 or RS485 interface	
	Signal Output	4 pin connector	
Enclosure	Output Terminals	M8 screw holes	
	Insulation Coordination	Rated insulation voltage : 1kV DC Or 2.8kV AC (50Hz, 10sec) Rated impulse withstand voltage : 6kV DC	IEC 61287-1 (Cat. : OV II)
	Protection Degree	IP 65 (Dust-tight and protected against water jets)	IEC 60529
	Vibration & Shock Resistance	SAE J2380 : Vibration SAE J2464 : Shock	
	Mounting	8 locations, M8 holes on top and bottom covers	

Figure-A III-1 Supercapacitor module specifications

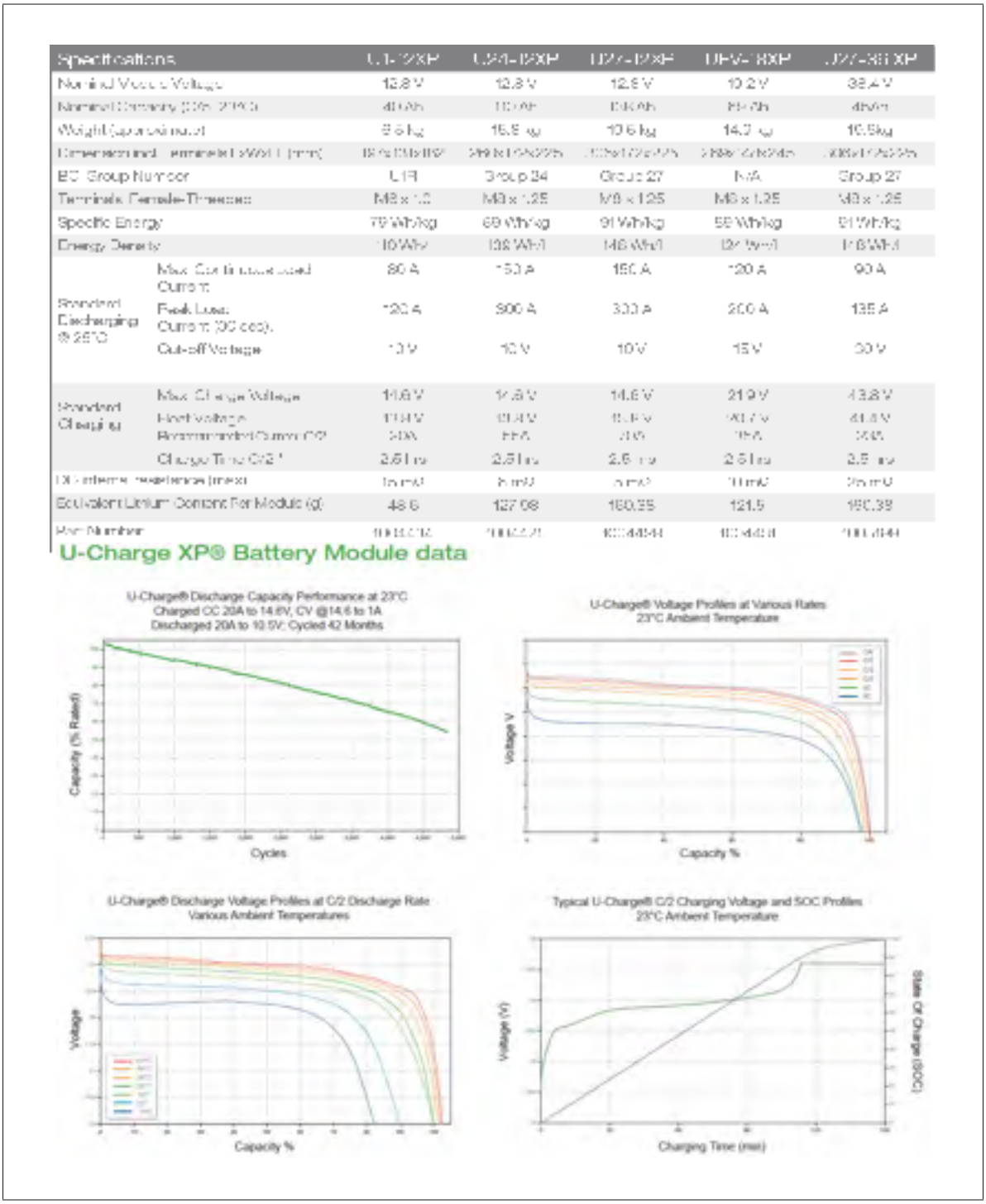

Figure-A III-2 Battery module specifications

Table 3-1: FCPM Technical Specifications

PROPERTY	UNIT	VALUE
PRODUCT INFORMATION		
Model Number		HyPM® HD 12
Part Number		1037312
PHYSICAL		
Dimensions of FCPM (L x W x H)[1]	mm	847 x 446 x 301
Mass[2]	kg	85
Volume of FCPM[3]	L	114
PERFORMANCE		
Rated Electrical Power[4]	kW	12.5
Maximum Electrical Overload		None permitted
Operating Current[4,5]	A_{dc}	0–380
Operating Voltage	V_{dc}	30–60
Peak Efficiency[6]	%	53
Time from Off Mode to Idle[7]	s	≤ 25
Time from Idle to Rated Power[7]	s	≤ 5
FUEL SYSTEM REQUIREMENTS		
Gaseous Hydrogen[8]	%	≥ 99.99
CO	µmol/mol	≤ 0.2
Sulfur (total, ex. H_2S, COS)	µmol/mol	≤ 0.004
Total Hydrocarbons	µmol/mol	≤ 2
Supply Pressure[9]	kPa	515–690
Stack Operating Pressure[9]	kPa	≤ 120
Consumption[10]	L/min	≤ 190
Hydrogen Temperature	°C	2–40

Figure-A III-3 Fuel cell power module specifications-1

Table 3-1: FCPM Technical Specifications

Property	Unit	Value
Fuel System Requirements		
Air Delivery System		
Maximum Air Flow Rate[11]	L/min	≤ 1300
Air Filtration[12]		Chemical and Particulate
Composition		Ambient Air
Sulfur	µmol/mol	≤ 0.004
Air Inlet Temperature	°C	2-40
Operating Environment		
Storage Air Temperature[13]	°C	-20–46
Ambient Air Temperature	°C	2–40
Maximum FCPM Interior Temperature[14]	°C	46
Relative Humidity (Operation and Storage)[15]	%	≤ 95
Altitude Range[16]	m	0-400
Orientation	°	±30
Emissions		
Allowable Pressure Drop of Customer Cathode Exhaust	kPa	≤ 3
Water Collected:[17]		
Anode	mL/min	≤ 18
Cathode	mL/min	≤ 24
Noise[18]	dBA	≤ 70

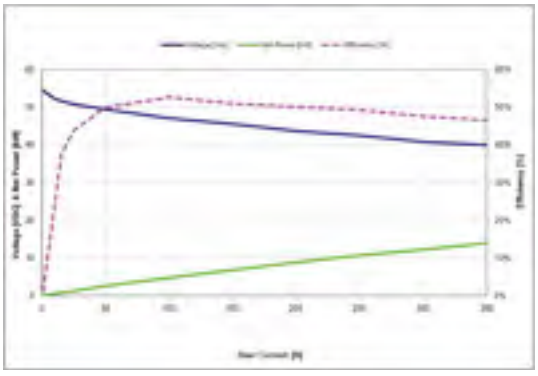

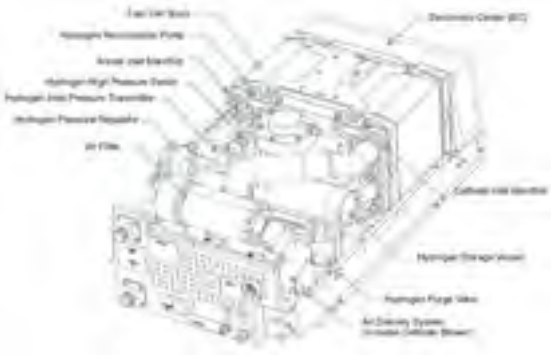

Figure-A III-4 Fuel cell power module specifications-2

APPENDIX IV

RAT POWER SEQUENCE

This section presents the RAT power sequence (Figure-A IV-1) during a 5 min. emergency situation. The loads to be supplied by the emergency power system are also presented in Figure-A IV-2 along with the description of each event and time of occurrence. Figures-A IV-3-IV-5 show the power flow sequence during a typical emergency situation. As observed, when the main generators are loss, the essential loads are supplied by the Avionic and APU battery systems till the RAT is fully deployed.

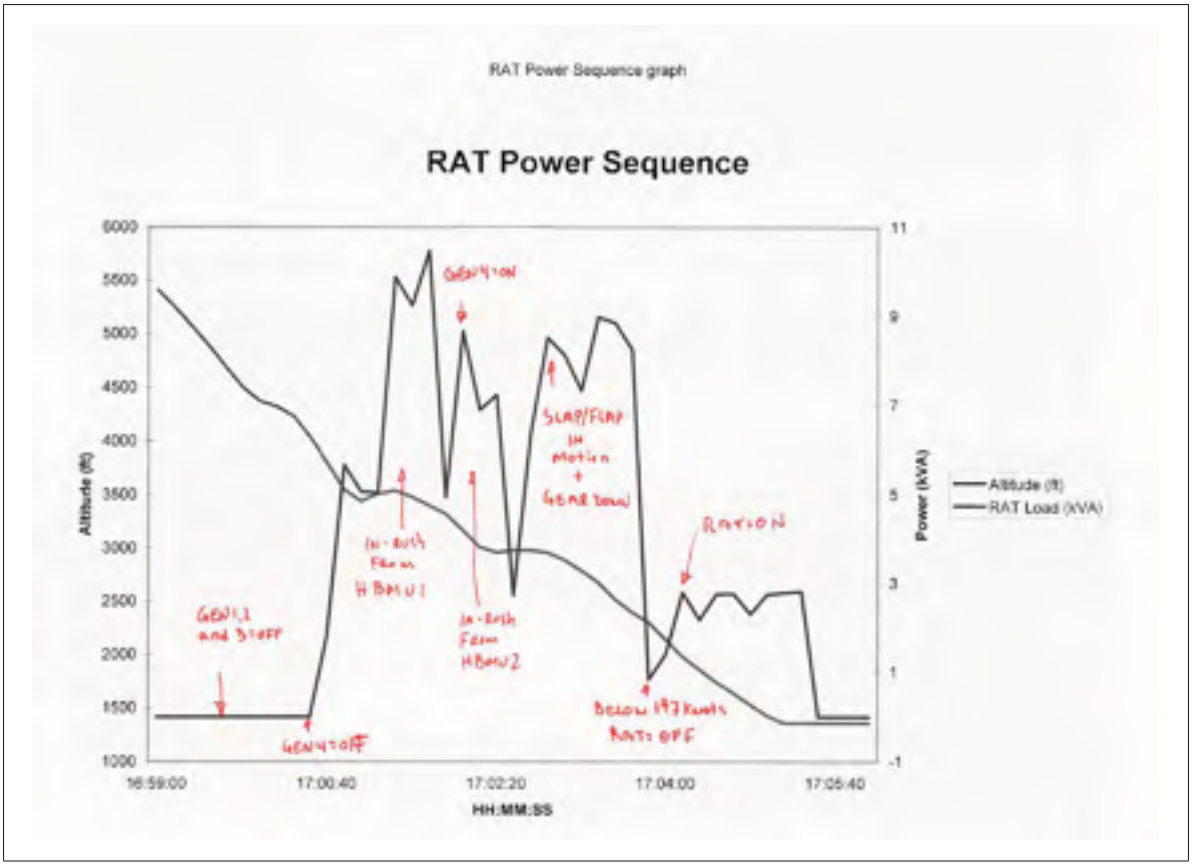

Figure-A IV-1 RAT power

Time	Event
16:59:50	Gen 1 = OFF
17:00:00	Gen 2 and Gen 3 = OFF
17:00:30	Gen 4 = OFF; AV Battery and APU Battery = ON
17:00:50	RAT = ON; AV Battery and APU Battery = OFF
17:01:00	HBMU 1 = In-rush power
17:02:00	HBMU 2 = In-rush power
17:02:50	Flap/Slat in motion
17:03:06	Gear down
17:03:20	Flap/Slat in motion
17:03:50	RAT OFF (below 147 knots)
17:04:10	RAT ON
17:05:20	RAT OFF

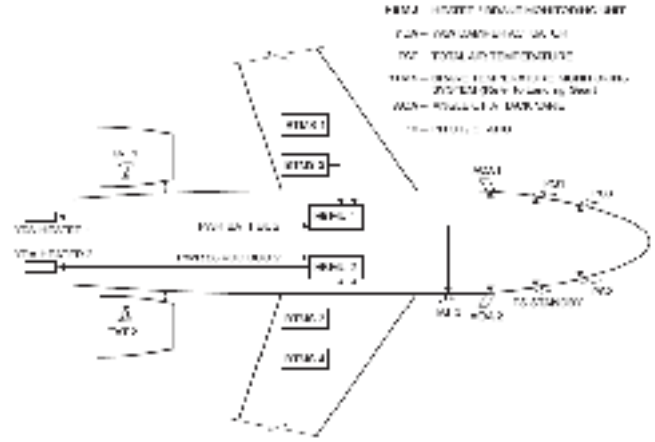

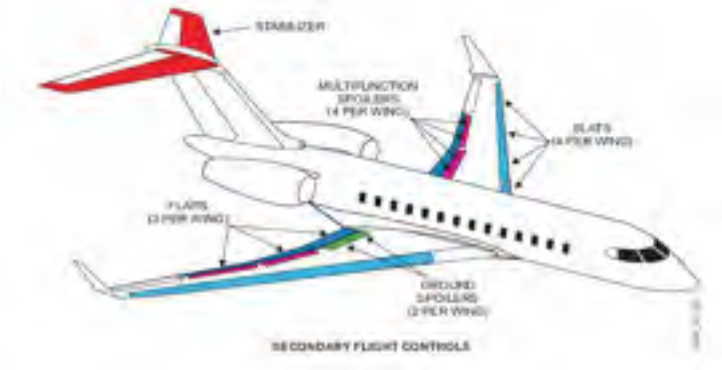

Figure-A IV-2 Load sequence

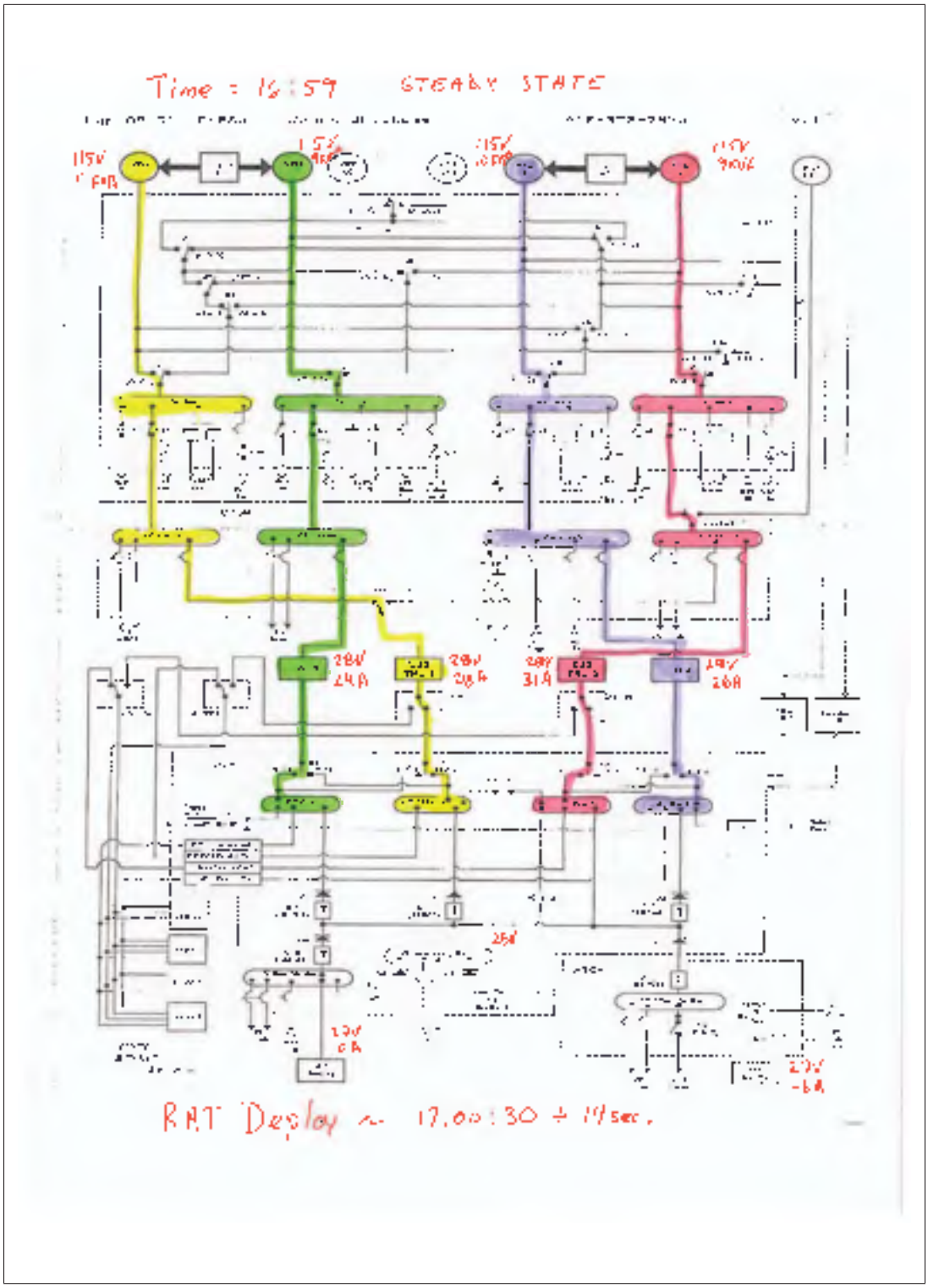

Figure-A IV-3 Emergency supply sequence - phase 1

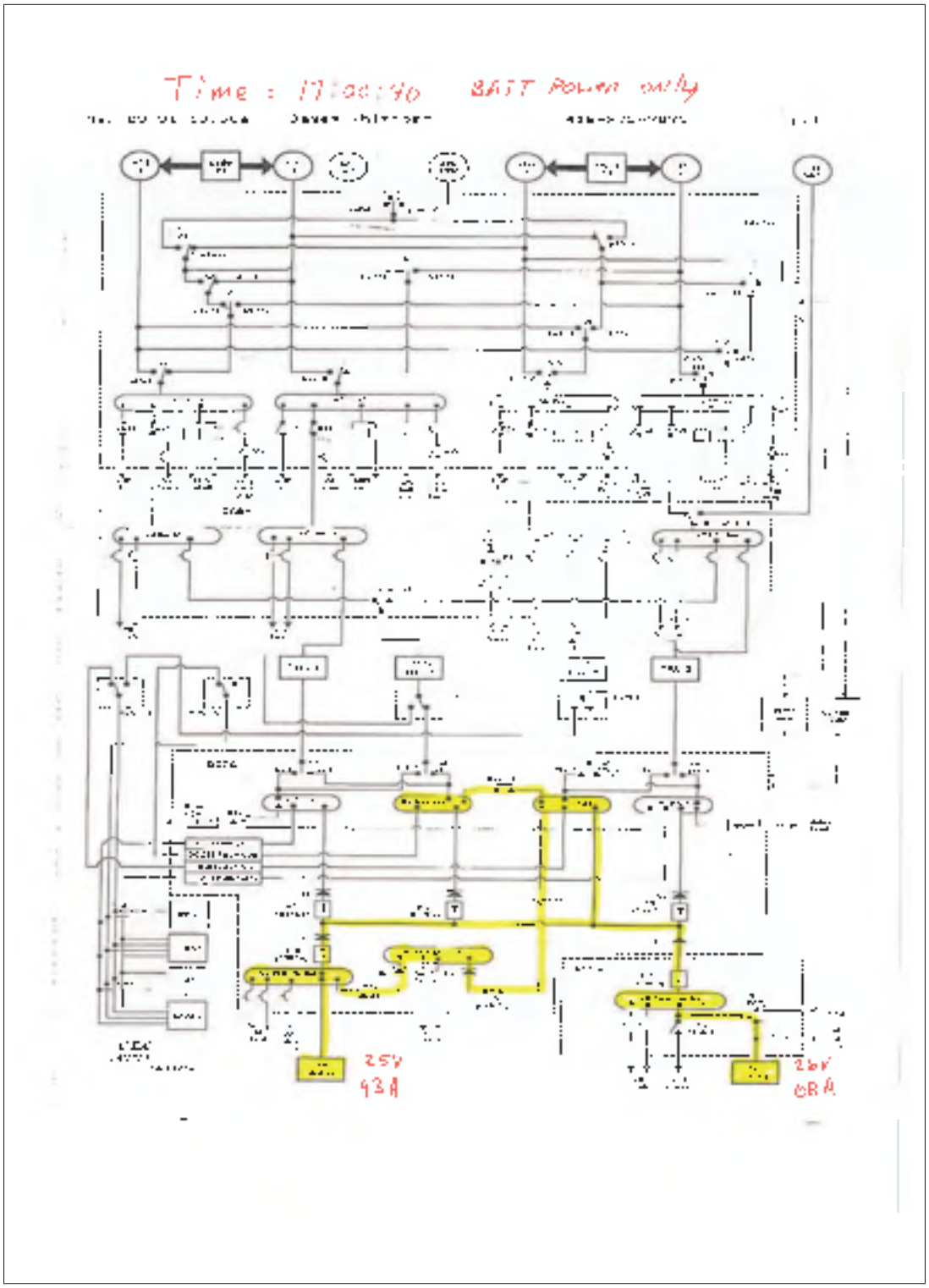

Figure-A IV-4 Emergency supply sequence - phase 2

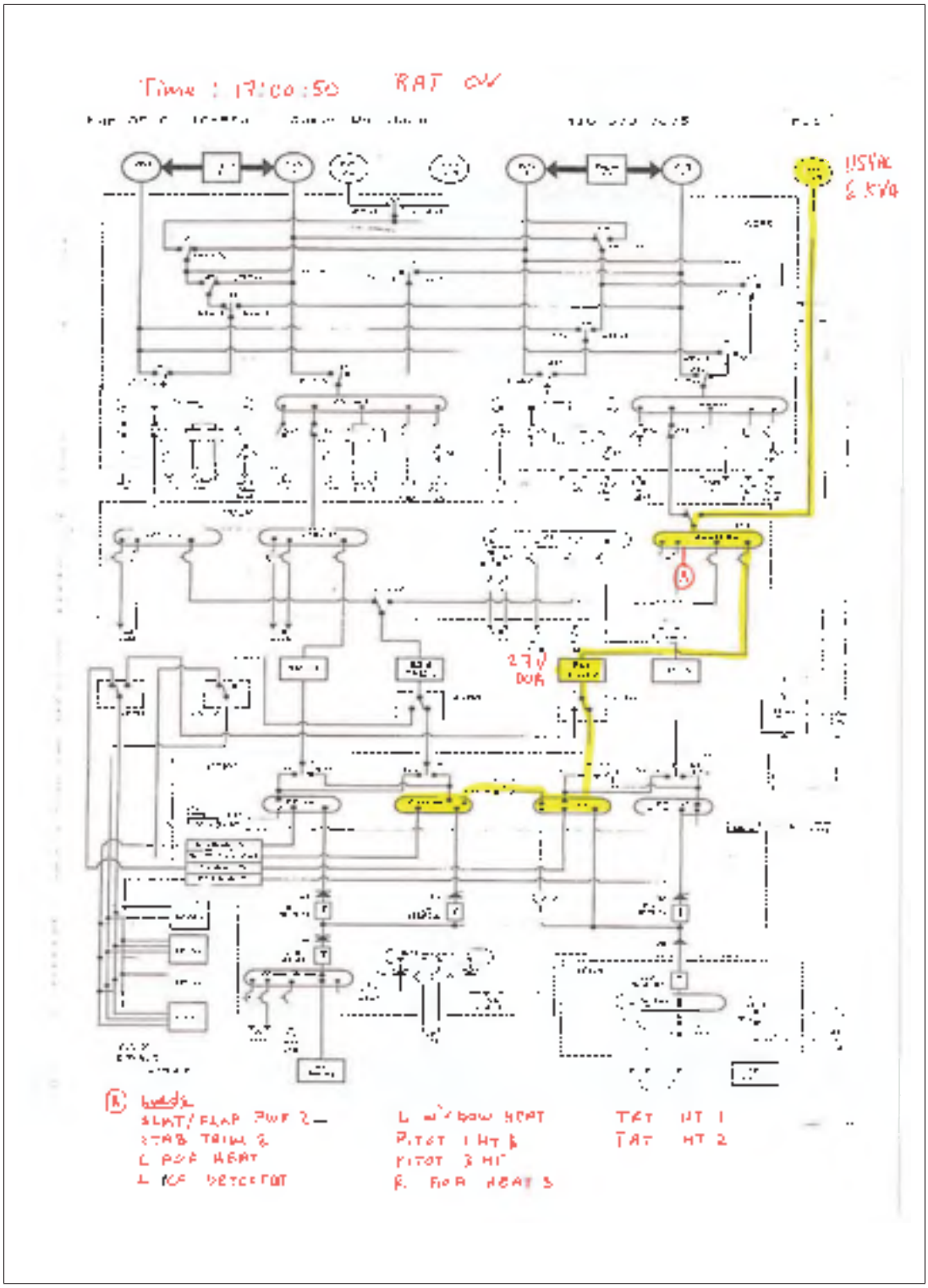

Figure-A IV-5 Emergency supply sequence - phase 3

REFERENCES

Amokrane, S. 1996. "Microscopic Description of the Electrode Surface and Double Layer Capacity at the Electrode/solution Interface". *Electrochimica Acta*, vol. 41, n. 14, p. 2097–2105.

Ates, Y., O. Erdinc, M. Uzunoglu, and B. Vural. 2010. "Energy management of an FC/UC hybrid vehicular power system using a combined neural network-wavelet transform based strategy". *International Journal of Hydrogen Energy*, vol. 35, n. 2, p. 774-783.

Attaianese, C., M. Di Monaco, and G. Tomasso. 2012. "Power Control for Fuel-Cell–Supercapacitor Traction Drive". *IEEE Transactions on Vehicular Technology*, vol. 61, n. 5, p. 1961-1971.

Ballard. 2012. "Mark9 SSL". <http://www.ballard.com/>.

Bauman, J. and M. Kazerani. 2008. "A Comparative Study of Fuel-Cell—Battery, Fuel-Cell—Ultracapacitor, and Fuel-Cell–Battery—Ultracapacitor Vehicles". *IEEE Transactions on Vehicular Technology*, vol. 57, n. 2, p. 760-769.

Bernard, J., S. Delprat, F. Buechi, and T. M. Guerra. 2006. "Global Optimisation in the power management of a Fuel Cell Hybrid Vehicle (FCHV)". *Vehicle Power and Propulsion Conference*, p. 1-6.

Blaud, Pierre Clément . 2012. "Développement d'un modèle de simulation de supercondensateur et validation expérimentale". In *École de technologie supérieure*. En ligne. <http://espace.etsmtl.ca/id/eprint/1084>. Mémoire de maîtrise électronique, Consulté le 10 Septembre 2012.

Boaventura, M., J. M. Sousa, and A. Mendes. 2011. "A dynamic model for high temperature polymer electrolyte membrane fuel cells". *International Journal of Hydrogen Energy*, vol. 36, n. 16, p. 9842-9854.

Bombardier. 2004. "Global express/ Global 5000 Electrical load analysis report". *Eng. Doc No: RAE-L700-103*, p. 1-46.

Bordons, C., M. A. Ridao, A. Perez, A. Arce, and D. Marcos. 2010. "Model Predictive Control for power management in hybrid fuel cell vehicles". *IEEE Vehicle Power and Propulsion Conference (VPPC)*, p. 1-6.

Buller, S., E. Karden, D. Kok, and R. De Doncker. 2002. "Modeling the dynamic behavior of supercapacitors using impedance spectroscopy". *IEEE Transactions on Industry Applications*, vol. 38, n. 6, p. 1622 – 1626.

Cadar, D., D. Petreus, I. Ciocan, and P. Dobra. 2009. "An improvement on empirical modelling of the batteries". *32nd International Spring Seminar on Electronics Technology*, p. 1-6.

Caux, S., W. Hankache, M. Fadel, and D. Hissel. 2010. "On-line fuzzy energy management for hybrid fuel cell systems". *International Journal of Hydrogen Energy*, vol. 35, n. 5, p. 2134-2143.

Chun-Yan, L. and L. Guo-Ping. 2009. "Optimal fuzzy power control and management of fuel cell/battery hybrid vehicles". *Journal of Power Sources*, vol. 192, n. 2, p. 525-533.

DLR. 2010. "Fuel cell demonstrator aircraft". <www.dlr.de>.

Erdinc, O. and M. Uzunoglu. 2010. "Recent trends in PEM fuel cell-powered hybrid systems: Investigation of application areas, design architectures and energy management approaches". *Renewable and Sustainable Energy Reviews*, vol. 14, n. 9, p. 2874-2884.

Erdinc, O., B. Vural, and M. Uzunoglu. 2009. "A wavelet-fuzzy logic based energy management strategy for a fuel cell/battery/ultra-capacitor hybrid vehicular power system". *Journal of Power Sources*, vol. 194, n. 1, p. 369-380.

Erickson, R. and D. Maksimovic, 2001. *Fundamentals of Power Electronics*. éd. 2nd.

Fadel, A. and B. Zhou. 2011. "An experimental and analytical comparison study of power management methodologies of fuel cell–battery hybrid vehicles". *Journal of Power Sources*, vol. 196, n. 6, p. 3271-3279.

Faleiro, L. 2005. "Beyond the more electric aircraft". *Aerospace America*, p. 35-40.

Faleiro, L. 2006. "Power optimised aircraft". *Aerodays 2006, Liebherr-Aerospace*, p. 1-19.

Fernandez, L. M., P. Garcia, C. A. Garcia, and F. Jurado. 2010. "Comparison of control schemes for a fuel cell hybrid tramway integrating two dc/dc converters". *International Journal of Hydrogen Energy*, vol. 35, n. 11, p. 5731-5744.

Fernandez, L. M., P. Garcia, C. A. Garcia, and F. Jurado. 2011. "Hybrid electric system based on fuel cell and battery and integrating a single dc/dc converter for a tramway". *Energy Conversion and Management*, vol. 52, n. 5, p. 2183-2192.

Ferrero, R., M. Marracci, M. Prioli, and B. Tellini. 2012. "Simplified model for evaluating ripple effects on commercial PEM fuel cell". *International Journal of Hydrogen Energy*, vol. 37, n. 18, p. 13462-13469.

García, P., J. P. Torreglosa, L. M. Fernandez, and F. Jurado. 2012. "Viability study of a FC-battery-SC tramway controlled by equivalent consumption minimization strategy". *International Journal of Hydrogen Energy*, vol. 37, n. 11, p. 9368-9382.

Garcia, A. M. 2007. "Theoretical study of a power generation unit based on the hybridization of a fuel cell stack and ultracapacitors". PhD thesis, Institut national polytechnique de Toulouse.

Graham, M., M. C. Andrew, H. W. Andreas, and J. K. Robert. 2012. "Three-dimensional particle-resolved models of Li-ion batteries to assist the evaluation of empirical parameters in one-dimensional models". *Electrochimica Acta*, vol. 64, p. 118-129.

Honda. 2009. “FCX Clarity”. <http://world.honda.com/FuelCell/>.

Kermani, S., S. Delprat, T. M. Guerra, R. Trigui, and B. Jeanneret. 2012. “Predictive energy management for hybrid vehicle”. *Control Engineering Practice*, vol. 20, n. 4, p. 408-420.

Kim, M. J., Huei Peng, Chan-Chiao Lin, E. Stamos, and D. Tran. 2005. “Testing, modeling, and control of a fuel cell hybrid vehicle”. *American Control Conference*, vol. 6, p. 3859 - 3864.

Langlois, O. 2006. “Conception d’un réseau de secours électrique pour l’aéronautique”. PhD thesis, Institut national polytechnique de Toulouse.

Langlois, O., E. Foch, X. Roboam, and H. Piquet. 2005. “De l’avion plus électrique à l’avion tout électrique: état de l’art et prospective sur les réseaux de bord”. *J3eA, Journal sur l’enseignement des sciences et technologies de l’information et des systèmes*, vol. 4, p. 1-8.

Larminie, J. and A. Dicks, 2003. *Fuel cell systems explained*. éd. 2nd.

Li, Q., W. Chen, Y. Li, S. Liu, and J. Huang. 2012. “Energy management strategy for fuel cell/battery/ultracapacitor hybrid vehicle based on fuzzy logic”. *International Journal of Electrical Power and Energy Systems*, vol. 43, n. 1, p. 514-525.

Liangfei, X., L. Jianqiu, H. Jianfeng, L. Xiangjun, and O. Minggao. 2009. “Adaptive supervisory control strategy of a fuel cell/battery-powered city bus”. *Journal of Power Sources*, vol. 194, n. 1, p. 360-368.

Liebherr. 2007. “Fuel cell emergency power system (FCEPS)”. <www.liebherr.com>.

Lin, W.-S. and C-H. Zheng. 2011. “Energy management of a fuel cell/ultracapacitor hybrid power system using an adaptive optimal-control method”. *Journal of Power Sources*, vol. 196, n. 6, p. 3280-3289.

Min-Joong, K. and P. Huei. 2007. “Power management and design optimization of fuel cell/battery hybrid vehicles”. *Journal of Power Sources*, vol. 165, n. 2, p. 819-832.

Mingruo, H., G. Anzhong, W. Minghua, Z. Xinjian, and Y. Lijun. 2004. “Three dimensional, two phase flow mathematical model for PEM fuel cell: Part I. Model development”. *Energy Conversion and Management*, vol. 45, n. 11-12, p. 1861-1882.

Moreno, J., M. E. Ortuzar, and J. W. Dixon. 2006. “Energy-management system for a hybrid electric vehicle, using ultracapacitors and neural networks”. *IEEE Trans. Ind. Electron.*, vol. 53, n. 2, p. 614- 623.

Musardo, C., G. Rizzoni, and B. Staccia. 2005. “A-ECMS: An Adaptive Algorithm for Hybrid Electric Vehicle Energy Management”. *44th IEEE Conference on Decision and Control*, p. 1816- 1823.

Nissan. 2011. “Fuel cell vehicles”. <http://www.nissan-global.com>.

Njoya, S. M., O. Tremblay O, and L-A. Dessaint. 2009. “A generic fuel cell model for the simulation of fuel cell vehicles”. *IEEE Vehicle Power and Propulsion Conference*, p. 1722-1729.

O’Hayre, R., S-W. Cha, W. Colella, and F. B. Prinz, 2005. *Fuel cell fundamentals*. éd. 1.

Oldham, K. B. 2008. “A Gouy-Chapman-Stern model of the double layer at a (metal)/(ionic liquid) interface”. *Journal of Electroanalytical Chemistry*, vol. 613, n. 2, p. 131–138.

Padulles, J., G.W Ault, and J. R. McDonald. 2000. “An integrated SOFC plant dynamic model for power systems simulation”. *Journal of Power Sources*, vol. 86, n. 1-2, p. 495-500.

Parashuram, B., B. T. Dhananjay, P. M. Uday, and B. Ramesh. 2000. “Development, modeling and characterization of aqueous metal oxide based supercapacitor”. *Energy*, vol. 40, n. 1, p. 131-138.

Pisu, P. and G. Rizzoni. 2007. “A Comparative Study Of Supervisory Control Strategies for Hybrid Electric Vehicles”. *IEEE Transactions on Control Systems Technology*, vol. 15, n. 3, p. 506-518.

Piyush, B., G. A. Suresh, and K. P. Ajay. 2012. “Integration of batteries with ultracapacitors for a fuel cell hybrid transit bus”. *Journal of Power Sources*, vol. 199, p. 360-366.

Prats, M. A. M. 2007. “PEM fuel cell emergency electrical power”. *Research report, Bombardier Aerospace*, p. 1-75.

Pukrushpan, J. T., A. G. Stefanopoulou, and H. Peng, 2002. *Control of fuel cell power systems: principles, modeling, analysis, and feedback design*. éd. 2nd.

Ramos-Paja, C. A., A. Romero, R. Giral, J. Calvente, and L. Martinez-Salamero. 2010. “Mathematical analysis of hybrid topologies efficiency for PEM fuel cell power systems design”. *International Journal of Electrical Power and Energy Systems*, vol. 32, n. 9, p. 1049-1061.

Renouard-Vallet, G., M. Saballus, G. Schmithals, J. Schirmer, J. Kallo, and A. K. Friedrich. 2010. “Improving the environmental impact of civil aircraft by fuel cell technology: concepts and technological progress”. *Energy Environ. Sci.*, p. 1458-1468.

Renouard-Vallet, G., M. Saballus, G. Schmithals, J. Schirmer, J. Kallo, and A. K. Friedrich. 2011. “Fuel Cells For Aircraft Applications”. *ECS Trans.*, vol. 30, n. 1, p. 271-280.

Rodatz, P., G. Paganelli, A. Sciarretta, and L. Guzzella. 2005. “Optimal power management of an experimental fuel cell/supercapacitor-powered hybrid vehicle”. *Control Engineering Practice*, vol. 13, n. 1, p. 41-53.

Rosero, J., J. A. Ortega, E. Aldabas, and L. Romeral. 2007. “Moving towards a more electric aircraft”. *IEEE Aerospace and Electronic Systems Magazine*, vol. 22, n. 3, p. 3-9.

Runtz, K. and M. D. Lyster. 2005. "Fuel cell equivalent circuit models for passive mode testing and dynamic mode design". *Canadian Conference on Electrical and Computer Engineering*, p. 794 - 797.

Sciarretta, A., M. Back, and L. Guzzella. 2004. "Optimal control of parallel hybrid electric vehicles". *IEEE Transactions on Control Systems Technology*, vol. 12, n. 3, p. 352- 363.

Shepherd C. M. 1963. "Theoretical design of primary and secondary cells. part 3: Battery discharge equation". In *Naval Research Lab Washington DC*. En ligne. <http://oai.dtic.mil/oai/oai?verb=getRecord&metadataPrefix=html&identifier=AD0405904>. Consulté le 10 Septembre 2012.

SimPowerSystems. 2012. "Model and simulate electrical power systems". <http://www.mathworks.com/products/simpower/>.

Sripakagorn, A. and N. Limwuthigraijirat. 2009. "Experimental assessment of fuel cell/supercapacitor hybrid system for scooters". *International Journal of Hydrogen Energy*, vol. 34, n. 15, p. 6036-6044.

Sungwoo, C., J. Hyeonseok, H. Chonghun, J. Shanshan, H. L. Jae, and O. Jeonkeun. 2012. "State-of-charge estimation for lithium-ion batteries under various operating conditions using an equivalent circuit model". *Computers and Chemical Engineering*, vol. 41, p. 1-9.

Thanh-Son, D., P.V. Chandrika, and M. John. 2012. "Simplification and order reduction of lithium-ion battery model based on porous-electrode theory". *Journal of Power Sources*, vol. 198, p. 329-337.

Thounthong, P. and S. Raël. 2009. "The benefits of hybridization". *IEEE Industrial Electronics Magazine*, vol. 3, n. 3, p. 25-37.

Thounthong, P., V. Chunkag, P. Sethakul, S. Sikkabut, S. Pierfederici, and B. Davat. 2011. "Energy management of fuel cell/solar cell/supercapacitor hybrid power source". *Journal of Power Sources*, vol. 196, n. 1, p. 313-324.

Torreglosa, J. P., F. Jurado, P. García, and L. M. Fernández. 2011. "Hybrid fuel cell and battery tramway control based on an equivalent consumption minimization strategy". *Control Engineering Practice*, vol. 19, n. 10, p. 1182-1194.

Tremblay, O. and L-A. Dessaint. 2009. "Experimental Validation of a Battery Dynamic Model for EV Applications". *World Electric Vehicle Journal*, p. 1-10.

Valero, I., Seddik Bacha, and Elisabeth Rulliere. 2006. "Comparison of energy management controls for fuel cell applications". *Journal of Power Sources*, vol. 156, n. 1, p. 50 - 56.

Vural, B., A. R. Boynuegri, I. Nakir, O. Erdinc, A. Balikci, M. Uzunoglu, H. Gorgun, and S. Dusmez. 2010. "Fuel cell and ultra-capacitor hybridization: A prototype test bench based analysis of different energy management strategies for vehicular applications". *International Journal of Hydrogen Energy*, vol. 20, n. 35, p. 11161-11171.

Wells, J. R., M. Amrhein, E. Walters, Steve Iden, Austin Page, Peter Lamm, and Anthony Matasso. 2008. "Electrical Accumulator Unit for the Energy Optimized Aircraft". *SAE 2008 Power System Conference*, p. 1071-1077.

Wikipedia. 2012. "Ram air turbine". <http://en.wikipedia.org/wiki/Ram_air_turbine>.

Wilhelm, J., H. Janssen, J. Mergel, and D Stolten. 2010. "Energy management for a fuel cell/battery hybrid system". *Emobility - Electrical Power Train*, p. 1-6.

Wong, J. H., N. R. N. Idris, and M. Anwari. 2011. "Parallel configuration in energy management control for the fuel cell-battery-ultracapacitor hybrid vehicles". *IEEE Applied Power Electronics Colloquium (IAPEC)*, p. 69-74.

Xiaosong, H., L. Shengbo L, and P. Huei. 2012. "A comparative study of equivalent circuit models for Li-ion batteries". *Journal of Power Sources*, vol. 198, p. 359-367.

Xin, K., A.M. Khambadkone, and K.T. Soy. 2005. "A hybrid model with combined steady-state and dynamic characteristics of PEMFC fuel cell stack". *Industry Applications Conference, Fourtieth IAS Annual Meeting*, vol. 3, p. 1618- 1625.

Yang, Y.-P., R-M. Guan, and Y-M. Huang. 2012. "Hybrid fuel cell powertrain for a powered wheelchair driven by rim motors". *Journal of Power Sources*, vol. 212, p. 192-204.

Yongping, H., Y. Zhihua, and W. Gang. 2010. "An improved dynamic voltage model of PEM fuel cell stack". *International Journal of Hydrogen Energy*, vol. 35, n. 20, p. 11154-11160.

Zandi, M., A. Payman, J-P. Martin, S. Pierfederici, B. Davat, and F. Meibody-Tabar. 2011. "Energy Management of a Fuel Cell/Supercapacitor/Battery Power Source for Electric Vehicular Applications". *IEEE Transactions on Vehicular Technology*, vol. 60, n. 2, p. 433-443.

Zhang, X., C. Chunting Mi, A. Masrur, and D. Daniszewski. 2008. "Wavelet-transform-based power management of hybrid vehicles with multiple on-board energy sources including fuel cell, battery and ultracapacitor". *Journal of Power Sources*, vol. 185, n. 2, p. 1533-1543.

Zheng, C. H., N. W. Kim, and S. W. Cha. 2012. "Optimal control in the power management of fuel cell hybrid vehicles". *International Journal of Hydrogen Energy*, vol. 37, n. 1, p. 655-663.

Zubieta, L. and R Bonert. 2002. "Characterization of double-layer capacitors for power electronics applications". *IEEE Transactions on Industry Applications*, vol. 36, n. 1, p. 199 – 205.